The Effect of Support Conditions on the Fire Resistance of a Reinforced Concrete Beam

cand.-ing. Daniela Bernhart

Supervised by

Prof. Dr. Andrew Buchanan
Assoc. Prof. Dr. Peter Moss
Dipl.-Ing. Martin Larcher

Fire Engineering Research Report 04/5

August 2004

This report was presented as a thesis in partial fulfilment of the requirements for the Degree of Diplom-Bauingenieurin at the University of Karlsruhe.

Department of Civil Engineering
University of Canterbury
Private Bag 4800
Christchurch, New Zealand

For a full list of reports please visit http://www.civil.canterbury.ac.nz/fire/fe_resrch_reps.html

ABSTRACT

This report examines the behaviour of reinforced concrete beams with rectangular cross-section exposed to fire from the bottom and the sides. The study was performed with 2D finite element analysis using SAFIR.

The effect of various support conditions was studied during the exposure to a four-hour ISO-fire for single-span beams with pinned and rotationally restrained supports, allowing for varying levels of horizontal restraint in both cases. The results showed that the provision of horizontal restraint was beneficial to the fire resistance of the beams in both cases. The provision of rotational restraint greatly improved the behaviour of the beams compared to the pinned supported case.

The effect of continuity was investigated with beams spanning over two and three bays subjected to a four-hour ISO-fire. Within this analysis the effect of different lengths of the top reinforcing bars at the supports was investigated. Compared to the single span beam, the continuous beams resisted the fire exposure for a longer period of time. The different lengths of the reinforcing bars did not greatly increase the fire resistance of the beams.

The influence of the full process of fire development was analysed with one, two and three-bay beams without horizontal restraint. These beams were exposed to the ISO-fire for 30, 60 and 90 minutes followed by a decay phase. The analysed beams showed good behaviour. Failure only occurred when the decay phase started close to the failure time reached during the full ISO-fire.

ACKNOWLEDGEMENTS

I would like to extend my appreciation and gratitude to the following people who helped me with my research:

- Professor Andrew Buchanan for supervising my project and providing invaluable assistance and guidance.
- Associate Professor Peter Moss for supervising my project and providing invaluable assistance as well as methodically proof reading this report.
- Associate Professor Athol Carr for compiling and improving my Fortran files needed for data extraction.
- Dr. Rajesh Dhakal, Dr. Richard Fenwick and Prof. Desmond Bull for their help.
- Prof. Dr.-Ing. Lothar Stempniewski for supporting my wish to make my thesis in New Zealand.
- Dipl.-Ing. Martin Larcher for supervising me back home in Germany.
- Jerry Chang for his assistance with the SAFIR program and his overall support.
- The *DAAD* and the *Studienstiftung des Deutschen Volkes* for providing me with a scholarship.
- Finally, my family and friends for their unwavering support, patience and belief in me.

TABLE OF CONTENTS

1 INTRODUCTION

Concrete frame structures form the basis of most modern multi-storey buildings. Concrete structures in general have a reputation of having very good behaviour in fire conditions as not many fires have led to a collapse of the structure even in severe fires. However, tragic events like September 11th have made people more aware of the extent of damage a fire could have on the behaviour or the stability of the entire structure. There is now a greater interest in investigating the effects a local collapse might have on the total building structure.

One of the main types of structural elements within concrete structures are the beams. As the beams form the supports for other load-bearing elements like slabs, their collapse during a fire can be detrimental to the stability of the rest of the structure.

The behaviour of concrete beams in fires is complex, as thermal and load induced stresses are combined, but the most obvious consequence of a fire is the degradation in strength of the concrete and the reinforcing steel which may lead to collapse. Accompanied by the heating of the beam is the high thermal expansion, which may cause the surrounding structure to impose high axial forces on the beam. These forces are normally not included in the design process. Most design procedures assume sufficient fire resistance, if certain criteria, mainly the distance of the reinforcing bars from the concrete surface, are kept.

1.1 Motivation

At the University of Canterbury, considerable research has been carried out into the effect of fire on the behaviour of steel and composite beams and reinforced concrete slabs, while no similar research has been undertaken into the behaviour of concrete beams.

Reinforced concrete beams within real structures may be subjected to varying support conditions because neither total horizontal restraint nor total rotational restraint is likely to be realised. Thus, the behaviour of the beams with varying support conditions has to be analysed.

The previous research on steel and composite beams has shown that the effect of a decay phase of the fire can have detrimental consequences on the structure. Therefore

there is great interest in the behaviour of a concrete beam exposed to the full process of fire development.

In view of all the factors outlined above, this research project set out to investigate the behaviour of reinforced concrete beams having a range of support conditions and subjected to ISO and parametric fires.

1.2 Objectives

The objectives of this research are to:

- Investigate the effect of various support conditions on the flexural behaviour of a single concrete beam under fire exposure.
- Determine the effect of fire on the flexural behaviour of continuously designed beams.
- Investigate the effect of fires with a decay phase on the flexural behaviour of concrete beams.
- Compare the design recommendations of Eurocode and DIN with the numerical results.

1.3 Scope of this research

The scope of this research covers the effect of various support conditions on the behaviour of a single span beam subjected to the ISO-fire from the bottom and the sides. The support conditions include pin-roller and pin-pin supports with varying levels of horizontal restraint and fix-slide and fix-fix supports also with varying levels of horizontal restraint.

The effect of continuity is studied by analysing beams spanning over two and three bays subjected to the ISO-fire. Within this section the influence of varying the length of the top reinforcement at the inner supports is also investigated.

The effect of the full process of fire development is analysed with beams spanning from one to three bays subjected to growing ISO-fires with a decay-phase.

The analysis is carried out as a 2D analysis using the non-linear finite element program SAFIR.

1.4 Outline of the thesis

Following this introduction, Chapter 2 provides a review of the literature dealing with previous research with particular reference to aspects of structural analysis for fire situations and design implementation in codes. The material properties of concrete and steel at elevated temperatures are summarized in Chapter 3. An introduction to the SAFIR program used in the analyses and its capabilities is given in Chapter 4.

The numerical analyses on the effect of varying support conditions on the fire resistance of single-span reinforced concrete beams subjected to the ISO fire are described in Chapter 5. The effect of continuity of the beams over one and two supports is presented in Chapter 6. Chapter 7 shows the effects of fires with a decay phase on various beams. The conclusions and recommendations from this research can be found in Chapter 8.

2 BASIC PRINCIPLES

This section gives an overview of the basic principles of fire design. It shows the meaning of fire resistance and summarizes code recommendations and design methods for concrete members, including design fires. The principal behaviour of beams under fire exposure is shown and a reference to large-scale fire tests is given. The effects of elevated temperatures on the material behaviour of concrete and steel are outlined separately in section 3.

2.1 Fire resistance

Fire resistance is the measure of the ability of a building element to resist a fire. Fire resistance is most often quantified as the time for which the element can meet certain criteria during exposure to a standard fire-resistance test. It is a property assigned to building elements; individual materials do not possess fire resistance.

During a fire test, a structural element must perform its load-bearing function and carry the load for the duration of the test without collapse. It then meets the stability criteria. Barriers like walls and slabs additionally have to meet the integrity and insulation criteria to prevent fire spreading from the room of origin. Therefore, the test specimen must not develop any cracks or fissures which allow smoke or hot gases to pass through and the temperature of the cold side must not exceed a specified limit (Buc-01).

It is important to realise that the fire-resistance time does not express the time a structure might resist in a real fire, as the duration of an actual fire cannot be precisely specified. The construction in a building may perform satisfactorily for a shorter or a longer period depending upon the characteristic of the fire (Mal-82).

2.2 Code recommendations for fire design of concrete beams

This section gives an overview of the regulations concerning the design of fire resistance of different codes, with emphasis on the design of concrete beams.

2.2.1 Eurocode

Eurocode 1 Part 1-2: ”Actions on structures exposed to fire” (EC1-03) regulates calculation models for the determination of temperature and load effects. The fire scenario is treated as “exceptional action” and does not need to be superimposed with other, independent exceptional actions. For the fire design, different time-temperature curves for the determination of the hot-gas-temperature are provided. These are stated in section 2.4.

Eurocode 2 Part 1-2: “Design of Concrete Structures – Structural Fire Design” (EC2-02) (EC2-95) deals with the design of concrete structures for the case of fire. It states the design values for material properties and combination factors for actions and treats methods of the passive and structural fire precautions; active fire protection methods are not included.

For the determination of a sufficient fire rating, Eurocode 2 (EC2-02) (EC2-95) gives three alternatives of design methods:

- **Tabulated data**

  In dependence on the fire resistance rating, the tabulated data gives minimum values for cross-sectional dimensions and the axial distances of the longitudinal reinforcement to the concrete surface. For beams there is a distinction between simply supported and continuous beams.

  For statically determinate structures the axial distance of the reinforcement is determined such, that for the fire resistance time, the critical temperature in the steel bars is 500°C. Reaching this critical temperature, the reinforcement reaches its yield stress if the loads under fire conditions equal 0.7 times the load under cold conditions. If the applied load in the event of fire is less, the tabulated axial distances may be reduced.

- **Simplified calculation methods for specific types of members**

  Eurocode 2 provides several calculation methods to assess the strength of the concrete members at any time for any fire exposure. These methods are based on a reduced cross-section consisting of cooler parts of the member. Therefore, the temperature profiles within the member and data of the temperature dependant changes of the material properties are needed. More details on simplified calculation methods are given in section 2.3.1.

- **Advanced calculation methods**

  Advanced calculation methods can be used for the simulation of the structural behaviour of single members, parts of the structure, or the entire structure.

  The advanced calculation methods provide a realistic analysis of the structures exposed to fire. They are based on fundamental physical behaviour leading to a reliable approximation of the expected behaviour under fire conditions.

  Thermal analysis shall be based on acknowledged principles and assumptions of the theory of heat transfer and include the temperature dependant thermal properties of the materials. Mechanical analysis shall be based on the acknowledged principles and assumptions of the theory of structural mechanics, taking into account the changes of mechanical properties with temperature. Non-linear geometrical effects and the effects of thermally induced strains and stresses shall be considered, as well as all strains due to the temperature, mechanical loads, creep and transient creep (EC2-02).

  The code provides details on the thermal and mechanical properties of concrete and reinforcing steel when they are subjected to elevated temperatures.

2.2.2 German Standard

The German regulations on determining the fire resistance of concrete structures are regulated according to DIN 4102-4 (DIN-4102-4). DIN 4102-4 gives tabulated data considering the size of the member, the axial distance of the longitudinal reinforcement to the concrete surface and the minimum number of reinforcing bars within the beam, related to the fire resistance rating.

At present, DIN 4102-4 is not applicable to the current German concrete standard DIN 1045-1, as it is based on stress analysis and not on the partial safety coefficient

concept used in DIN 1045-1. This discrepancy is going to be closed with the introduction of DIN 4102-22, which is a direction for use of DIN 4102-4. At the moment, the first draft of DIN 4102-22 (DIN-4102-22) has been published. For the design of concrete beams the application of DIN 4102-22 will not result in great changes in the use of the tabulated data.

At the moment, the determination of the fire resistance has to be performed using the tabulated data of Eurocode 2 (EC2-95), considering additional regulations stated in “DIBt-Richtlinie zur Anwendung von DIN V ENV 1992-1-2 in Verbindung mit DIN 1045-1" (DIBt-02).

2.2.3 New Zealand Standard

The New Zealand Concrete Structures Standard NZS 3101 (NZS-95) sets the requirements for the design of concrete structures and members to resist the effects of fire. Within the code, the fire resistance of a concrete member can be determined according to stated data, prescribing the minimum size of the member and the minimum concrete cover of the longitudinal reinforcing bars.
Additionally the code allows the determination of the fire resistance ratings from fire tests or a recognized method of calculation such as that given in “BRANZ Technical Recommendation No.8” (Wad-91).

Currently the New Zealand Concrete Structures Standard is being revised. Thus, the parts considering fire resistance will be changed, and some parts will be more closely aligned with the Eurocode and with the Australian Standard AS 3600 (Buchanan, pers. comm.).

2.3 Design methods

2.3.1 Simplified calculation methods

The design of beams under fire conditions is normally performed in the strength domain. Thus it has to be demonstrated, that the design resistance under fire conditions is greater than the design action at a particular duration of the fire. For the determination of the design resistance, the reduced strength of the concrete and the reinforcement has to be determined.

Eurocode 2 (EC2-02) gives two methods to determine the residual strength of a structural member using reduced cross-sections:

- The “500°C isotherm method” comprises a general reduction of the cross-section size with respect to a heat-damaged zone at the concrete surfaces. The thickness of the damaged zone is made equal to the average depth of the 500°C isotherm in the compression zone of the cross-section. Thus concrete with temperatures in excess of 500°C is assumed not to contribute to the load bearing capacity of the member, whilst the residual cross-section retains its initial values of strength and modulus of elasticity. Taking the reduced strength of the reinforcement bars into account, the ultimate load bearing capacity can be determined using conventional calculation methods, such as those stated in the Eurocode (EC2-02), by the CRSI (Gut-80), Harmathy (Har-93), or the ACI Committee (ACI-81).
- The “Zone method” subdivides the cross-section into several zones of equivalent thickness and evaluates the reduced strength of each zone. Out of the single value of each zone, a damaged zone and the residual strength of the reduced cross-section can be determined. For the standard fire curve, the Eurocode provides several diagrams which allow for a quicker determination of the reduced cross-section. This method is more accurate, but also more laborious, compared to the 500°C isotherm method.

For the determination of the temperature profiles needed, published generic temperature contours for structural members can be used. Temperature contours have been published among others by FIP (FIP-78), ACI (ACI-81), Wade (Wad-91) and the Eurocode (EC2-95) (EC2-02) for standard fires. For fire conditions other than standard fires, the temperature profiles should be determined using suitable computer programs.

2.3.2 Computer programs

Several computer programs have been developed for the analysis of steel and concrete structures in fires, most of which are based on the finite element method and are not user-friendly enough to be used as design tools and are typically used for research purposes. Several programs are listed below, but more detailed summaries have been given by Sullivan (Sul-94) and Lim (Lim-03).

Terro (Ter-98) has developed two programs for the 3D analysis of concrete structures in fire, TEMP and STRUCT. The TEMP program is used for the thermal analysis and the

temperature distributions are then fed into the program STRUCT, to perform the structural analysis. STRUCT was developed within the shell of a general purpose finite element program called LUSAS (London University Stress Analysis System).

At the University of Sheffield, the program VULCAN has been developed with the objective of enabling three-dimensional modelling of the behaviour of composite buildings in fire (Hua-00) (Hua-01). The program has been verified with several experimental results of the Cardington full-scale fire tests. Cai (Cai-03) states that the VULCAN program has been extended in such a way that steel, concrete and composite members such as reinforced concrete beams and concrete filled columns can be modelled.

SAFIR (Fra-00) has been developed at the University of Liège, Belgium. It is a non-linear finite element program based on an earlier program, CEFICOSS. The program is divided into a thermal and a structural analysis part. It is possible to model 2D and 3D elements of steel, concrete and composite members. SAFIR will be used for the analysis of this report and will be described in further detail in section 4.

Franssen and Gens (Fra-04) state that recently an algorithm has been implemented in the SAFIR program that allows considered acceleration terms in the analysis of structures subjected to fire. This allows the simulation to run beyond the moments when the stiffness matrix is temporarily or locally not positive, thus local failures and temporary unstable states can be accommodated. The algorithm also allows much larger displacements than with the succession of static analyses.

Other programs have been developed by Zha (Zha-03) and Bratina et al. (Bra-03). Commercial general-purpose finite element programs, such as ABAQUS, have been used among others by Sanad et al. (San-00), Lamont (Lam-01) (Lam-01), and Gillie (Gil-00) to model structures in fire. However, users have reported severe convergence problems (Lam-01) (Gil-00) due to the non-linear material properties and the geometric non-linearity of structures exposed to fires.

2.4 Fire Models

Several models of time-temperature relationships are available for the simulation of fires for design purposes:

The ISO 834 fire is the basis of most fire resistance tests and is defined according to the following equation:

$$T = 345 \cdot \log_{10}(8 \cdot t + 1) + T_0 \tag{2.1}$$

where t is the time (minutes) and T_o is the ambient temperature (°C).

Where a structural member is engulfed in flames from a large pool fire, the hydrocarbon fire curve according to EC1 (EC1-03) should be used. The hydrocarbon fire curve is defined as follows:

$$T = 1080 \cdot (1 - 0.325 \cdot e^{-0.167 \cdot t} - 0.675 \cdot e^{-2.5 \cdot t}) + 20 \tag{2.2}$$

where t is the time (minutes).

Structural members located outside a burning compartment will be exposed to lower temperatures than the members inside a compartment unless they are engulfed in flames. They can be designed according to:

$$T = 660 \cdot (1 - 0.687 \cdot e^{-0.32 \cdot t} - 0.313 \cdot e^{-3.8 \cdot t}) + 20 \tag{2.3}$$

where t is the time (minutes).

The fires mentioned above are shown in Figure 2.1:

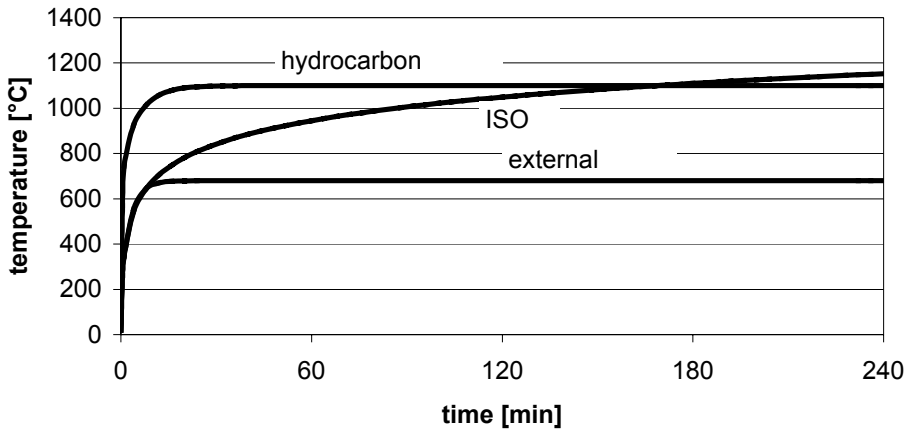

Figure 2.1: Time-temperature relationship for different fire models

The Eurocode (EC1-03) also provides an equation for parametric fires, which allows a time-temperature relationship considering any combination of fuel loads, ventilation openings and wall lining materials. Thus the fire curve can be adjusted to any existing fuel load to produce a realistic temperature development to allow for a performance-based design.

The temperature during the heating period is defined as:

$$T = 20 + 1325 \cdot (1 - 0.324 \cdot e^{-0.2 \cdot t^*} - 0.204 \cdot e^{-1.7 \cdot t^*} - 0.472 \cdot e^{-19 \cdot t^*}) \quad (2.4)$$

where

$t^* = t * \Gamma$ [h]

t time [h]

$$\Gamma = \frac{[O/b]^2}{[0.04/1160]^2}$$

$b = \sqrt{(\rho c \lambda)}$ in the limits $100 < b < 2200$ [$J/m^2 s^{\frac{1}{2}} K$]

ρ = density [kg/m^3]

c = specific heat [J/kgK]

λ = thermal conducitvity [W/mK]

O = ventilation factor : $A_v \sqrt{h_{eq}} / A_t$ with $0.02 < O < 0.2$ [$m^{1/2}$]

A_v = total area of vertical openings in all walls [m^2]

h_{eq} = hight of the window opening [m]

A_t = total area of the bounding surfaces of the room [m^2]

2.5 Simply supported beam under fire conditions

When a simply supported beam, as shown in Figure 2.2, is exposed to fire, it will expand outwards and gradually deflect downwards. The expansion is due to the thermal elongation of the materials. The deflection results from the non-linear temperature gradients that form across the cross-section of the beam and lead the beam to bow thermally. The high temperatures at the bottom and the sides of the beam will cause the tensile reinforcement to lose its flexural strength as well as the concrete in the compression zone to lose its compressive strength. This reduction in the flexural strength of the beam will result in increasing deflections. When the applied bending moment exceeds the residual strength of the beam, a plastic hinge will form and failure will occur.

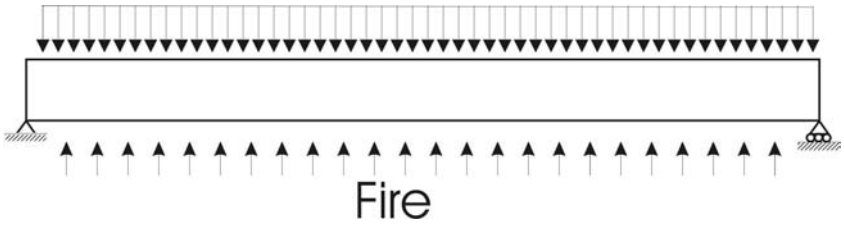

Figure 2.2: Simply supported beam subjected to fire exposure

Experimental tests on simply supported members have been carried out by the Portland Cement Association. In three different studies the fire resistance of prestressed concrete members has been investigated. Study A investigated the influence of thickness of concrete cover of the prestressing steel strands (Car-62). The tests showed that an increase in covering did increase the fire resistance, but not proportionally. Study B studied the influence of aggregate and load intensity (Sel-64). It was shown that beams made of concrete containing expanded shale aggregates exhibited longer fire endurance than did beams of normal weight aggregate concrete. Beams made of normal weight aggregate mainly failed in tension as the steel elongated at critical amounts, whereas lightweight concrete members showed a compression failure at the top of the beams as their compression zones were subjected to higher temperatures due to the longer fire endurance. Heavier loading led to a more rapid midspan deflection and failure occurred at lower average temperatures, and so shorter endurance times, than did the lighter loading. In study C, the type of reinforcement, the type of bond and the influence of aggregate were investigated (Gus-71). Beams with reinforcing bars showed longer fire endurance than those with post-tensioned high-strength alloy bars or cold drawn wire. General effects of the type of bond and the aggregate could not be obtained in those tests.

2.6 Effect of axial restraint

Axial restraint can have a significant influence on the fire performance of concrete beams. It results when a heated member is restrained from thermal expansion by a more rigid surrounding structure and thus compressive axial forces develop in the beam.

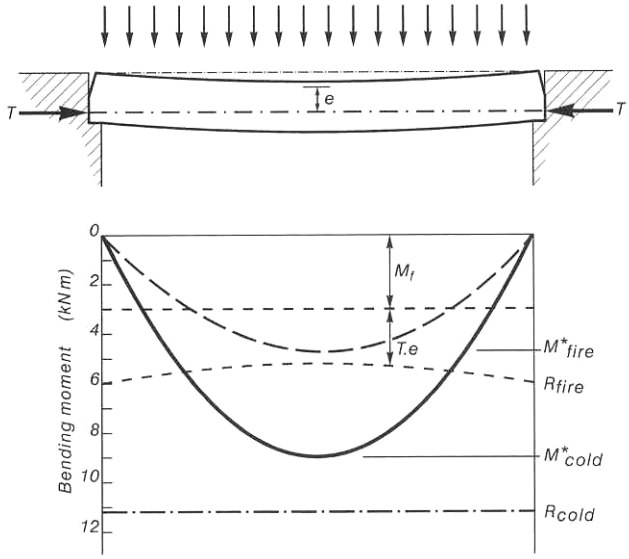

Figure 2.3: Effect of axial restraint force on bending moment diagram (Buc-01)

Figure 2.3 shows the effect of axial restraint on a simply supported concrete beam restrained by rigid supports as stated by Buchanan (Buc-01). Due to the heating of the beam an axial thrust *T* develops, which can be considered as external prestressing. It can be seen that the applied moment M^*_{fire} can be resisted, although the flexural moment capacity at elevated temperatures M_f may be smaller than M^*_{fire}. This is due to the additional bending moment *T*e* induced in the structure by the axial force, where *e* is the eccentricity between the line of action of the thermal thrust and the centroid of the compression block near the top of the beam, as shown in Figure 2.4.

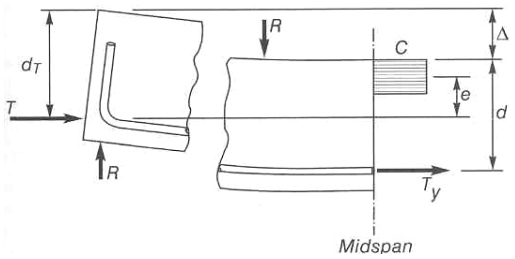

Figure 2.4: Free body diagram of beam with axial restraint force (Buc-01)

The total flexural resistance R_{fire} can thus be calculated as:

$$R_{fire} = M_f + T * e \tag{2.5}$$

It can be seen from equation (2.5) that the positive effect of the thermal thrust is strongly dependant on the position of the axial force. The additional moment may become negative if large deflections occur or the axial force acts at the top of the beam. Consequently, the resulting moment will tend to deflect the beam downwards. Unless *T* is large enough to induce sufficient compressive stress to counteract the tensile stresses caused by *T*e* and the applied moment, structural failure will occur earlier (Car-65).

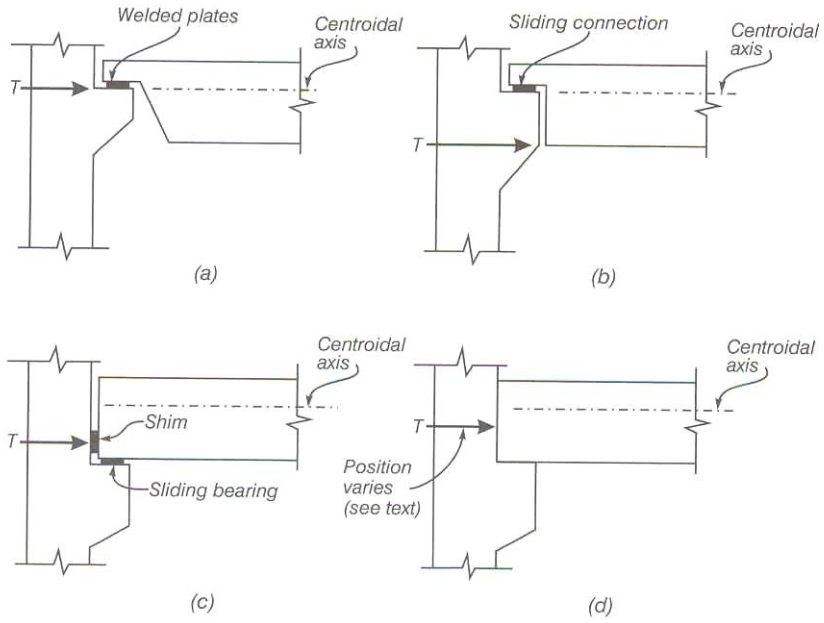

Figure 2.5: Location of axial thrust for several support conditions (PCI-77)

The position of the line of thrust can only be located accurately for specific support conditions where the line of thrust is well defined due to the method of construction. Figure 2.5 (a) to (c) show such determinate support conditions which mainly exist in precast concrete construction. Figure 2.5 (d) represents a situation, such as cast-in-place concrete, where the position of the thrust line is not clearly defined. Fire tests have shown, that when only minimal thrust occurs, the thrust line is near the bottom of the member throughout the fire exposure. For highly restrained members the thrust line will be at the bottom of the member at the start of the fire, with the position rising slowly during the fire (PCI-77).

In order to develop the beneficial effects of axial restraint, the surrounding structure has to provide sufficient strength and stiffness to restrain the thermal elongation. According to Gustaferro (Gus-86), the thrust forces that occur can be quite large but are always considerably less than that calculated by use of elastic properties of concrete and steel together with appropriate coefficients of expansion as at high temperatures, creep and stress relaxations play an important role.

Experimental investigations of the effects of axial restraint on fire exposed concrete members have first been executed by the Portland Cement Association (Sel-63). A series of double-tee shaped specimens were exposed to the American standard fire ASTME119. Each specimen was permitted to expand a given amount and then further expansion was prevented. Issen (Iss-70) reported that all tested beams supported their load longer than would have anticipated for simply supported beams. The tests have also shown that the maximum thrust for a given allowed expansion is proportional to the “heated perimeter” and the concrete’s modulus of elasticity, where the heated perimeter is defined as the perimeter of the cross-section of the specimen, perpendicular to the direction of the thrust, which is exposed to fire. Based on the test results, a step-by-step method incorporating several nomograms was developed to estimate the thrust requirements for a given fire endurance for simply supported beams (PCI-77).

The applicability of this approach to slabs and beams other than those tested has not been demonstrated. Besides, Anderberg and Forsén (And-82) have shown, using the non-linear finite element program CONFIRE, that the PCI method over-predicts the developing axial force. Wade (Wad-91) recommends that the positive effects of thermal restraint be disregarded where the location of the thrust is difficult to determine.

Numerical analyses on the effect of a moveable line of thrust on the behaviour of one-way concrete slabs have been carried out by Lim (Lim-03). Lim showed that the slab behaviour is very sensitive to the position of the line of thrust. If the position of the line of thrust is located much above the soffit of the slab, the slabs will rapidly undergo large deformations and sag into a catenary, imposing axial tensile forces at the supports. The analyses have also shown that even if the line of thrust is located close to the soffit, the slab can still deform into a catenary if there is insufficient horizontal axial restraint (Lim-03) (Lim-04).

2.7 Effect of continuity

Continuous flexural elements have a considerably greater fire resistance than simply supported elements. Their superior performance is due to beneficial changes in the moment distribution that take place in response to fire exposure, and their higher level of redundancy against failure (Har-93) (Buc-01) (Gut-80).

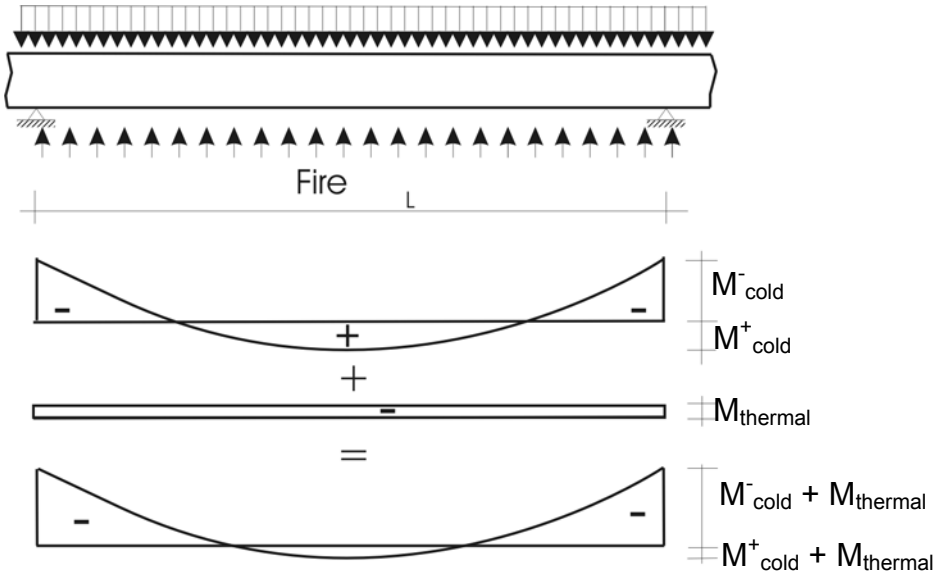

Figure 2.6: Components of moments in a continuous beam

Figure 2.6 shows the centre beam of a member that is continuous over several supports. When it is heated, the beam wants to deflect downwards due to the temperature gradient which produces different amounts of thermal elongation on the top and the bottom of the beam. This thermally induced curvature results in a uniform negative bending moment $M_{thermal}$ along the length of the beam. Consequently the support moments M^{-}_{cold} of the beam increase and the bending moment at the span M^{+}_{cold} decreases. This is beneficial to the beam's fire endurance, as the moment is reduced at the midspan where the beam's flexural capacity is reduced faster due to higher temperatures in the steel bars. The change in bending moment will always be limited to between the reduced positive and negative flexural capacity of the beam. Gustaferro and Martin (PCI-77) state that the amount of redistribution that occurs is sufficient to cause yielding of the negative reinforcement. By increasing the amount of negative moment reinforcement, a greater negative moment will be attracted. To avoid a compression failure in the negative moment region, the amount of negative moment reinforcement should be small enough so that

$\omega = A_s f_y / b d f_c$ is less than about 0.30 even after reductions due to temperature are taken into account. In contrast to simply supported members, a continuous beam will not fail until three plastic hinges form.

Experimental tests on the behaviour of continuous beams carried out by Ehm and v. Postel (Ehm-65) showed that the negative flexural capacity at the supports is reached quite early during the fire exposure. The reduction in flexural stiffness due to cracks forming at the support reduced the induced moment. As the temperatures increased and the flexural stiffness of the span dropped, the support moment increased again.
Tests carried out by the Portland Cement Association (Lin-81) (Lin-88) report beneficial effects of the continuity over the supports. The tests were also simulated with mathematical models, which showed sufficient accuracy (Ell-91).
However, Malhotra (Mal-69) reports as a result of tests that the continuity over supports without any horizontal restraint showed only marginal effects on the overall performance of beams compared to simply supported ones. The beams failed through the formation of three plastic hinges, but those formed more or less simultaneously.

2.8 Shear

Shear failure is not usually a problem in fire exposed concrete structures, with the exception of precast pre-tensioned slabs with narrow webs (Buc-01). Tests by Lin et al. (Lin-88) on highly loaded reinforced concrete beams showed that shear cracks developed during the fire exposure before flexural cracks occurred. But as the latter extended rapidly, all the beams tested failed in flexure rather than in shear.

Eurocode 2 (EC2-02) also states, that shear failure is very uncommon, and thus provides calculation methods that are stated as not having been fully verified. Normal temperature design methods are recommended, using the reduced cross sections and material properties obtained with the simplified calculation methods stated in section 2.3.1. If there is no shear reinforcement provided, or the shear capacity relies mainly on the reduced tensile strength of the concrete, the actual shear behaviour of the concrete at elevated temperatures must be considered.

Franssen and Brul (Fra-97) assumed that the shear resistance of concrete is less affected by the temperature than the compressive strength. Thus, they showed that the concrete contribution to the shear strength reduces more slowly than the contribution of steel stirrups or any prestressing forces.

Desai (Des-98) has proposed a similar design rule for estimating shear capacities of rectangular beams exposed to fire. The method takes the contribution of the concrete and the links into account. Additionally, the provision of a central reinforcing bar as a part of the web reinforcement is proposed. The contribution of this to the shear strength could be useful for beams with smaller dimensions. The method showed good agreement with test results, but is only applicable to rectangular beams.

2.9 Large-scale fire tests

In order to obtain information, on how a building in its entirety resists or accommodates the large thermal expansions from the heated parts of the structure and to identify beneficial and detrimental modes of whole-building behaviour which can not be shown from standard small-scale fire tests, large scale fire tests have been carried out at the Cardington Large Building Facility in recent years.

During 1995 and 1996 a series of fire tests were carried out on an eight-storey steel-framed building with composite deck flooring. During the compartmental fire tests, the steel beams and the soffit of the slabs were unprotected whereas all columns were protected up to the underside of the floorslabs. Temperatures of over 900°C were reached in the steel bars and large deflections in the beams and the slabs could be observed, but collapse did not occur (Bai-99). The good performance was assumed to be due to the composite slabs acting in tensile membrane action and the effect of restraint. The Cardington tests formed the basis of the approach of several researchers when modelling the response of the Cardington frame with finite element methods in order to improve the understanding of the observed behaviour and investigate the implications for the rational design of those kinds of buildings. Work related to the Cardington steel-composite building tests can be found among others by Sanad et al. (San-00), Elghazouli and Izzuddin (Elg-01), Gillie et al. (Gil-04), Huang et al. (Hua-01) and Moss and Clifton (Mos-04).

In 2001 a fire test on a seven-storey column-slab in-situ concrete structure was carried out in order to gain more insight into the behaviour of an entire concrete structure. During the test, a compartment of 225 m² including several columns was exposed to a parametric fire. Although there was a considerable amount of spalling, the building resisted the fire without showing signs of collapse during or after the fire. The thermal expansion of the slab resulted in large lateral residual movements of the outer columns, but did not lead to failure. The slabs carried their imposed loads with low residual vertical displacements.

Observations suggest that the slab carried the loads acting as a compressive membrane (Bai-02) (Cha-03). Bailey (Bai-02) states that analytical research is needed to understand the entire behaviour and to enable the creation of design guidance based on the observed behaviour in a similar way as this has already been realised for steel-framed structures with composite slabs.

3 MATERIAL PROPERTIES AT ELEVATED TEMPERATURES

3.1 General reactions of concrete at high temperatures

When concrete is subjected to heat, a number of transformations and reactions of many different kinds take place. Apart from the crystal transformations occurring mainly in the aggregates, these phenomena comprise the so-called degradation reactions. They are reactions which bring a progressive breakdown in the structure of the concrete. They arise predominantly from the hardened cement paste, but also in the aggregates.

The reactions initiated during the heating of concrete can be studied with the aid of differential thermal analysis. Figure 3.1 shows the differential thermal analysis of various normalweight concretes. At temperatures of about 100°C water expulsion occurs and at 180°C the first stage of dehydration in the form of the breakdown of gel can be observed. The decomposition of portlandite and the transformation of quartz take place at 500°C and 570°C respectively. The decomposition of the CSH phase starts from 700°C onwards. For limestone aggregate concretes the decarbonation of limestone commences from 800°C onwards. The concrete starts to melt at about 1150°C-1200°C (Schn-82).

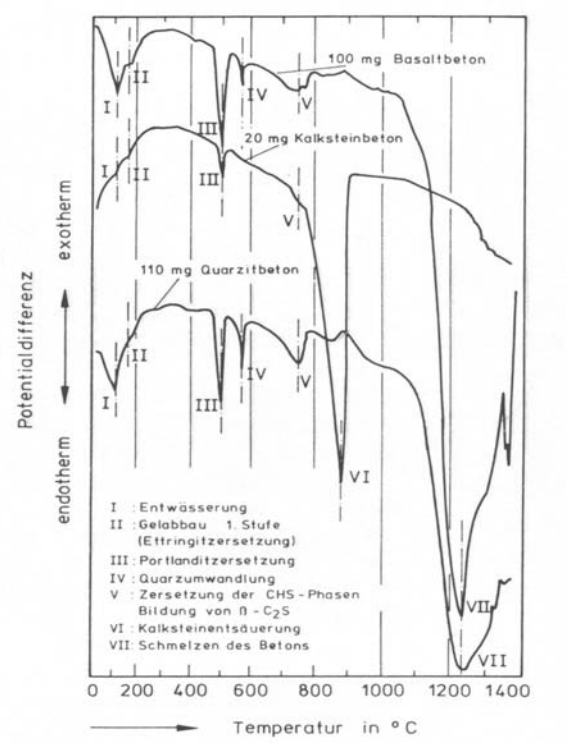

Figure 3.1: Differential thermal analysis of various normalweight concretes (Schn-82)

3.2 Thermal properties of concrete

3.2.1 Density

The density of concrete shows little dependence on temperature as can be seen in Figure 3.2. This change in density during heating is mostly influenced by water loss. The significant decrease of density for limestone concrete at about 800°C is due to the decomposition of the calcareous aggregate (Schn-88).

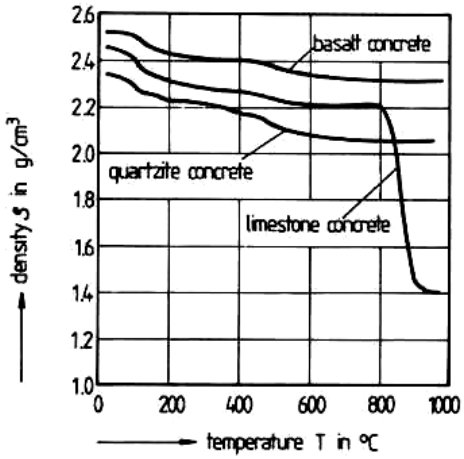

Figure 3.2: Density of structural concretes at high temperatures (Schn-88)

In Eurocode 2 (EC2-02) the variation of density with temperature is defined as follows and plotted in Figure 3.3:

$$\begin{aligned}
\rho(\theta) &= \rho(20°C) && \text{for } 20°C \le \theta \le 115°C \\
\rho(\theta) &= \rho(20°C) \cdot \{1 - 0.02 \cdot (\theta - 115)/85\} && \text{for } 115°C < \theta \le 200°C \\
\rho(\theta) &= \rho(20°C) \cdot \{0.98 - 0.03 \cdot (\theta - 200)/200\} && \text{for } 200°C < \theta \le 400°C \\
\rho(\theta) &= \rho(20°C) \cdot \{0.95 - 0.07 \cdot (\theta - 400)/800\} && \text{for } 400°C < \theta \le 1200°C
\end{aligned} \tag{3.6}$$

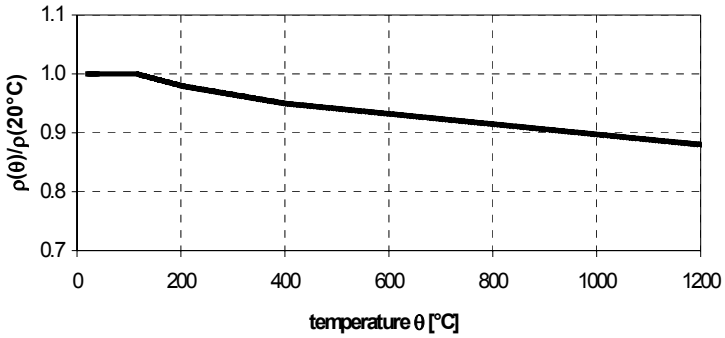

Figure 3.3: Variation of density according to EC2 (EC2-02)

3.2.2 Thermal conductivity

Thermal conductivity is the ability of a material to conduct heat. It is defined as the ratio of the heat flux to temperature gradient. It represents the uniform flow of heat through a material of a unit thickness over a unit area subjected to a unit temperature difference between two opposite faces and is measured in W/mK (Baz-96).

The thermal conductivity of concrete depends on the conductivity of its components. Thus, the major factors are the moisture content, the type of aggregate and the mix portions.

At ambient temperatures the conductivity of any given concrete varies approximately linearly with its moisture content. Thus, the loss in conductivity is greater for the concretes with a high initial thermal conductivity due to the loss of moisture during heating. The thermal conductivity also depends on the mix portions by the volume of free water, hydrated cement and aggregate. For normal concrete the conductivity of the aggregates is higher than that of the cement paste. Therefore lean mixes tend to have a higher conductivity. For lightweight concrete the opposite holds, as the aggregates, which influence the thermal conductivity directly, are less conductive (Schn-82). Figure 3.4 shows the thermal conductivity of different structural concretes.

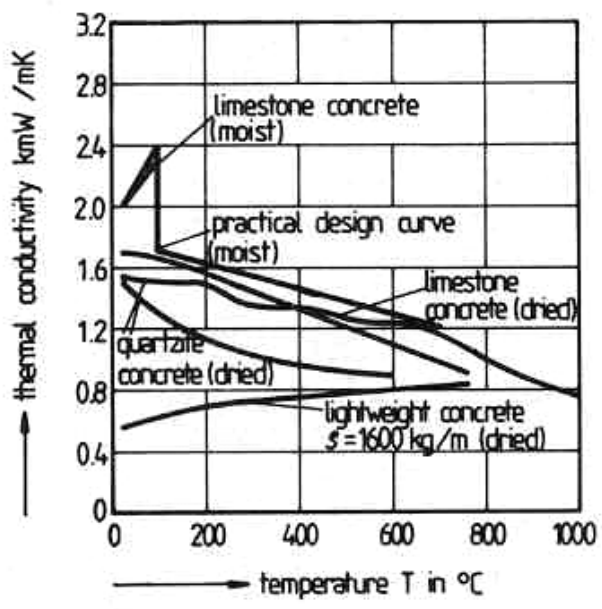

Figure 3.4: Thermal conductivity of different structural concretes (Schn-88)

The thermal conductivity of normal weight concrete as defined in Eurocode (EC2-02) may be determined between lower and upper limit values, with the upper limit given as

$$\lambda_c = 2 - 0.2451 \cdot (\theta_c / 100) + 0.0107 \cdot (\theta_c / 100)^2 \text{ W/mK} \quad (3.7)$$

and the lower limit given as

$$\lambda_c = 1.36 - 0.136 \cdot (\theta_c / 100) + 0.0057 \cdot (\theta / 100)^2 \text{ W/mK} \quad (3.8)$$

for 20°C ≤ θ_c≤ 1200°C.

The lower limit has been derived from comparisons with temperatures measured in fire tests of different types of concrete structures, whereas the upper limit has been derived from tests for steel/composite structures. Hence the lower limit gives more realistic values for concrete structures. Both limits are shown in Figure 3.5.

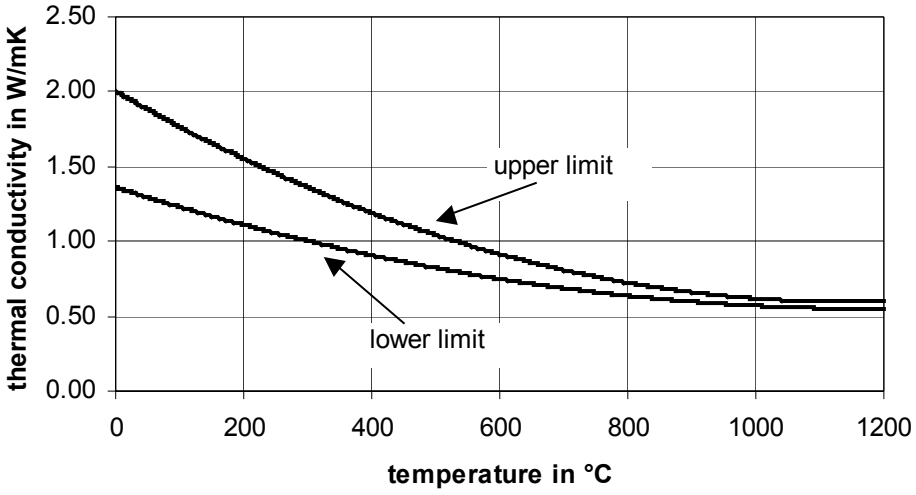

Figure 3.5: Thermal conductivity according to EC2 (EC2-02)

3.2.3 Specific heat

The specific heat, also called thermal or heat capacity, is the amount of heat per unit mass required to change the temperature of the material by one degree (Baz-96).

At constant pressure, the specific heat c_p is defined as

$$c_p = \left(\frac{\partial H}{\partial T} \right)_p \tag{3.9}$$

where H is enthalpy, T is temperature and p is pressure (Schn-82). If the heating of the material is accompanied by chemical reactions, the enthalpy is a function of both the degree of conversion from reactants into the products ξ and the temperature. Equation (3.9) can thus be rewritten as:

$$c_p = \left(\frac{\partial H}{\partial T} \right)_{p,\xi} + \left(\frac{\partial H}{\partial \xi} \right)_{p,T} \frac{d\xi}{dT} \tag{3.10}$$

In this case c_p is usually referred to as “apparent” heat. The first term on the right-hand side of equation (3.10) represents the sensible heat contribution to the specific heat at a given degree of conversion; the second term represents the latent heat contribution from the reactions that occur (Baz-96).

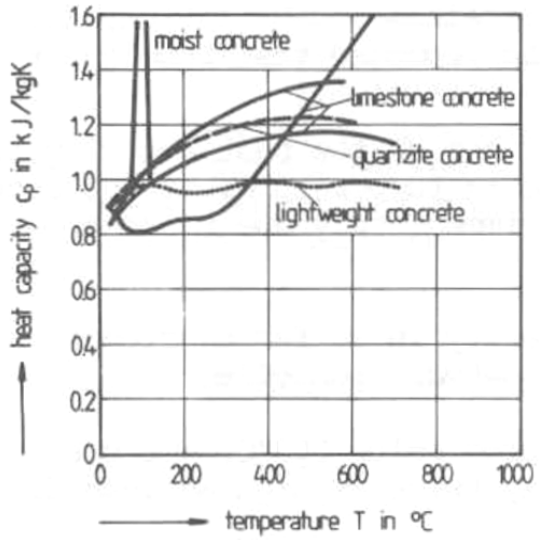

Figure 3.6: Heat capacity of different concretes (Schn-88)

Figure 3.6 shows the heat capacity of different concretes. The available data shows that the type of aggregate does not have a significant effect on the heat capacity, if temperatures below 800°C are considered. For calcareous concrete, the apparent specific heat rises immediately when reaching temperatures above 800°C due to decarbonisation. Richer concrete mixes show greater heat capacity as they are influenced by dehydration effects. The determining factor below temperatures of 200°C is the water content. Initially wet concretes around 100°C show an apparent specific heat nearly twice as high as oven-dried concretes (Schn-82). This is due to the relatively high specific heat of water (4.19 kJ/kgK) (Baz-96).

According to the Eurocode (EC2-02), the specific heat of dry siliceous and calcareous concrete may be determined from the following:

$$\begin{aligned} c_p(\theta) &= 900 \text{ (J/kgK)} && \text{for } 20°C \le \theta \le 100°C \\ c_p(\theta) &= 900 + (\theta - 100) \text{ (J/kgK)} && \text{for } 100°C \le \theta \le 200°C \\ c_p(\theta) &= 1000 + (\theta - 200)/2 \text{ (J/kgK)} && \text{for } 200°C \le \theta \le 400°C \\ c_p(\theta) &= 1100 \text{ (J/kgK)} && \text{for } 400°C \le \theta \le 1200°C \end{aligned} \qquad (3.11)$$

where θ is the concrete temperature (°C).

Where the moisture content is not considered explicitly in the calculation method, the function given above may be modelled including a constant peak value at 100°C depending on the moisture content.

Figure 3.7 shows the variation of the specific heat according to Eurocode.

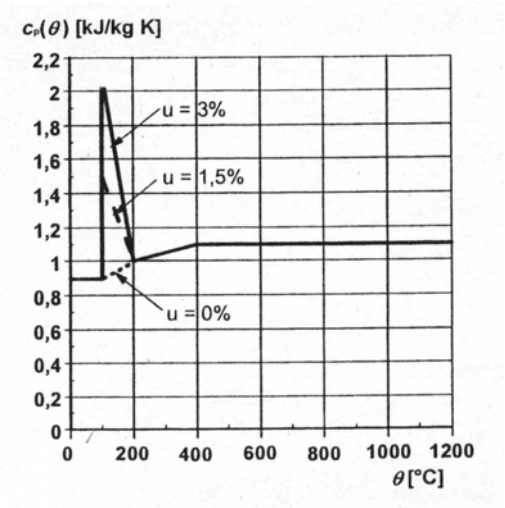

Figure 3.7: Specific heat according to Eurocode 2 (EC2-02)

3.2.4 Thermal diffusivity

Thermal diffusivity indicates the rate at which temperature changes can take place in a material. Diffusivity can be calculated from the equation,

$$D = k/c\rho \tag{3.12}$$

where *k* is thermal conductivity, *c* is specific heat and *ρ* is the density of the material. Thermal diffusivity can also be determined by direct measurement (Baz-96).

Schneider (Schn-82) states that the type of aggregate, mix portions and water content of the concrete have the same effect on thermal diffusivity as was noted previously for the thermal conductivity. Therefore the values of the thermal diffusivity display roughly the same trend as the values of the thermal conductivity. The variation in thermal diffusivity of siliceous concrete as determined by different researchers can be seen in Figure 3.8. Due to the considerable effect of moisture content upon thermal conductivity and density, the largest differences in the value of the diffusivity are to be observed in the temperature range below 200°C. At higher temperatures the measured values are relatively close to each other (Schn-82).

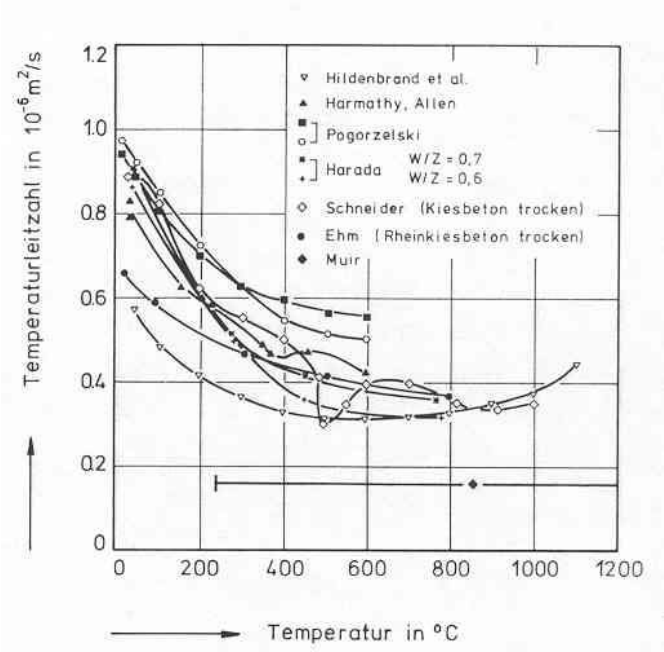

Figure 3.8: Thermal diffusivity of concrete adopted from Schneider (Schn-82)

3.2.5 Thermal expansion

The thermal expansion of concrete is mainly affected by the thermal strain of the type of aggregate, especially the coarse aggregate fraction. Figure 3.9 shows the influence of the type of aggregate on the thermal expansion. It can be seen that thermal strain is a non-linear function even at low temperatures (Schn-82). The expansion generally increases with temperature, notwithstanding the shrinkage that takes place in hardened cement paste at temperatures greater than about 150 to 300°C. The reason is that the expansion of the aggregates usually predominates over the contraction of the cement paste (Baz-96). At very high temperatures (600-800°C), most concretes show no further expansion. In some cases the concrete shrinks due to chemical or physical reaction in the aggregates.

The moisture content, water/cement ratio and the type of aggregate are in general only of relevance to the thermal expansion at comparatively low temperatures (< 200°C). Schneider (Schn-82) considers thermal expansion to be irreversible, while Anderberg (And-76) states that the main part of the thermal expansion is reversible.

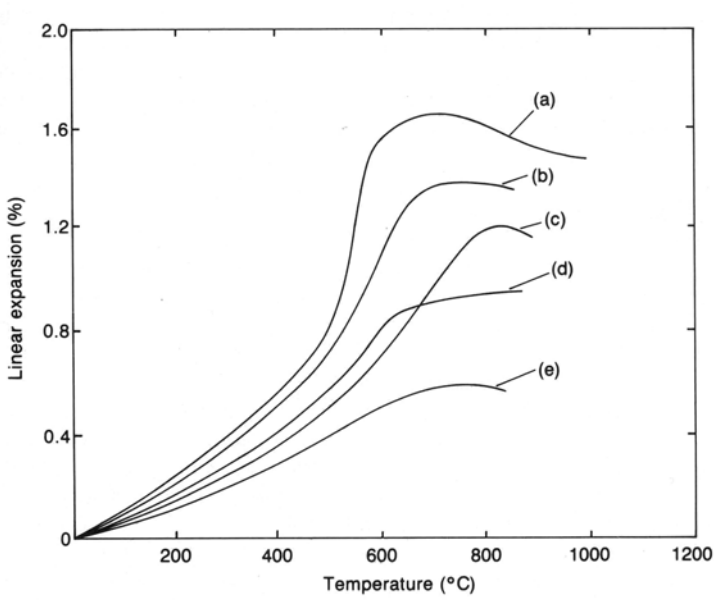

Figure 3.9: Thermal expansion of concrete with different aggregates
(a) quartzite; (b) sandstone; (c) limestone; (d) basalt; (e) expanded slag (Baz-96)

Eurocode 2 (EC2-02) states the following definitions to determine the thermal strain of concrete related to the length at 20°C.

For siliceous aggregates:

$$\begin{aligned} \varepsilon_c(\theta) &= -1.8 \cdot 10^{-4} + 9 \cdot 10^{-6} \cdot \theta + 2.3 \cdot 10^{-11} \cdot \theta^3 && \text{for } 20°C \le \theta \le 700°C \\ \varepsilon_c(\theta) &= 14 \cdot 10^{-3} && \text{for } 700°C < \theta \le 1200°C \end{aligned} \tag{3.13}$$

For calcareous aggregates:

$$\begin{aligned} \varepsilon_c(\theta) &= -1.2 \cdot 10^{-4} + 6 \cdot 10^{-6} \cdot \theta + 1.4 \cdot 10^{-11} \cdot \theta^3 && \text{for } 20°C \le \theta \le 805°C \\ \varepsilon_c(\theta) &= 12 \cdot 10^{-3} && \text{for } 805°C < \theta \le 1200°C \end{aligned} \tag{3.14}$$

where θ is the concrete temperature.

The variation of the thermal elongation with temperature is illustrated in Figure 3.10.

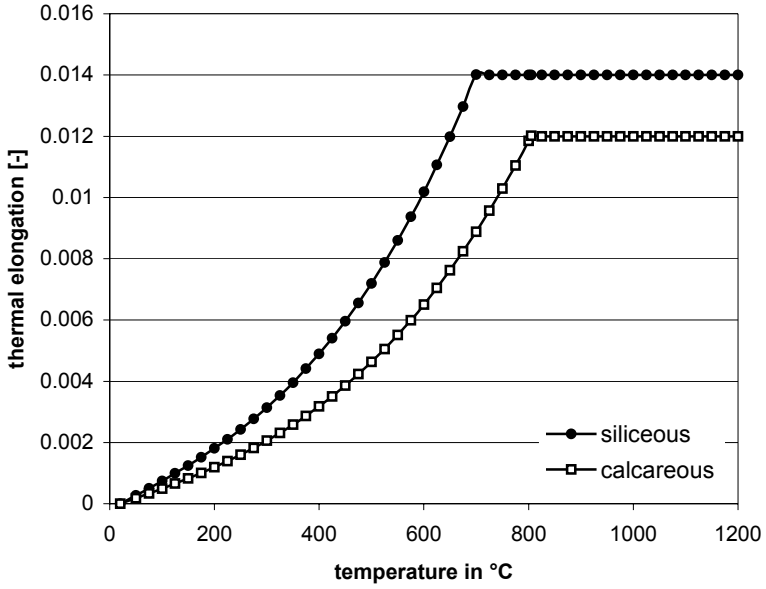

Figure 3.10: Thermal elongation for siliceous and calcareous concrete according to Eurocode 2 (EC2-02)

3.2.6 Spalling

Spalling is the breaking off of layers or pieces of concrete from the surface of a structural element, when exposed to high and rapidly rising temperatures, such as experienced in fire. This process may be insignificant in amount and consequence, but it also may seriously affect the stability of the structure. Spalling has been categorised into three different types on the basis of its extent, severity and the nature of occurrence.

1) Surface pitting

This occurs when small pieces, up to about 20mm in size, fly off the surface of a concrete element during early parts of its exposure to a fire. It is usually caused by splitting of pieces of aggregate close to the surface because of the physical or chemical changes which occur at high temperatures in siliceous aggregate.

2) Explosive spalling

This is the violent form of spalling which occurs at the early part of a fire test, usually within the first 30 minutes. It is characterized by the forcible separation of pieces of concrete, accompanied by a loud noise. The severity of explosive spalling can lead to the formation of holes through the sickness of the section (see Figure 3.11) (Mal-84).

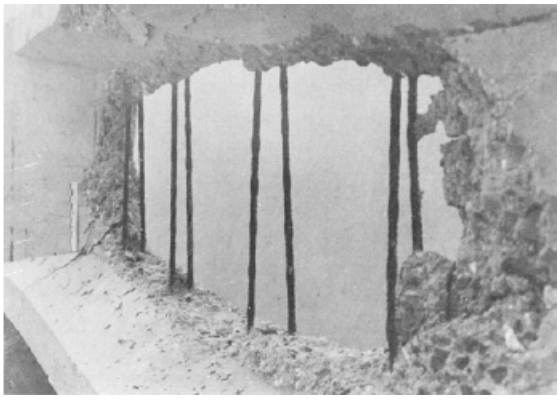

Figure 3.11: Severe spalling in the stem of a prestressed I-beam (Kor-65)

3) Corner break-off/ Sloughing off

This is a gradual progressive form of breakdown, involving partial separation of layers of surface material from the member. It occurs during the later stages of fire exposure when the concrete has become weak and cracks develop along edges and corners. Supplementary reinforcement can keep the damaged layer in place so that it can act as

an insulation layer. Even though it cannot contribute to the members' strength anymore (Bob-75) (Mal-84).

Explosive spalling is most harmful to structures. According to Hertz (Her-03), there are several different reasons which affect this form of spalling:

- Low tensile strength in the concrete increases the risk of spalling because it decreases the energy and the pressure required to explode the material.
- Dense reinforcement and large aggregates can increase the tensile stresses in the cement matrix because of their thermal expansion, and thereby contribute to spalling, but are not a cause in themselves.
- The heating conditions influence the appearance of spalling. Rapid heating produces large temperature and moisture gradients which again result in thermal stresses. Asymmetric heating or longitudinal restraint influence the thermal stresses induced in the member.
- Thin cross-sections are more susceptible to spalling due to rapid heating.
- Prestress and compression stresses seem to increase the risk of spalling.
- Free water and moisture gradients in the concrete must be considered to be the main reason for explosive spalling. Normal dense concrete will not spall if it is dry, even under the presence of all the other reasons mentioned above.

Eurocode (EC2-02) allows the assumption that the explosive spalling is unlikely to occur when the moisture content of the concrete is less than 3% by weight. This is consistent with the statement given by Hertz (Her-03), that traditional concrete in the moisture range of 3-4% by weight has limited risk of spalling, and concrete with less than 3% moisture content by weight does not give rise to spalling.

3.3 Mechanical properties of concrete

The properties of concrete at elevated temperatures can be defined by starting from a number of different viewpoints. Under fire conditions, materials are subjected to transient processes. Therefore, the material properties measured under such conditions have to be distinguished from those which can be derived from steady-state analysis.

In high temperature tests the three main test parameters are heating, the application of load and the control of strain. These parameters can have constant values or may be varied during testing sometimes leading to difficulties in comparing the results of different tests. Figure 3.12 shows the combination of different parameters and the mechanical properties which can be determined in each case.

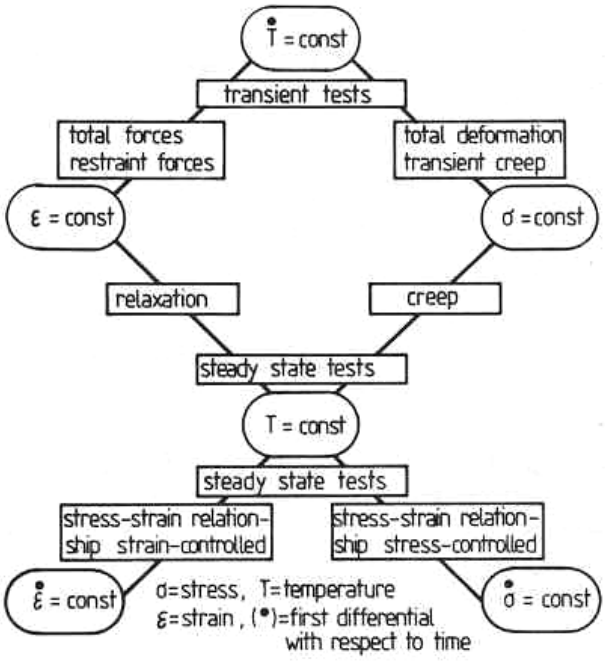

Figure 3.12: Different testing regimes to determine mechanical properties of concrete at high temperatures (Schn-88)

As indicated in Figure 3.12, the stress-strain relationships can be determined by steady state methods. Here, the specimen is heated to a specified temperature without applying any load. After the temperature is stabilized, either a load is applied as a controlled rate of stress increase while strain is measured, or the strain is increased at a constant rate while the corresponding stress is measured, depending if the stress or the strain rate controlled method respectively is used. Both tests allow the determination of compressive or tensile

stress, modulus of elasticity and ultimate strain at collapse. The strain rate controlled test can also be used to establish the mechanical dissipation energy.

Steady-state tests also allow the testing of long-term creep and relaxation.

Transient tests are used to establish critical temperature values for different stress levels. Therefore, the specimens are heated at a constant rate after a specified load is applied and the strain is measured until the strain rate is approaching infinity.

Restraint forces can also be measured under transient conditions, by applying an initial strain, which is maintained during the test, and the stress is measured during the heating process (Schn-88) (Schn-82).

3.3.1 Components of strain

Generally, the constitutive law for concrete under high temperatures may be expressed as the sum of four different strain components as follows (And-76):

$$\varepsilon = \varepsilon_{th}(T) + \varepsilon_{\sigma}(\tilde{\sigma}, \sigma, T) + \varepsilon_{cr}(\sigma, T, t) + \varepsilon_{tr}(\sigma, T) \tag{3.15}$$

where

ε = total strain
ε_{th} = thermal strain
ε_{σ} = stress – related strain
ε_{cr} = creep strain
ε_{tr} = transient strain
T = temperature
σ = stress
$\tilde{\sigma}$ = stress history

TOTAL STRAIN

The total deformation of loaded concrete specimens during heating is illustrated in Figure 3.13. The expansion that occurs during heating of unloaded specimens is significantly reduced when loads are imposed on the specimens. For loads exceeding about 40% of the strength at ambient temperatures, the specimens do not expand but shorten instead.

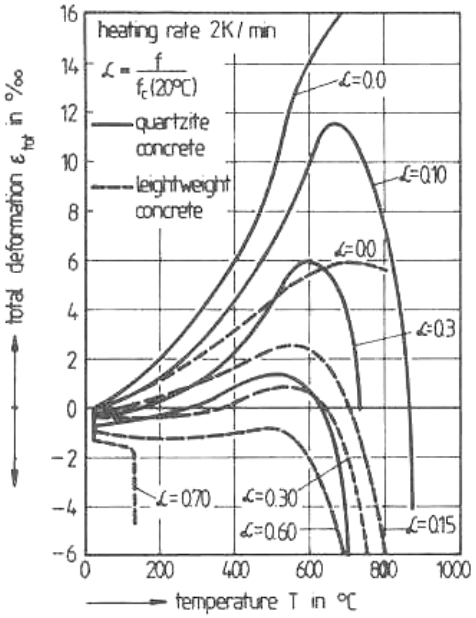

Figure 3.13: Total deformation of different concretes being loaded during heating (Schn-88)

THERMAL STRAIN

Thermal strain of unstressed specimens is caused by the elongation of concrete. This is shown in section 3.2.5.

INSTANTANEOUS STRESS-RELATED STRAIN

The stress-related strain includes the elastic and plastic components of strain induced from applied stresses (Buc-01). Figure 3.14 and Figure 3.15 show the relationship between stress and strain at elevated temperatures derived from stress controlled and strain controlled tests respectively.

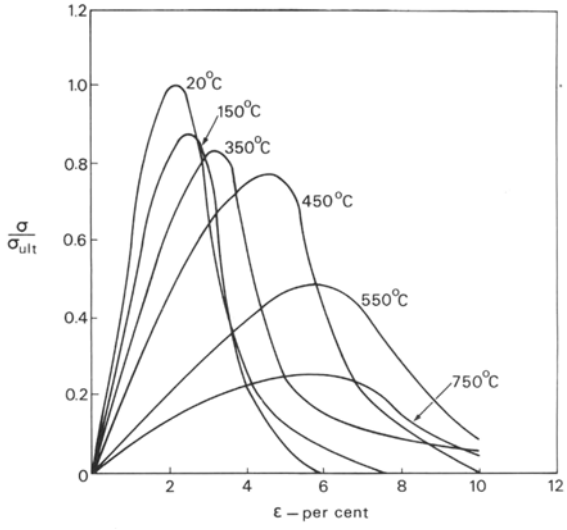

Figure 3.14: Stress-strain relationship derived from stress controlled tests (Mal-82)

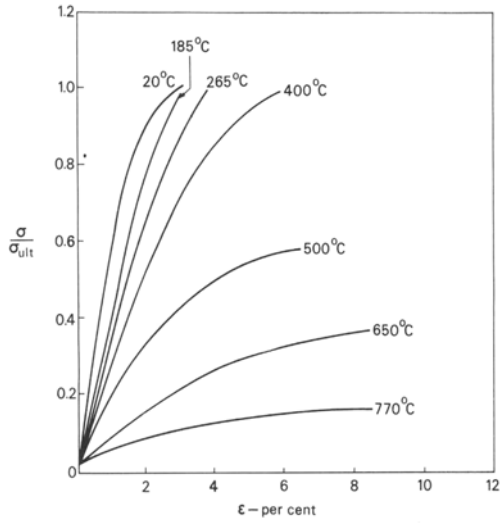

Figure 3.15: Stress-strain relationship derived from strain controlled test (Mal-82)

The ultimate strains increase with increasing temperatures, whereas the ultimate stress limits decrease. It can be seen that if the rate of increase in strain is controlled during the tests, higher stresses in conjunction with lower strains can be observed.

Schneider (Schn-82) states that induced stresses influence the stress-strain relationship considerably. Specimens under a sustained load during the heating period demonstrate a significant increase of compressive strength. On the other hand the ultimate strain is reduced (see Figure 3.16).

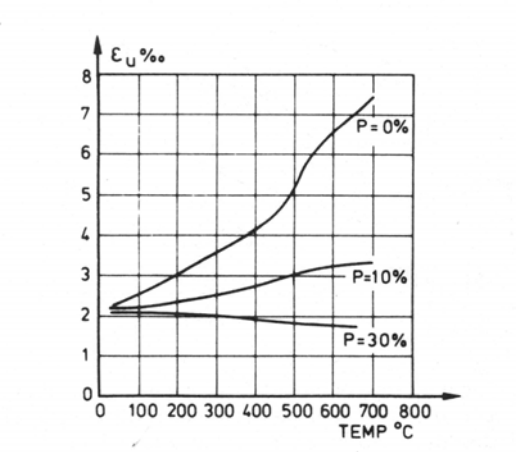

Figure 3.16: Ultimate strain as a function of temperature for concrete specimens, exposed to different stress levels (FIP-78)

The Eurocode (EC2-02) stipulates the strength and deformation properties of uniaxially stressed concrete at elevated temperatures as seen in Figure 3.17.

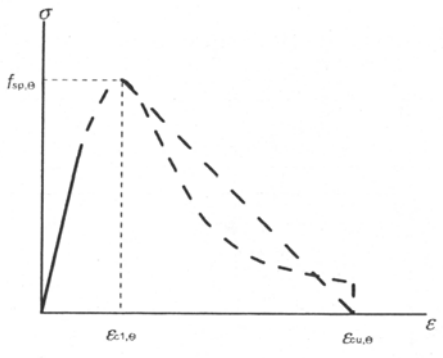

Figure 3.17: Stress-strain relationship according to EC2 (EC2-02)

with

$$\sigma(\theta) = \frac{3 \cdot \varepsilon \cdot f_{c,\theta}}{\varepsilon_{c1,\theta} \cdot \left(2 + \left(\frac{\varepsilon}{\varepsilon_{c1,\theta}}\right)^3\right)} \qquad \text{for } \varepsilon \le \varepsilon_{c1,\theta} \tag{3.16}$$

and $f_{c,\theta}$ and $\varepsilon_{c1,\theta}$ to be chosen according to Table A 2 in appendix A.2.

In the range of $\varepsilon_{c1,\theta} < \varepsilon \le \varepsilon_{cu,\theta}$ the adoption of linear and non-linear models for numerical purposes are permitted.

CREEP STRAIN

For any given combination of constant temperature and constant compressive strength, the basic creep ε_{cr} can be expressed by the formula (And-76).

$$\varepsilon_{cr} = \beta \frac{\sigma}{\sigma_u(T)} \left(\frac{t}{t_r} \right)^p e^{k_1 (T-20)} \tag{3.17}$$

where

$\beta_0 = -0.53 * 10^{-3}$
$\sigma_u(T) = ultimate\ stress\ at\ current\ temperatures\ T$
$t = time$
$t_r = 3h$
$p = 0.5$
$k_1 = 3.04 * 10^{-3} C^{-1}$

Typical curves of creep strain are shown in Figure 3.18. When the temperature and the stress vary with time, the basic creep can be evaluated on the strain hardening principle (And-76).

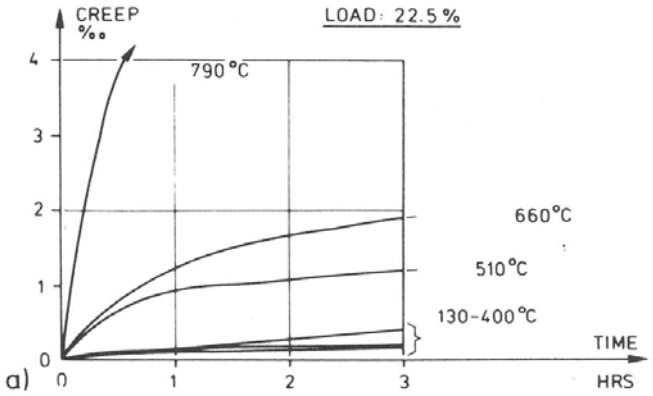

Figure 3.18: Basic creep at different stabilized temperatures (FIP-78)

TRANSIENT STRAIN/CREEP

Transient strain develops under stress when the temperature increases. It accounts for the effect of temperature change, which will produce instability of the material and activate the reactions responsible for the decomposition (And-76). Transient creep accommodates the thermal strain incompatibilities between aggregates and cement paste. Thus, it helps

to avoid excessive concrete damage due to relaxation processes and the redistribution of thermal stresses. Transient creep is seated in the cement paste and restrained by the aggregates. Transient creep only occurs during first heating and is irrecoverable (Kho-85b).

Transient creep cannot be evaluated from tests and therefore has to be calculated according to equation (3.18).

$$\varepsilon_{tr} = \varepsilon_{tot} - \varepsilon_{th} - \varepsilon_{\sigma} - \varepsilon_{cr} \tag{3.18}$$

Figure 3.19 shows the total strain and the different strain components for a specimen tested with a load of 35% of its ultimate strength at cold conditions. The considerable effect of the transient creep is noticeable.

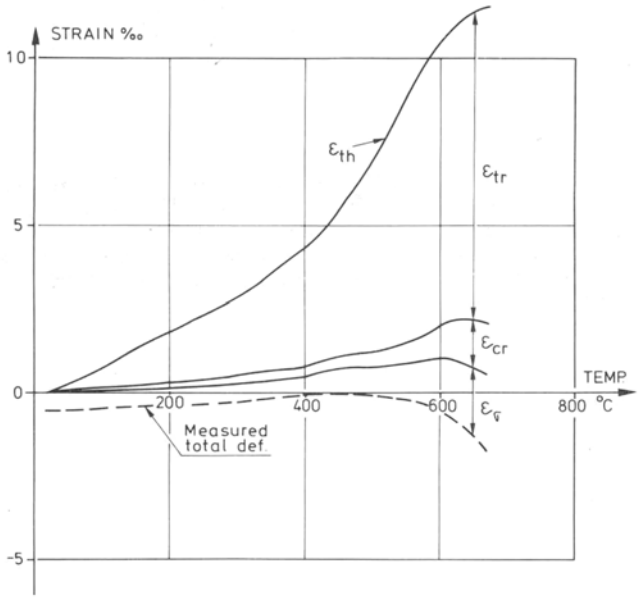

Figure 3.19: Relation between different strain components (And-76)

3.3.2 Modulus of elasticity

During heating the modulus of elasticity decreases. This is due to the breakage of bonds in the microstructure of cement paste as well as to the increase of short-time creep at increasing temperature (Baz-96).

Figure 3.20 and Figure 3.21 show the strong influence of the aggregates on the modulus of elasticity at elevated temperatures. The values derived by Schneider (Schn-88) and Cruz (Cru-66) differ significantly. As stated by Kaplan (Baz-96) this might be due to different definitions of the elastic modulus or the effect of simultaneous loss of moisture.

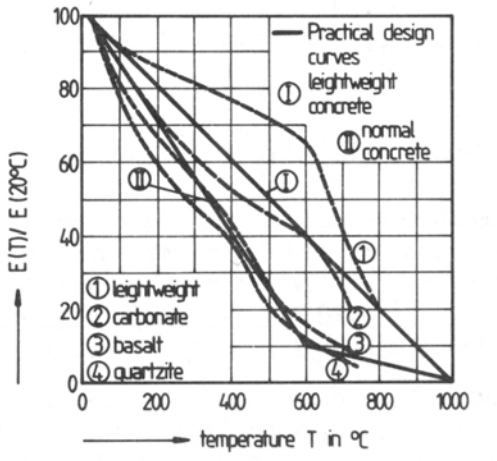

Figure 3.20: E-modulus according to Schneider (Schn-88)

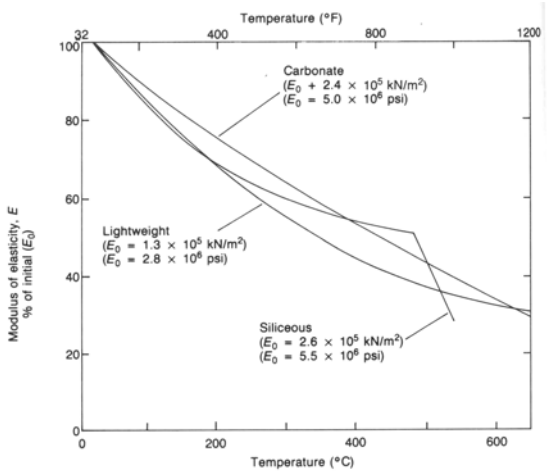

Figure 3.21: E-modulus according to Cruz (Cru-66)

The original strength, the water/cement ratio and the type of aggregate seem to have little influence on the E-modulus, whereas applied loads during heating can slow down the decrease of the modulus of elasticity. Tests with dynamic loads show higher temperature reductions in the modulus of elasticity than in static tests (Schn-82).

Kaplan (Baz-96) states further that during the drying process, which occurs simultaneously with temperature increase, the apparent value of elasticity is reduced. This occurs because any movement of moisture results in some bond rupture and consequently in the decrease of the stiffness.

3.3.3 Compressive strength

The compressive strength of concrete drops with increasing temperature.

Figure 3.22 shows the effect of aggregate on the compressive strength of unsealed specimens. It can be seen that concrete with siliceous aggregates undergoes a rapid loss in strength at a temperature around 450°C, whereas for calcareous and lightweight concretes the strength reduction does not occurs until a temperature around 700°C.

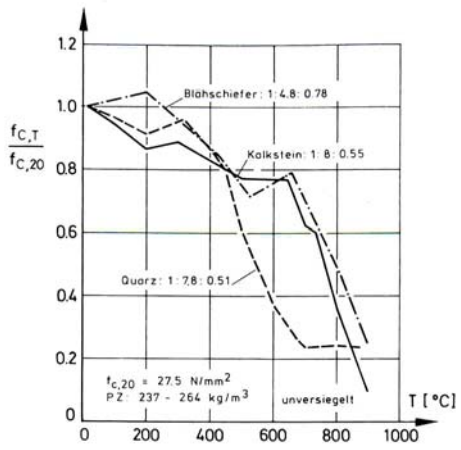

Figure 3.22: Compressive strength of concrete with different aggregates (Schn-82)

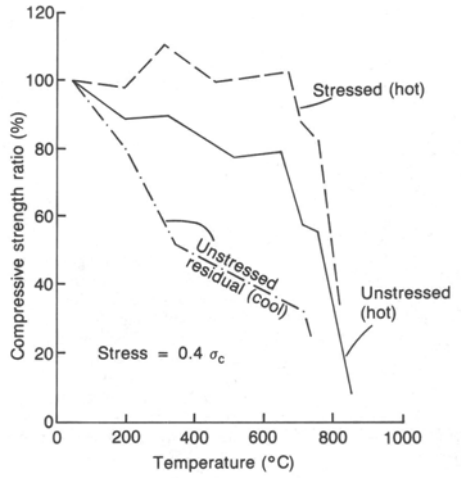

Figure 3.23: Strength ratio of calcareous aggregate concrete under various conditions (Baz-96)

Sustained stresses during the heating period influence the shape of the strength-temperature relationship significantly (see Figure 3.23). Specimens that were loaded between 0.25-0.55 σ_c could sustain higher stresses compared to unstressed specimens and specimens tested after cooling at equal temperatures. The stressed specimens even

showed an increase in strength of 10% at 300°C. Kaplan (Baz-96) states that the better performance of stressed specimens might be due to the retardation of crack formation owing to the imposed stress.

Figure 3.24 shows that the ratio of aggregate and cement also influences the strength of concrete exposed to high temperatures. The strength reduction is proportionally smaller for lean mixes than for rich mixes.

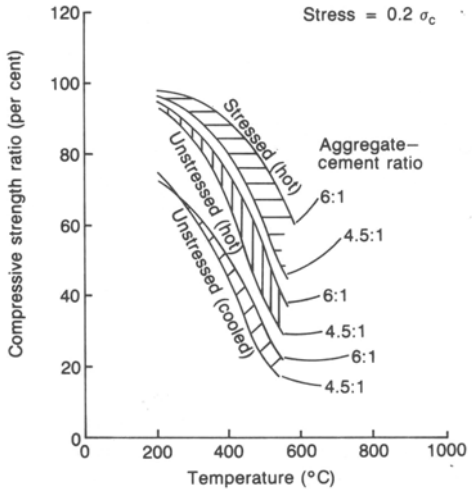

Figure 3.24: Dependence of compressive strength on aggregate-cement ratio (Baz-96)

The strength-temperature relationship defined in Eurocode (EC2-02) for concretes with siliceous and calcareous aggregates is plotted in Figure 3.25.

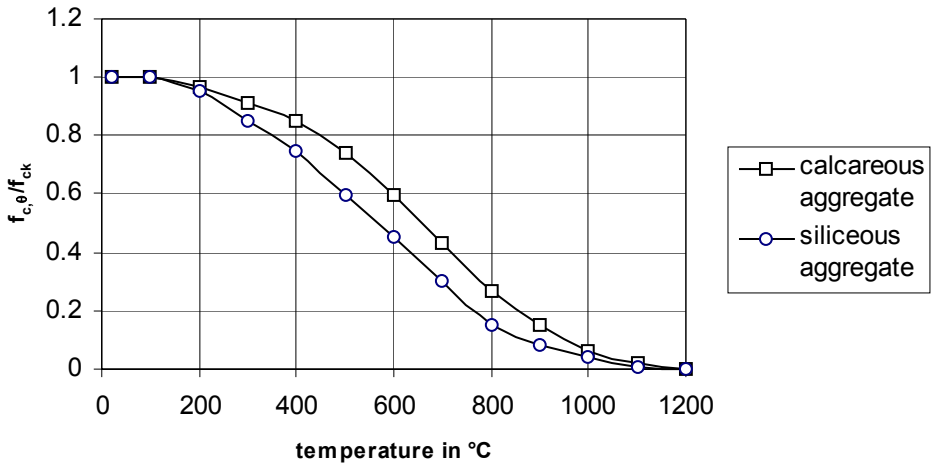

Figure 3.25: Ratio of compressive strength according to EC2 (EC2-02)

3.3.4 Tensile strength

The tensile strength of concrete also decreases with increasing temperatures. Figure 3.26 shows the tensile strength of concrete tested under high temperatures and after cooling. Compared to the compressive strength, the tensile strength shows a greater relative decrease and thus, is more responsive to the effects of temperature. The tensile strength is affected by the mix portions and significantly by the type of aggregate. The decrease in tensile strength of calcareous aggregate concrete is twice as high as for siliceous aggregate concrete at 500°C (Schn-82).

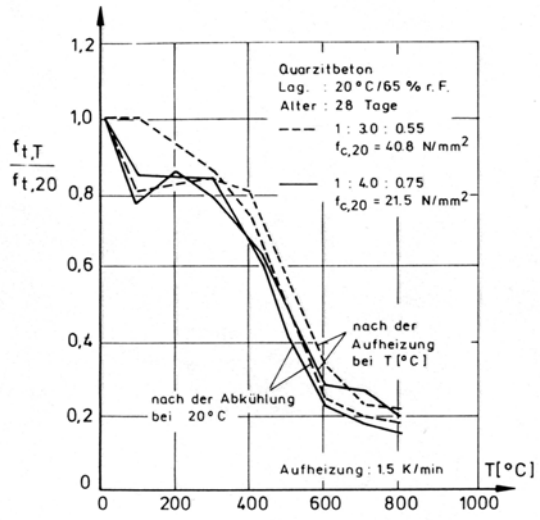

Figure 3.26: Split cylinder tensile strength of normal concrete (Schn-82)

Eurocode (EC2-02) recommends taking the tensile strength as zero as a conservative assumption. If it is necessary to take account of the tensile strength, the following equation for strength reduction may be used

$$f_{ck,t}(\theta) = k_{ck,t}(\theta) * f_{ck,t} \tag{3.19}$$

where $k_{ck,t}$ is defined as

$$\begin{aligned} k_{ck,t}(\theta) &= 1.0 && \text{for } 20°C \le \theta \le 100°C \\ k_{ck,t}(\theta) &= 1.0 - 1.0 \cdot (\theta - 100)/500 && \text{for } 100°C < \theta \le 600°C \end{aligned} \tag{3.20}$$

Figure 3.27 shows the values recommended by Eurocode.

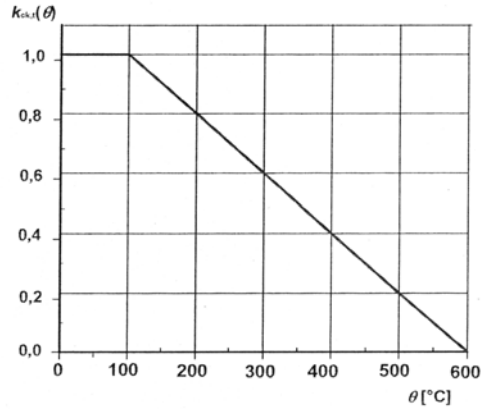

Figure 3.27: Reduction in tensile strength according to EC2 (EC2-02)

3.3.5 Poisson's ratio

The relation of the Poisson's ratio μ to the stress ratio at different temperatures is shown in Figure 3.28. The Poisson ratio at 20°C is constant until the load level exceeds 70% of the ultimate load. With increasing temperatures, a significant deviation of μ from its original value occurs. In some cases $\mu > 0.5$ was observed. These values indicate material effects far beyond the elastic range (Schn-88).

Tests performed by Maréchal are stated by Kaplan (Baz-96) and show inverse effects. There, the Poisson's' ratio decreases with increasing temperature.

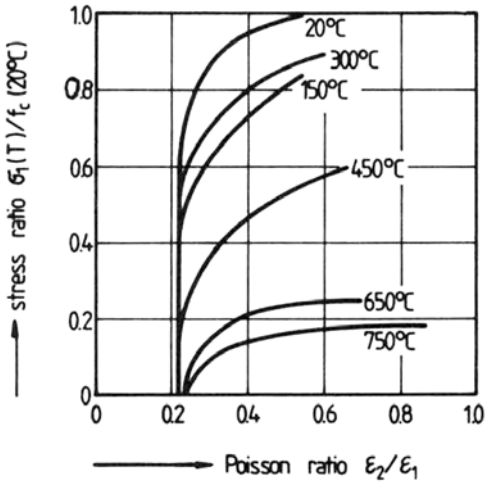

Figure 3.28: Poisson ratio plotted against stress ratio (Schn-88)

3.4 Thermal properties of steel

3.4.1 Density

The density of steel is remaining essentially constant with temperature (Buc-01) and therefore is assumed to be 7850 kg/m³.

3.4.2 Thermal conductivity

The thermal conductivity of steel depends mainly on the composition of the material and decreases with increasing temperature. The thermal conductivity of steel is assumed to be high enough to allow the assumption that normal size sections have a uniform temperature throughout (Mal-82).

The thermal conductivity according to Eurocode 3 (EC3-02) is determined from the following equations:

$$\begin{aligned} \lambda_a &= 54 - 3.33 \cdot 10^{-2} T \ \text{(W/mK)} && \text{for } 20°\text{C} \le \text{T} \le 800°\text{C} \\ \lambda_a &= 27.3 \ \text{(W/mK)} && \text{for } 800°\text{C} \le \text{T} \le 1200°\text{C} \end{aligned} \tag{3.21}$$

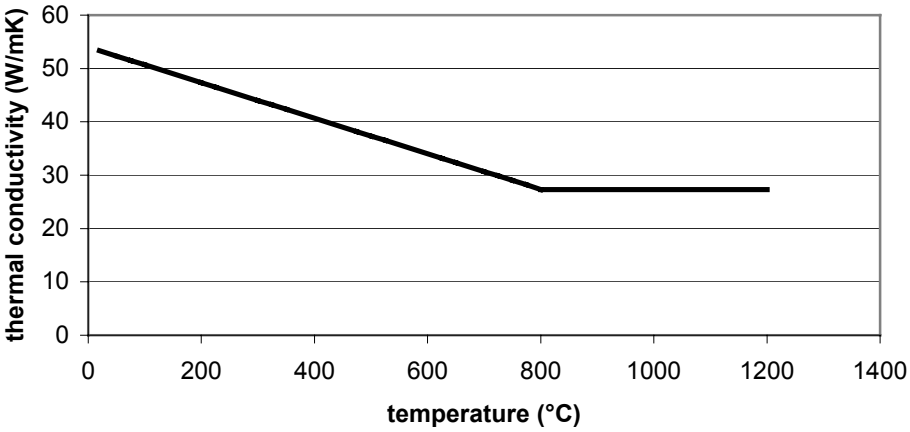

Figure 3.29: Thermal conductivity of steel according to EC3 (EC3-02)

3.4.3 Specific heat

The specific heat is independent of the composition of steel. Its variation with temperature is shown in Figure 3.30. The peak in specific heat at about 730°C results from a metallurgical change.

EC3 (EC3-02) stipulates equation (3.22) for the determination of the specific heat (J/kgK).

$$\begin{aligned} c_p &= 425 + 0.773 \cdot T - 1.69 \cdot 10^{-3} \cdot T^2 + 2.22 \cdot 10^{-6} \cdot T^3 && 20°C \le T \le 600°C \\ &= 666 + 13002/(738 - T) && 600°C \le T < 735°C \\ &= 545 + 17820/(T - 731) && 735°C \le T < 900°C \\ &= 650 && 900°C \le T \le 1200°C \end{aligned} \qquad (3.22)$$

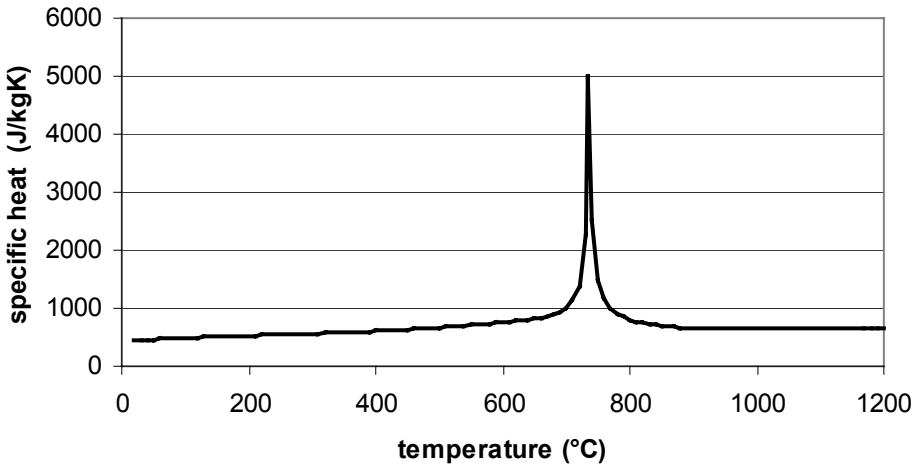

Figure 3.30: Specific heat of steel as a function of temperature according to EC3 (EC3-02)

3.4.4 Thermal expansion

Thermal expansion during heating is a simple function of the temperature and can be obtained directly from a conventional thermal expansion test. Figure 3.31 shows the relationship between the thermal expansion and the temperature for different reinforcing steels (FIP-78). The coefficient of thermal expansion is not constant with the temperature but increases slightly with increasing temperatures. Figure 3.32 shows the thermal elongation of steel according to EC3 (EC3-02) derived from the following formula:

$$\begin{aligned} \Delta L / L_s &= (-2.416 \cdot 10^{-4}) + (1.2 \cdot 10^{-5} \cdot T) + (0.4 \cdot 10^{-8} \cdot T^2) && \text{for } 20°C < T \le 750°C \\ \Delta L / L_s &= 11 \cdot 10^{-3} && \text{for } 750°C < T \le 860°C \\ \Delta L / L_s &= (-6.2 \cdot 10^{-3}) + (2 \cdot 10^{-5} \cdot T) && \text{for } T > 860°C \end{aligned} \quad (3.23)$$

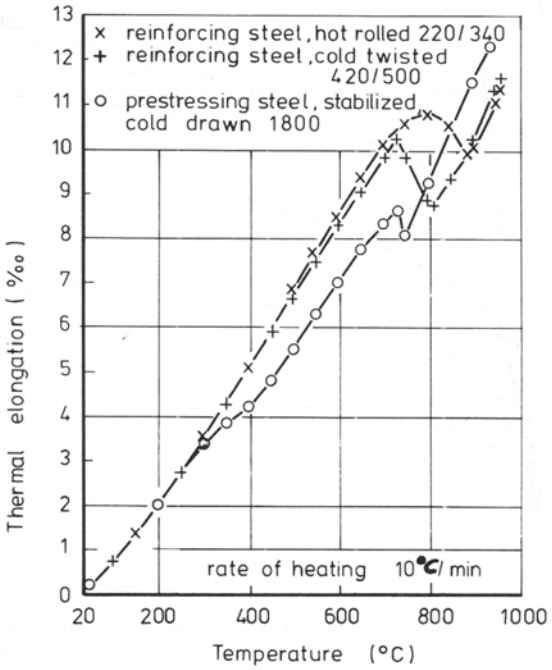

Figure 3.31: Thermal elongation of different steels (FIP-78)

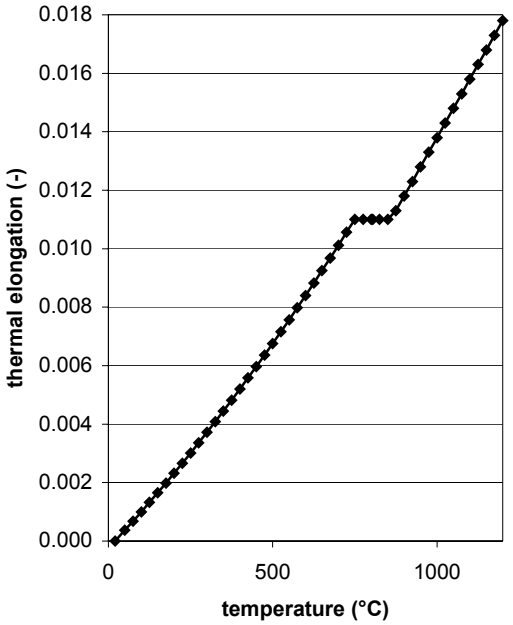

Figure 3.32: Thermal elongation according to EC3 (EC3-02)

3.5 Mechanical properties of steel

3.5.1 Strain

The total strain of steel can be calculated as the sum of three strain components similar to the total strain of concrete according the following formula (Buc-01):

$$\varepsilon = \varepsilon_{th}(T) + \varepsilon_{\sigma}(\sigma, T) + \varepsilon_{cr}(\sigma, T, t) \tag{3.24}$$

where

ε = total strain
ε_{th} = thermal strain
ε_{σ} = stress – related strain
ε_{cr} = creep strain
T = temperature
σ = stress

STRESS-RELATED STRAIN

Figure 3.33 shows typical stress-strain curves for structural steel elements at elevated temperatures.

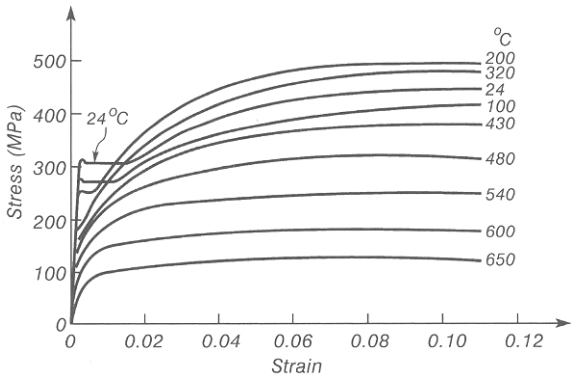

Figure 3.33: Stress-strain curves for hot-rolled steel at elevated temperatures (Buc-01)

It can be seen that the yield plateau becomes less noticeable with temperature rise and disappears at about 300°C. The ultimate strength increases slightly at moderate temperatures before decreasing at higher temperatures (Buc-01).

The stress-strain relationship according to Eurocode 2 (EC2-02) is defined by three parameters; the slope of the linear elastic range $E_{s,\theta}$, the proportional limit $f_{sp,\theta}$ and the maximum stress level $f_{sy,\theta}$. The entire mathematical model is plotted in appendix A.3. Stress-strain curves derived from that model are shown in Figure 3.34.

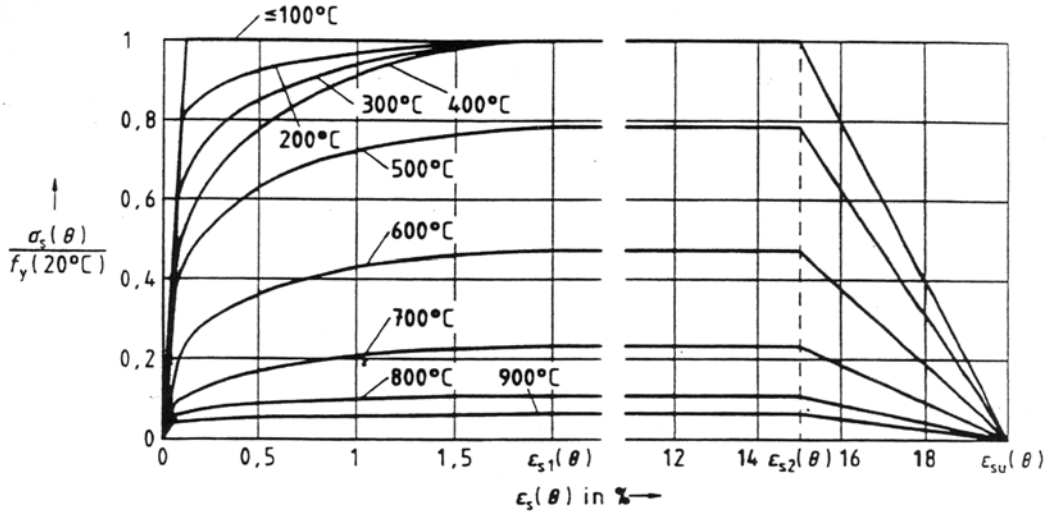

Figure 3.34: Stress-strain relationships of hot rolled reinforcing bars at elevated temperatures (EC2-95)

CREEP STRAIN

Creep strain is relatively insignificant in steel at normal temperatures but it has strong influence at temperatures above about 400°C. Figure 3.35 shows curves derived by Kirby and Preston (Kir-88) in transient tests.

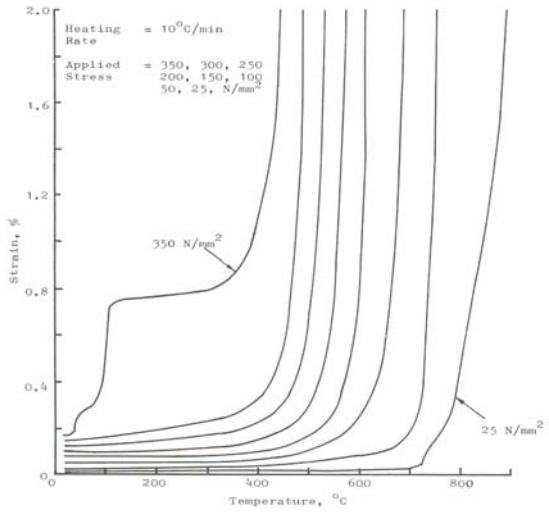

Figure 3.35: Creep of steel tested in tension (Kir-88)

It can be seen that the creep strain is highly dependant on temperature and the applied stress level. After a slight increase up to the critical temperature, the creep strain increases at a very rapid rate when this temperature is exceeded.

THERMAL STRAIN

The thermal strain of steel is equivalent to the thermal expansion coefficient described in section 3.4.4.

3.5.2 Modulus of elasticity

The modulus of elasticity decreases with increasing temperatures. It shows the same trend in reduction as the yield strength. Values recommended by Eurocode 2 (EC2-02) for the reduction of Young's Modulus of hot rolled and cold worked steel with increasing temperatures are shown in Figure 3.36.

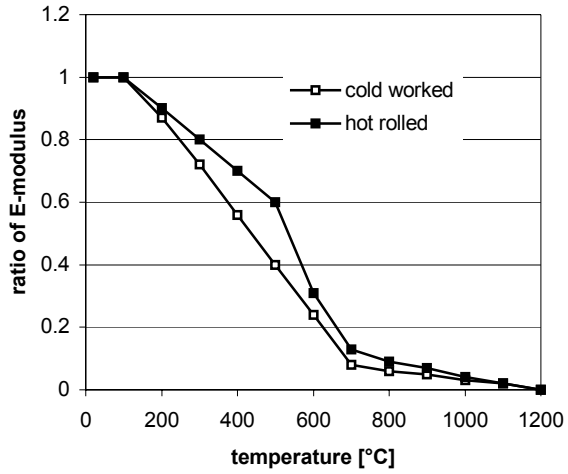

Figure 3.36: Variation of E-modulus with temperature
for cold worked and hot rolled steel according to EC 2 (EC2-02)

3.5.3 Ultimate and yield strength

Most normal steels have a very well defined yield strength at normal temperatures. However, this yield point disappears at elevated temperatures. The reduction of the ultimate and yield strength of cold-worked steel is shown in Figure 3.37. There is a

significant scatter in the results derived by various researchers which might be due to the lack of a clear definition of yield strength at elevated temperatures. The dashed straight line shows suggested values for design (Buc-01).

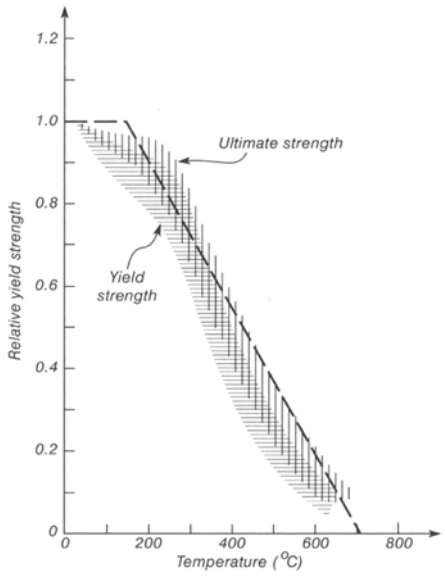

Figure 3.37: Ultimate and yield strength derived by various researchers (Buc-01)

The values for cold-worked steel recommended by Eurocode 2 (EC2-02) for the proportional limit and yield strength are plotted in Figure 3.38.

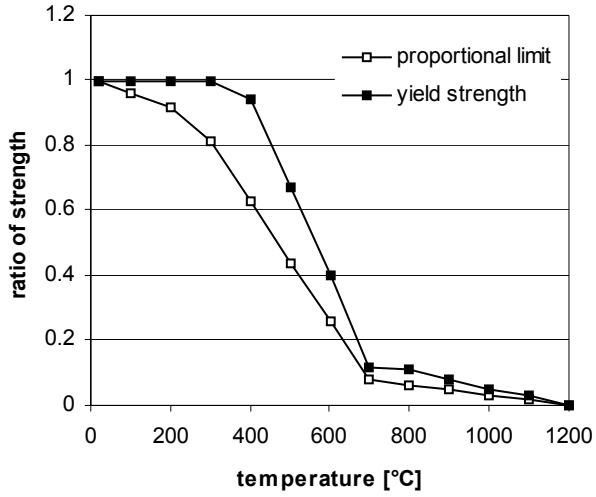

Figure 3.38: Variation of strength of steel according to EC2 (EC2-02)

4 SAFIR FINITE ELEMENT PROGRAM

4.1 General

The SAFIR computer program was developed at the University of Liège, Belgium, by J.M. Franssen based on a former existing program called Computer Engineering of the Fire design of Composite and Steel Structures (CEFICOSS). Specifications described in this chapter are based on the content of the Users Manual (Fra-02).

4.2 Capabilities of SAFIR

SAFIR is based on the Finite Element Method (FEM). The program can be used to analyse one to three-dimensional structures under ambient and elevated temperatures. For the idealization of the structure various elements and material models (linear and non-linear) are available and thermal, torsional and structural analysis can be performed either in 2 or 3D.

Within this report only 2D analysis were performed using 2D-SOLID elements for the thermal analysis and BEAM and TRUSS elements for the structural analysis.

4.3 Analysis procedure

The calculation process within the program consists of two steps, namely the ‘thermal analysis’ and the ‘structural analysis’.

The ‘thermal analysis’ predicts the temperature distribution inside the cross-section while the structure is exposed to fire. The discretisation for plane sections of all different shapes is possible by using triangular and/or quadrilateral elements. For each element the material can be defined separately, here steel and concrete are predefined, but other materials can be analysed if their physical properties at elevated temperatures are known. The variation of material properties as well as the evaporation of moisture can be considered.
The fire exposure is implemented as a function of time and either predefined code temperature curves can be used or other curves, also including a cooling phase, can be modelled.

For beams it is assumed that there is no heat transfer along the axis of the beam, as a two-dimensional model is used. If the modelled structure consists of different cross-sections, thermal analyses have to be performed for each section separately.
The assumed heat transfer mechanism for plane and solid sections is conduction, while inside internal cavities radiation is considered.
The results of the thermal analysis can be displayed with the post-processor DiamondXP, or the data can be evaluated using a text editor.

The ‘structural analysis’ determines the response of the structure due to static and thermal loading. The structure can be modelled with truss, beam, solid or shell elements thus allowing 2 and 3-dimensional analysis. The calculation is based on a step-by-step procedure integrating the temperature distribution obtained from the thermal analysis at each time step. For each step the program determines the successive position of equilibrium under the load using an incremental-iterative solver.

At each iteration step the following data is calculated:

- Displacements in all degrees of freedom for each node
- Axial forces and bending moments at each integration point
- Stresses at each integration point of beam elements
- Reaction forces at the supports

4.4 The SAFIR beam element

Three nodes define the beam element used within this report. Two nodes are needed for the definition of the end points of the beam element and thus its position in space. The additional third node is situated at the middle of the element and is used to support an additional degree of freedom, preventing the beam from being to stiff in bending. The end nodes of a 2D beam element have three degrees of freedom each; two displacements and one rotation. The single elements are connected to each other at the location of the nodeline, which can be defined within the thermal input file. The influence of the position of the nodeline is shown in appendix A.1.

The integration along the length of the beam is performed with Gauss integration; therefore the number of integration points can be varied from one to three. At each integration point the material behaviour is calculated at the centre of each fibre of the cross-section and is constant for the whole fibre.

For the beam element the following assumptions are stated in the User's Manual (Fra-00):

- The Bernoulli Hypothesis is considered
- Plasticity is only considered in the longitudinal direction of the member
- Non-uniform torsion is considered

4.5 Material properties

SAFIR provides numerous material models for the thermal and structural analysis. The material properties used for reinforced concrete are based on EC2 (1995) (EC2-95) allowing the use of siliceous or calcareous concrete.

The material properties defined in EC2 (1995) (EC2-95) are not entirely consistent to the properties defined according to EC2 (2002) (EC2-02) which are stated in section 3. Therefore the material properties that are defined differently are stated below.

Specific heat

The specific heat according to EC2 (EC2-95) is defined by the following equation:

$$c_c = 900 + 80 \cdot \theta/120 - 4 \cdot (\theta/120)^2 \text{ (J/kgK)} \quad \text{for } 20°\text{C} < \theta \leq 1200°\text{C} \tag{4.25}$$

The moisture content may be taken into account by assuming a peak value situated between 100°C and 200°C.

Figure 4.1 shows the specific heat according to different definitions of the Eurocodes (EC2-02) (EC2-95).

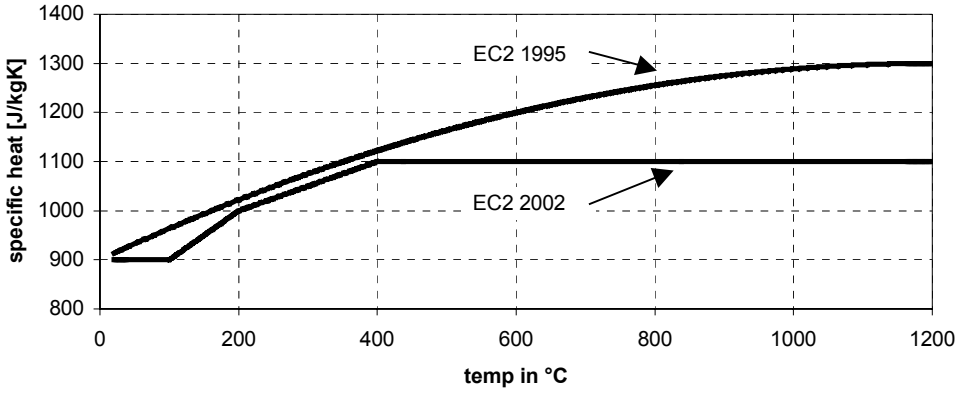

Figure 4.1: Specific heat of concrete according to (EC2-95) and (EC2-02)

Thermal conductivity

Version 2002 of EC2 determines the thermal conductivity between the upper and the lower limit, whereas the 1995 version distinguishes the thermal conductivity of siliceous and calcareous according to the following equations.

Siliceous aggregate concrete:

$$\lambda_c = 2 - 0.24 \cdot \theta/120 + 0.012 \cdot (\theta/120)^2 \,(\mathrm{W/mK}) \qquad \text{for } 20°\mathrm{C} < \theta \le 1200°\mathrm{C} \tag{4.26}$$

Calcareous aggregate concrete:

$$\lambda_c = 1.6 - 0.16 \cdot \theta/120 + 0.008 \cdot (\theta/120)^2 \,(\mathrm{W/mK}) \qquad \text{for } 20°\mathrm{C} < \theta \le 1200°\mathrm{C} \tag{4.27}$$

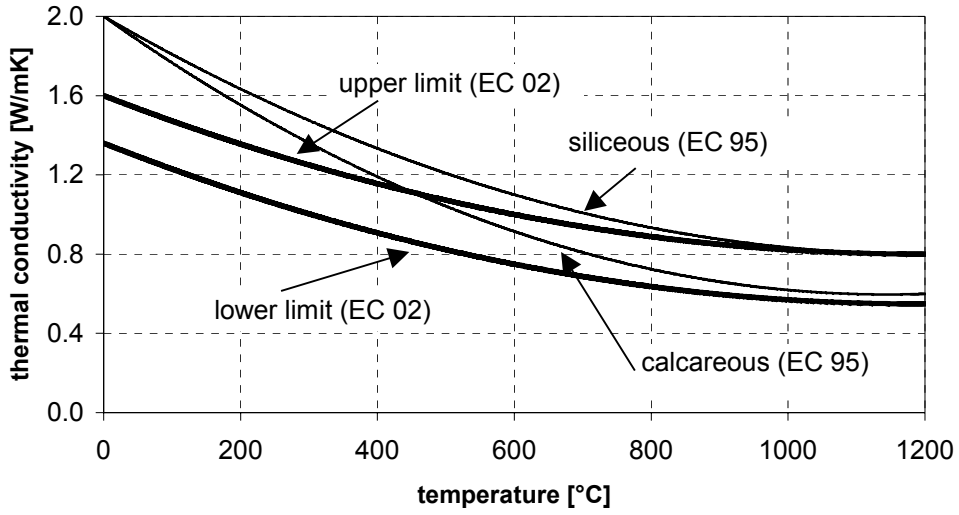

Figure 4.2: Thermal conductivity for concrete according to (EC2-02) and (EC2-95)

Stress strain-relationship for concrete

The stress-strain relationship according to EC2 (EC2-95) is defined as shown in Figure 3.17, but in comparison to EC2 (EC2-02) the strain values $\varepsilon_{c1,\theta}$ are smaller and the decrease in compressive strength is assumed to start at lower temperatures. Table A 2 in Appendix A.2 shows the values used in the analysis.

Assumptions within SAFIR

In the definition of material properties SAFIR makes the following assumptions:

- Perfect bond is assumed between materials and therefore slippage between steel and concrete cannot be taken into account.

- Spalling of concrete is non-existent.
- Shear failure cannot be considered in the structural analysis.
- Cracking and crushing of concrete can be included in the analysis.
- Creep, as time dependant material property, is not considered explicitly. Creep is implemented into the analysis using stress-strain-relationships that have been modified to allow for some creep.
- Contraction of concrete with decreasing temperatures is taken into account.

4.6 Applications

Franssen (Fra-04) recently used the SAFIR thermal analysis procedure to determine 3D temperature fields in steel joints to investigate the hypothesis that the temperature in the joints is always lower than that in the connected elements.

Lim et al. (Lim-04b) carried out numerical and experimental tests on a flat concrete slab, a *Hi-bond* slab (proprietary composite slab with a trapezoidal profiled steel deck) and a *Speedfloor* system slab (reinforced concrete flat slab with suspended steel joists) to validate the SAFIR program. For the flat slab and the *Speedfloor* slab, the SAFIR program predicted the behaviour observed in the tests with reasonable accuracy. The analysis of the *Hi-bond* slab showed that the temperatures and behaviour of the slab were difficult to predict, as the debonding of the steel decking, that was observed during the test, and the resulting insulating effects of the layer of air between the slab and the steel deck were not taken into consideration.

5 NUMERICAL ANALYSIS OF SINGLE-SPAN REINFORCED CONCRETE BEAMS SUBJECTED TO FIRE

5.1 Introduction

This chapter describes the numerical analysis of single reinforced concrete beams subjected to fire. The purpose of this analysis is to investigate the effect of various end support conditions on the structural behaviour and the fire resistance rating of reinforced concrete beams.

Two general models are analysed:

- Pin-supported beams with varying horizontal restraint as shown in Figure 5.1

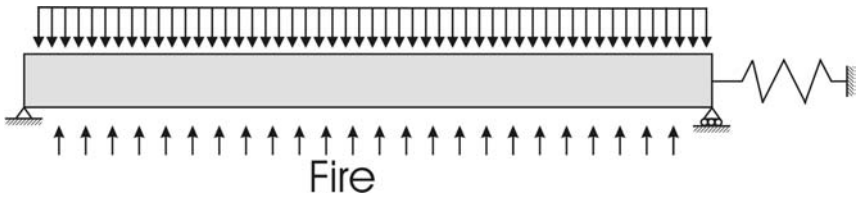

Figure 5.1: Pin-supported beam

The pinned supports allow for free rotation at the ends of the beam. The varying horizontal restraint of the beam is modelled with a spring.

- Rotationally restrained (fixed) beams with varying horizontal restraint as shown in Figure 5.2

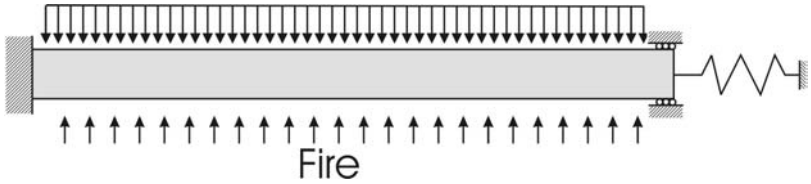

Figure 5.2: Fixed-supported beam

These beams are fixed into the supports, thus the rotation at the ends of the beam is disabled. The varying horizontal restraint is modelled with a spring.

The beams shown in Figure 5.1 and Figure 5.2 are modelled with several different levels of horizontal restraint, ranging from no restraint to total horizontal restraint. For the modelling of the varying horizontal restraint, a spring model is used. The axial stiffness of the spring is measured relative to the stiffness of the beam, such that 100% restraint is equivalent to an identical additional beam at the one support.

$$\text{restraint}\,(\%) = \frac{\text{stiffness of the spring}}{\text{stiffness of the beam}} = \frac{\left(\frac{EA}{L}\right)_{spring}}{\left(\frac{EA}{L}\right)_{beam}} \cdot 100\,\% \qquad (5.1)$$

The beams that are analysed have a cross-section of 300 x 600 mm and span 6 metres. The beams are assumed to be part of an office building carrying the loads of the simply supported slabs. The amount of reinforcement is chosen in a way that the beam can sustain the imposed load, if it is supported either as pinned-pinned or as fixed-fixed supported beam for the purpose of comparison. Therefore, the fact that a fixed-fixed supported beam would need less reinforcement at the bottom is neglected as well as the fact that a pinned-pinned supported beam does not need structural reinforcement at the top of the beam. The reinforcing bars are continuous through the whole length of the beam without considering the possibility of curtailment.

The cross-section of the beam used in the analyses is shown in Figure 5.3.

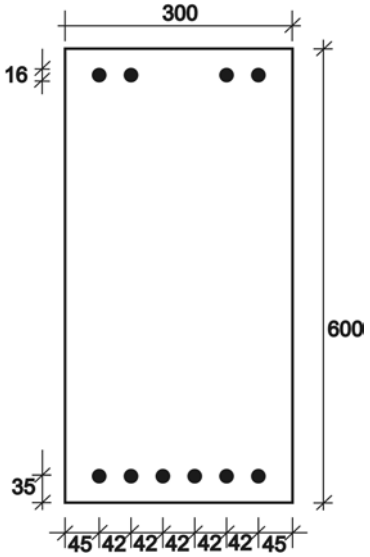

Figure 5.3: Beam geometry

The properties of the beam are as follows:

Beam geometry

Span, L:	6.0 m
Depth, h:	600 mm
Width, b:	300 mm

Concrete properties

Compressive strength (ambient temperatures):	30 N/mm²
Elastic modulus (ambient temperatures):	18000 N/mm²
Tensile strength:	Zero
Concrete model (thermal and mechanical):	Siliceous aggregate (EC2-95)
Axis distance of reinforcing bar to concrete surface:	
Bottom and top:	35 mm
Side:	45 mm

Reinforcing steel properties

Yield strength (ambient temperatures):	500 N/mm²
Elastic modulus (ambient temperatures):	210000 N/mm²
Steel model:	cold worked steel (EC2-95)
Bar diameter:	16 mm
Number of bars at the top:	4
Number of bars at the bottom:	6

Loads

Self-weight + superimposed dead load: G	34.0 kN/m
Live load: Q	9.0 kN/m
Ultimate load: 1.35·G+1.5·Q	59.4 kN/m
Fire load: 1.0·G+0.5·Q	38.5 kN/m
Fire exposure:	ISO 834 standard fire (4 hours)

5.2 Thermal analysis

The finite element discretisation of the cross-section for the numerical analyses with the SAFIR program is shown in Figure 5.4. Due to the symmetry of the cross-section, only half of the beam has been modelled. The discretisation of the finite-element mesh has been chosen to be very fine in order to determine the temperatures at the centre of the reinforcing steel bars as these are calculated at the nodes of the mesh.

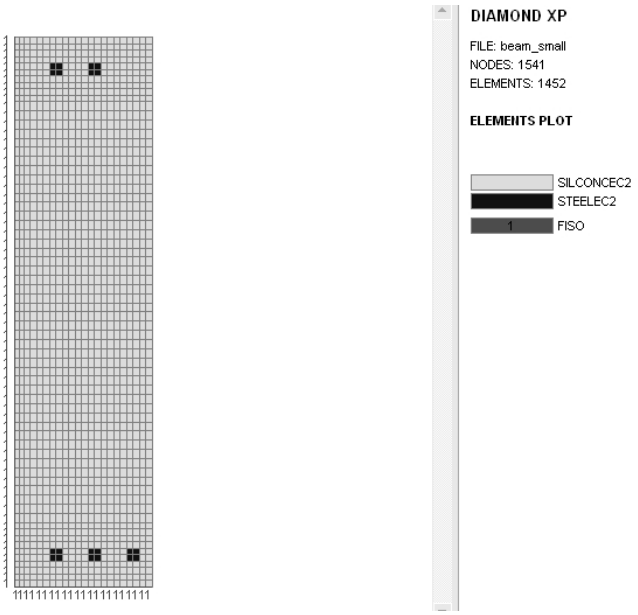

Figure 5.4: Discretisation of the beam cross-section using SAFIR thermal analysis

The beam is exposed to the ISO-fire time-temperature curve on the bottom and the sides. The analyses have been carried out for a duration of four hours. The temperature distribution along the cross-section obtained at different times during the ISO-fire is shown in Figure 5.5. For comparison, the temperature curves given in the tabulated data of the Eurocode (EC2-02) are plotted in Figure 5.6.

During the fire exposure the temperature contours moved inwards from the exposed surfaces to the cooler inner parts. At the sides and the bottom parts of the beam, the contours are mainly parallel to the surface. Much higher temperatures can be observed at the corners that are heated from two sides. It can also be seen in Figure 5.5 that the reinforcing bars do not have great influence on the temperature distribution.

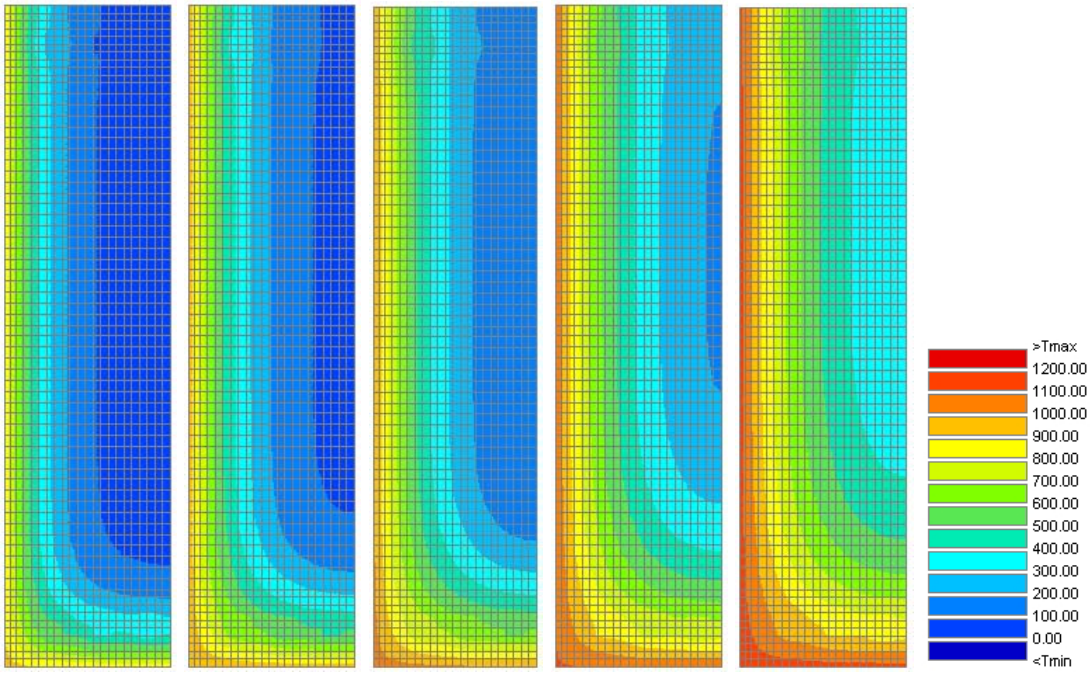

Figure 5.5: Temperature profiles in the cross-section at
60 min, 90 min, 120 min, 180 min, 240 min (from left to right), temperature unit: °C

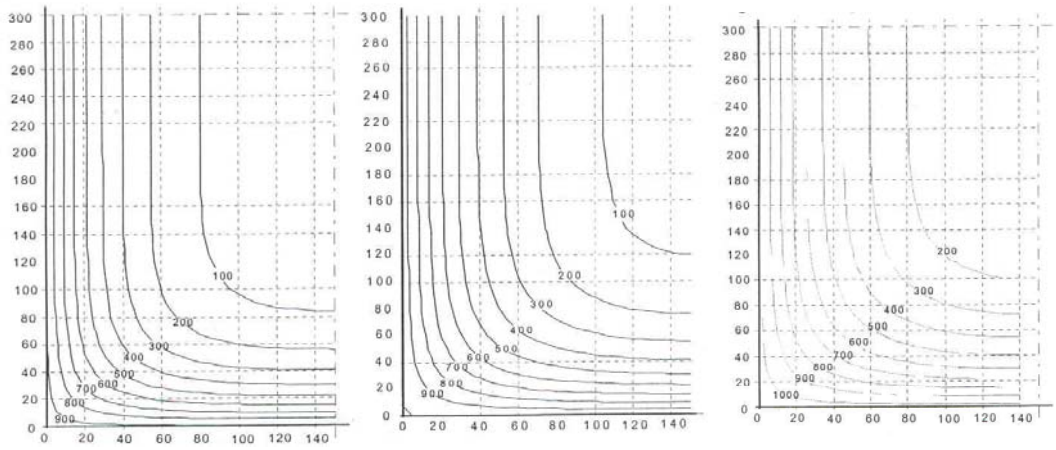

Figure 5.6: Temperature distribution according to EC2 (EC2-02) at 60 min, 90 min and 120 min, temperature in °C, length in mm

The comparison of the tabulated data with the results of the numerical analyses shows that the tabulated data are mostly on the conservative side as their stated concrete temperatures are always slightly higher at the outer layers of the beam. For the core of the cross-sections SAFIR predicted a somewhat faster increase in temperature.

The temperature development in the reinforcing bars during the four-hour exposure to the ISO-fire is shown in Figure 5.7. It can be seen that bar 1, which had heat contributions from the side and the bottom of the beam showed the steepest increase in temperature.

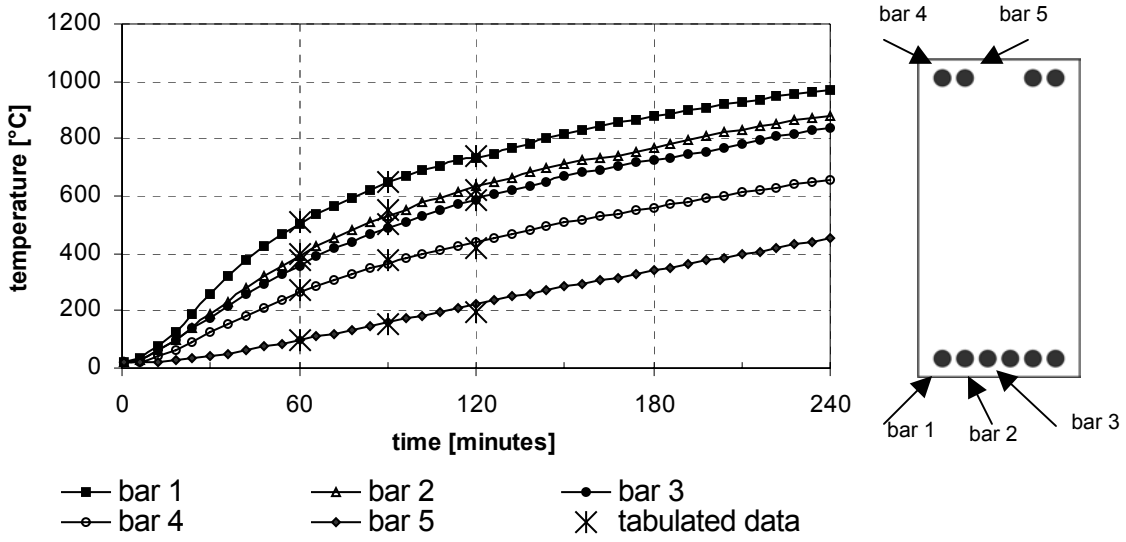

Figure 5.7: Temperature distribution in the reinforcing bars

Bars 2 and 3 were mainly heated from one side and thus their behaviour was similar and the temperatures reached were lower compared to those of bar 1. The temperature development in reinforcing bar 4 showed the same trend as bar 3, but since the concrete cover at the side for bar 4 was 10 mm thicker, the temperature development was delayed compared to bar 3. The temperatures in bar 5 increased gradually but were never very high. Compared to the tabulated data (shown by the crosses in Figure 5.7), the steel temperatures reached at 120 minutes showed slightly higher values for bar 2 and the top bars.

The metallurgical change of steel at temperatures of 730°C can be seen as a slight change of slope in the increase of temperatures.

5.3 Structural analysis

5.3.1 Structural model

The beams, spanning 6 metres, have been modelled using 2D beam finite elements. The elements each have a length of 0.25 m and are connected to each other at the centre of the cross-section shown in Figure 5.4. The spring, allowing for varying horizontal restraint, is modelled with a truss element. The supports and the spring are connected to the beam at the centre of the cross-section. The uniform load applied during the analyses equals the fire load of 38.5 kN/m as stated in section 5.1.

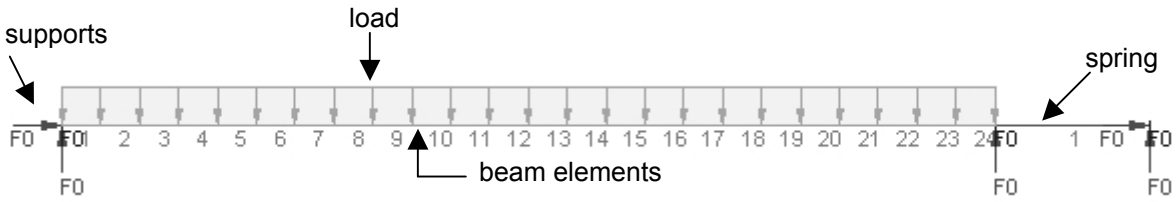

Figure 5.8: Discretisation of the beam with SAFIR for the structural analysis

5.3.2 Pin-supported beams with varying axial restraint

This section discusses the behaviour of the pin-supported beams with varying levels of axial restraint exposed to the 4-hours ISO-fire as shown in Figure 5.1. The spring stiffness is varied from 1% to 500%. The cases of no horizontal restraint (pin-roller) and total horizontal restraint (pin-pin) supports are considered as well.

The development of the axial force during the fire exposure for the different levels of spring stiffness is shown in Figure 5.9. It can be seen that with increasing spring stiffness, the compressive axial force developed in the beam increased as well. The beams with weaker springs develop their maximum force at a later stage into the ISO fire, as the weaker springs allow for more thermal elongation. The compressive stresses, which developed due to the restricted thermal expansion, shifted from the heated surface layers to the inner layers with increasing temperature. As concrete does not conduct heat well, this inwards moving of the compression block is limited to a few centimetres.

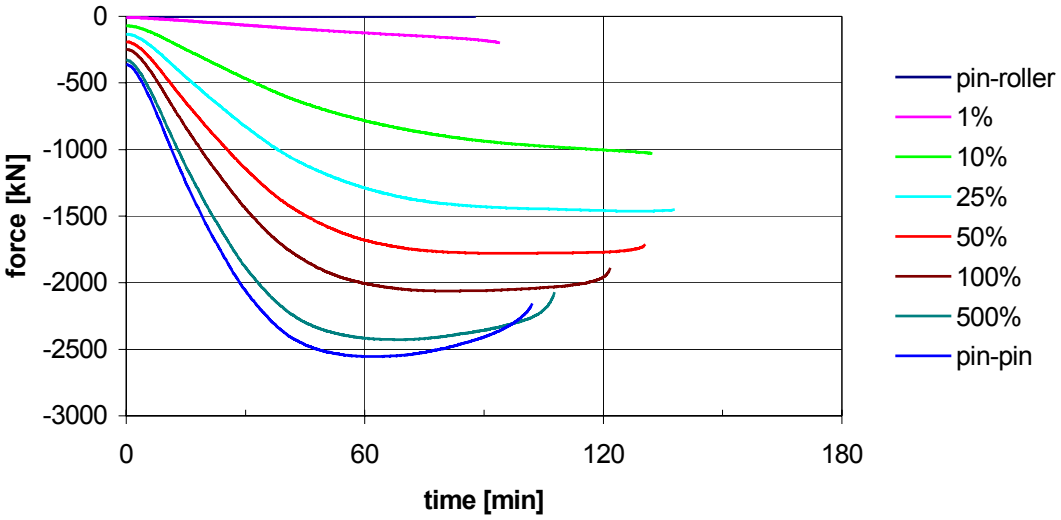

Figure 5.9: Axial force for different levels of spring stiffness

The axial force showed a linear trend for the spring with 1% stiffness. For beams with higher spring stiffness, the axial force had a fast increase at the beginning which slowed down later. For springs with stiffness higher than 50%, the axial force dropped after reaching the maximum value. This decrease in axial force might be due to reaching the compressive limit of the concrete fibres which causes a decrease in the extreme fibre stresses. For the pin-pin case it could be observed that the stresses in the concrete fibres at the top of the beam at the span reached values close to their compressive limit as the maximum force was reached. The initial axial force for the restrained beams is due to supporting the beam at the centroidal axis and not close to the neutral axis of the beam (see Appendix A.1).

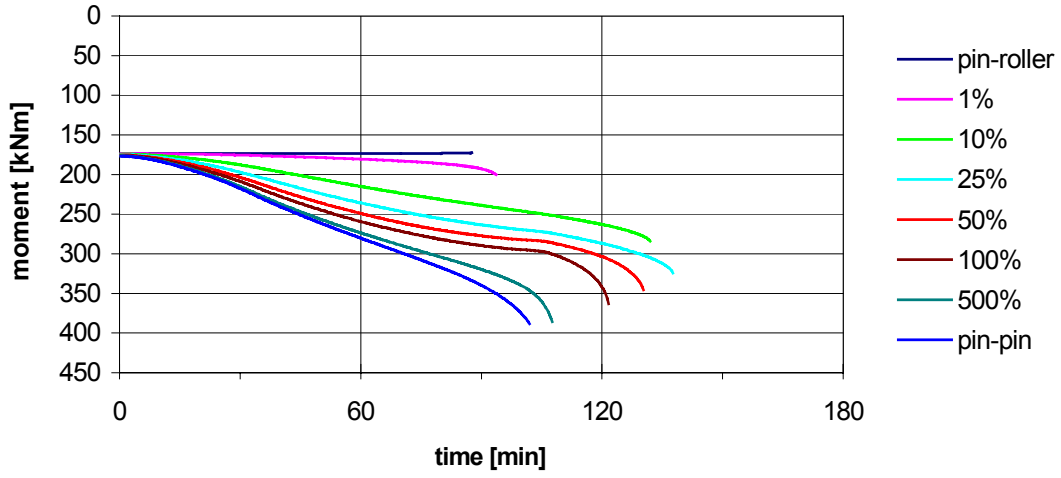

Figure 5.10: Midspan bending moment for different levels of spring stiffness

The development of the bending moment at midspan for the different amounts of spring-stiffness is shown in Figure 5.10. The initial moment at midspan was caused only by the imposed load and therefore was equal in all the beams. With increasing stiffness of the spring, the moment at the midspan increased during the fire exposure. This increase was caused by the resultant axial force which was induced at the centre of the beam and thus imposed an additional positive bending moment which equalled the deflection multiplied by the displacement.

The final bending moment reached during the analysis increased with increasing horizontal restraint. This is due to the compressive axial force which has the effect of prestressing the cross-section. For the same reason the pin-pin supported beam that developed the largest axial force reached the largest bending moment.

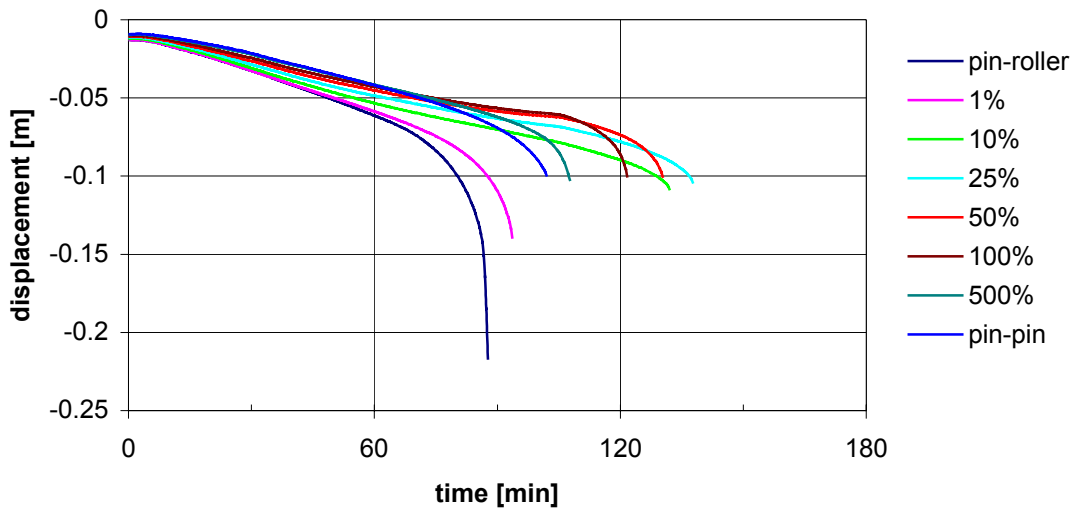

Figure 5.11: Displacement at midspan for different levels of spring stiffness

The displacements of all beams, as shown in Figure 5.11, showed a linear trend during the initial stages of the fire. At the beginning of the fire exposure, the beams with stiffer springs underwent smaller deflections than the beams with less stiff restraint.

The deflection was affected by the increasing bending moment which again was affected by the deflection, due to the axial force. This reciprocal influence led the beams with spring stiffness higher than 25% to reach their maximum moment at an earlier point of time during the analysis.

For beams with some amount of restraint, the SAFIR program was unable to converge after the last plotted time step shown in the diagrams, but the deflection of all beams

showed a trend to develop a vertical tangent by the time the calculation stopped. This observed increase in deflection would result in a snap-through behaviour of the beam. Consequently the beam would act as a catenary being held only by the reinforcement anchored into the supports. The compressive axial force would be expected to drop and eventually turn into tension if the computer program was able to continue.

Pin-roller and 1% spring stiffness:

The statically determinate pin-roller supported beam gradually deflected downwards during the initial stage of fire (see Figure 5.11). The initial deflection is caused by the steep temperature gradient at the bottom of the beam, which results in thermal bowing. At approximately 68 minutes the deflection increased, leading to runaway failure. The beam finally failed after 87 minutes. The fire resistance rating for statically determinate concrete beams with this particular cross-section according to the tabulated data of EC2 (EC2-02) is 60 minutes, as the requirements for the 90 minutes fire rating are not quite kept. Thus, the results of the analysis fit well in between the stated ranges of the code.

Figure 5.12 to Figure 5.14 show the stresses in the bottom reinforcing bars of the beam at midspan. Tensile stresses are positive and compressive stresses negative. The variation of the proportional limit and the yield limit of the reinforcing bars with temperature is shown by the broken and the continuous line respectively. The bars being referred to are indicated by the darkened bars in the sketch of the beam besides the figures.

The initial increase in the tensile stresses in the reinforcing bars is due to the expanding outer concrete layers. These went into compression as their elongation was restrained by the cooler inner concrete fibres, which consequently had to go into tension. As the concrete fibres cannot take any tensile stress, this tension had to be carried by the reinforcing bars. The tensile stress in the outer bottom bar (bar 1) decreased after about 18 minutes (point (a) in Figure 5.12). This drop in tensile stress might be caused by the increasing temperature of the bar which reduces the difference in expansion between the surrounding concrete and the bar and thus led to a decrease in the induced tensile stress, as well as the higher reduction in strength and elastic modulus due to the higher temperatures compared to the inner bars. This decrease had to be accommodated by the other reinforcing bars which carried on increasing stress until they reached their proportional limits (points (b) in Figure 5.13 and Figure 5.14). This limit was reached first for bar 3, as this one was the coldest and thus the stiffest one, attracting most of the stress. As the strength and the modulus of elasticity of the inner bars dropped due to the

rising temperatures, the outer bar had to increase in tension in order to enable the beam to sustain the imposed load.

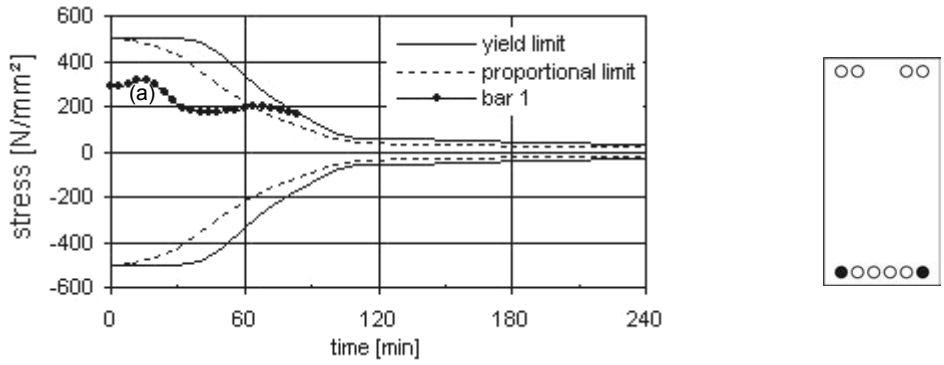

Figure 5.12 Stresses in reinforcing bar 1 for the pin-roller support (tension positive)

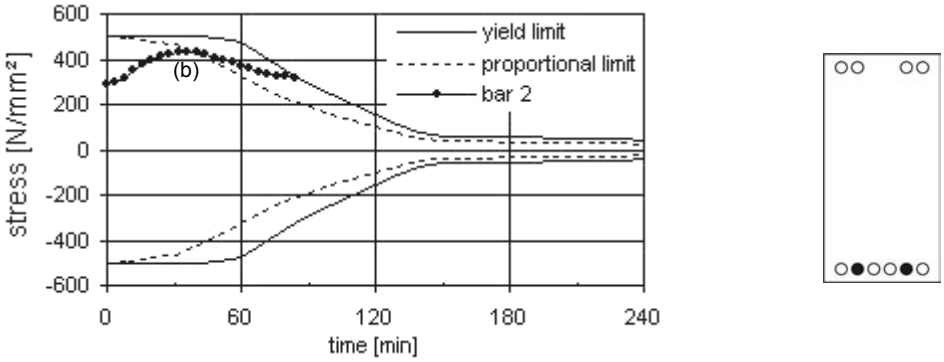

Figure 5.13 Stresses in reinforcing bar 2 for the pin-roller support (tension positive)

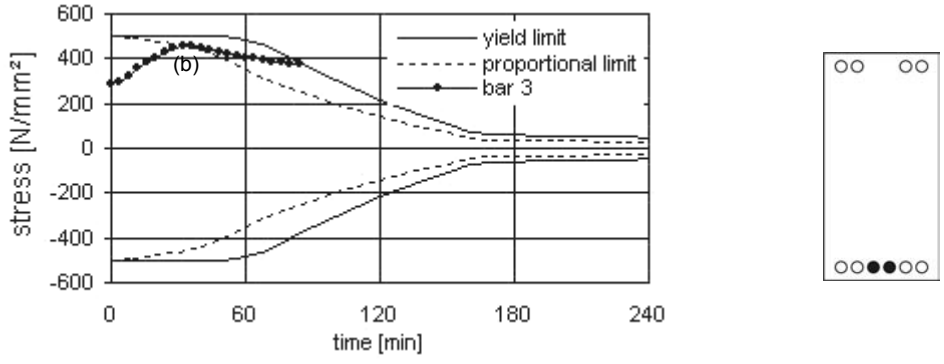

Figure 5.14 Stresses in reinforcing bar 3 for the pin-roller support (tension positive)

At the time the stresses in the reinforcing bars reached the tensile yield limit, a plastic hinge formed at midspan, and the beam deflected downwards at a high rate.

The beam with 1% spring stiffness showed equivalent behaviour to the pin-roller supported beam but lasted 8 minutes longer during the fire exposure due to the small axial force which reduced the tensile stresses in the bottom reinforcing bars.

Spring stiffness > 10%

The beams with spring stiffness higher than 10% showed a different behaviour during the fire exposure. The stresses in the reinforcing bars for the pin-pin supported beam at midspan are shown in Figure 5.15 as an example for these beams.

The stresses in the bottom reinforcing bars at midspan were initially in tension. Because of the increasing axial force, the tensile stresses dropped or even went into compression in the highly restrained beams. The corner bars showed higher compressive stresses than the inner bars, as the outer and thus hotter layers induced higher compression stresses due to thermal elongation. The stresses all became tensile at the end of the analyses and showed the trend of reaching the tensile proportional limit for beams with stiffness lower than 25%.

The top reinforcing bars of all beams increased in compression and reached their compressive proportional limit during the analysis (points (a) in Figure 5.15). At the end of the calculation the top reinforcing bars for the beams with spring stiffness higher than 100% were close to reaching the compressive yield limit (points (b) in Figure 5.15). For the pin-pin supported beam, the concrete fibres at the top of the beam showed values close to their compressive strength limit at the outer layers of the cross-section.

The beams showed very large compressive forces, but not all the fibres of the cross-section were under compression. At the beginning of the fire exposure, the compressive block at the top of the beams moved downwards and with increasing temperatures the fibres at the heated surfaces went into compression, but the inner fibres at the lower parts of the beams showed stresses of zero. This effect is caused by the thermally induced internal stresses, which cause the beam to go into compression at the outside and consequently the inner parts had to go into tension, but this is not possible for the concrete as zero tensile strength was assumed.

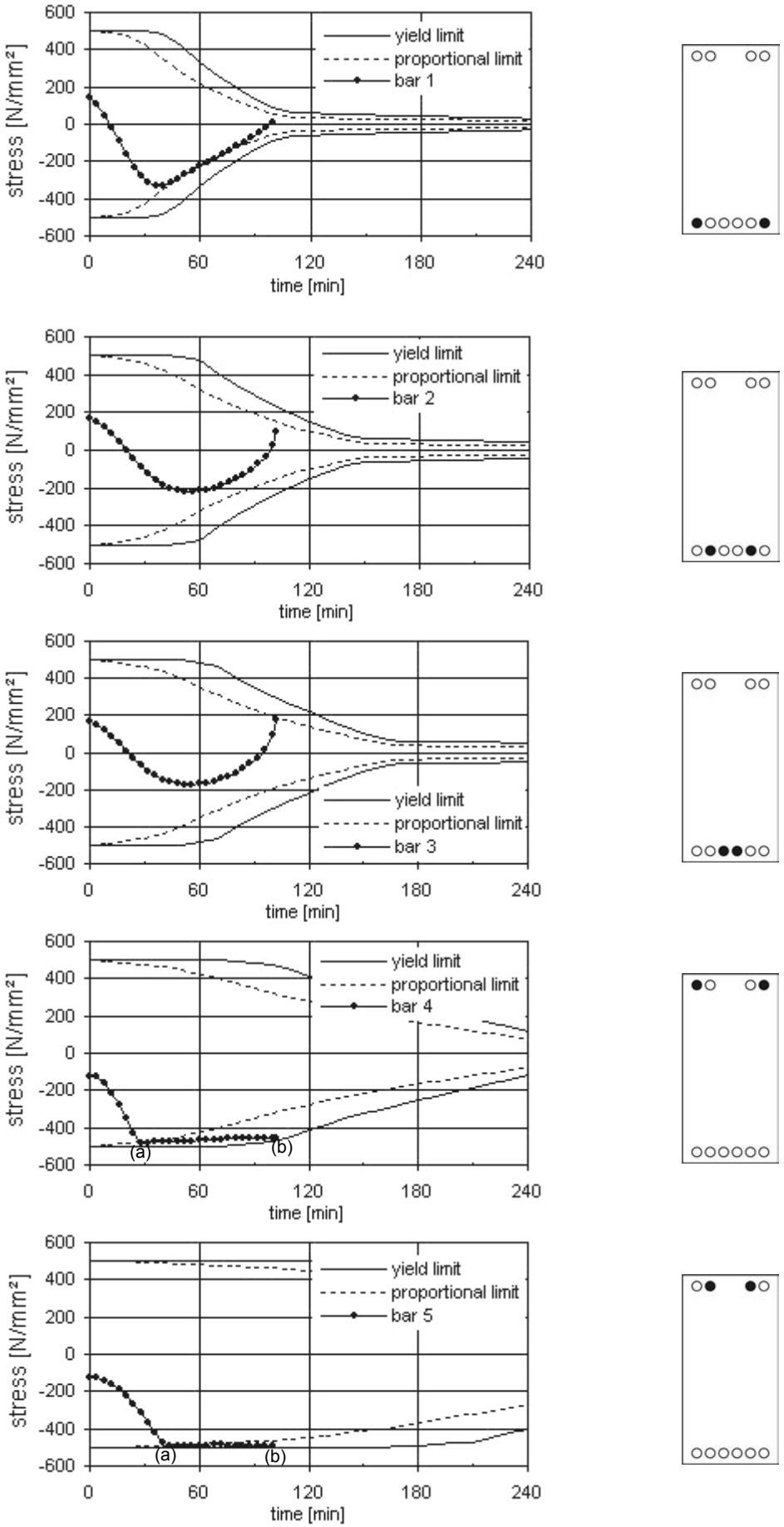

Figure 5.15: Stresses in the reinforcing bars for the pin-pin supported beam (tension positive)

The stresses in the reinforcing bars for the pin-pin supported beam show that the beam sustained the imposed load mainly due to the high compressive force, as all the reinforcing bars were in compression during most of the fire exposure. As the deflections of the beam did not exceed half of its depth, it is assumed that the beam developed a flat internal arch to sustain the imposed load. In order to enable this behaviour, large horizontal forces were needed. At the later stages of the fire, the beam changed its structural behaviour back into carrying the load with its flexural strength. This is indicated by the bottom reinforcement bars which went back into tension at the end of the analysis.

The definite failure mechanism of these beams cannot be determined as the program stopped when it could no longer converge on a solution, but the stresses in the reinforcing bars showed a trend that for beams with spring stiffness higher than 50%, the beams failed in compression at the top whereas for beams with spring stiffness lower than 25% the trend of the stresses in the bottom reinforcing bars was to fail in tension.

Conclusions:

The analysis of the pin-supported beams has shown:

- All beams with some amount of restraint resisted the ISO fire for more than 90 minutes and the pin-roller supported beam exceeded its tabulated fire rating time of 60 minutes.
- The axial force developed during the fire depends on the axial stiffness of the support system. High axial stiffness produces high axial forces. These forces have to be considered in the design calculation of the surrounding structure, as the beams can behave as calculated only if the high axial forces can be sustained.
- The high axial force increases the moment capacity of the beam, as it acts as a prestressing, but also leads to a faster increase in bending moment. Thus, beams with intermediate levels of restraint showed better behaviour during the fire exposure than highly restrained beams.
- For beams with some amount of restraint, the SAFIR program could not converge after the last plotted time step. The definite failure mechanism could therefore not be determined but highly restrained beams seemed to fail in compression while beams with less stiff restraint seemed to fail in tension.

5.3.3 Rotational restrained beams with varying axial restraint

The beams analysed in this section are rotationally restrained at both end supports, as shown in Figure 5.2. The axial spring, allowing for varying horizontal restraint, and the supports are connected to the centre of the cross-section of the beam. The spring stiffness is varied from 1% to 500% and the cases of complete restraint at both end supports (fix-fix) and no horizontal restraint (fix-slide) are considered in the analysis as well.

The fire resistance rating for concrete beams with rotational restraint according to DIN 4102 (DIN-4102-4) and EC2 (EC2-02) is 120 minutes for the given cross-section with an axial distance of the reinforcing bars of 35 mm to the bottom surface, of 45 mm to the side surface and a beam width of 300 mm.

The analysis showed that all beams with some amount of restraint survived the four-hour fire duration. The fix-slide beam failed after 195 minutes. For the totally restrained beam the SAFIR program could not converge after 237 minutes.

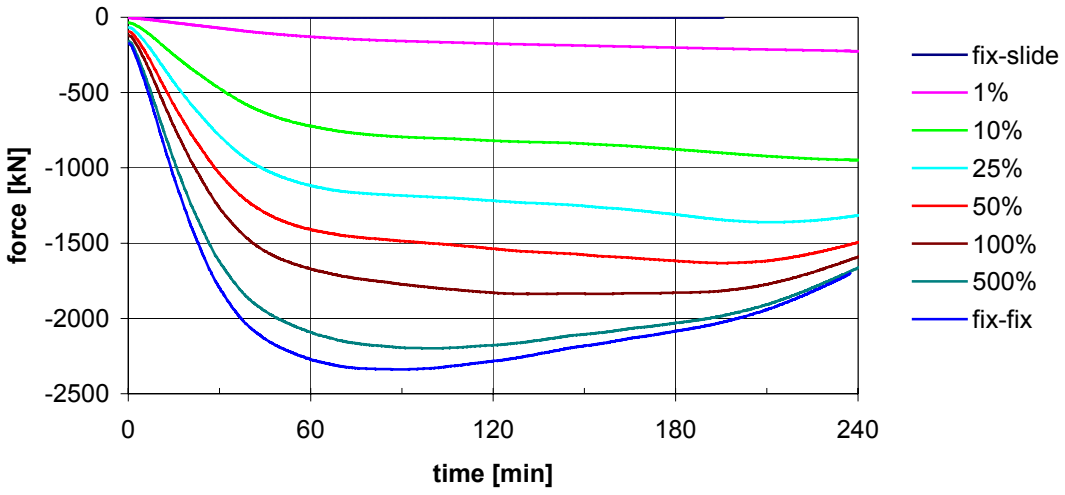

Figure 5.16: Axial force in the beam versus time

Figure 5.16 shows the development of the axial force in the beams during the fire exposure for the different amounts of spring stiffness. The axial forces increased very fast at the initial stages of the fire. This rapid increase slowed down after about 60 minutes. By the time the maximum force for the spring-restrained beams was reached, the horizontal

moveable support reached its maximum horizontal displacement as well. Beams with stronger restraint showed higher axial forces. At the later stages of the fire the axial force decreased for beams with spring stiffness higher than 25%. Compared to the pin-supported beams analysed in the previous section, the development of the axial force showed similar behaviour at the beginning of the fire, but the values reached were slightly lower for the rotationally restrained beams.

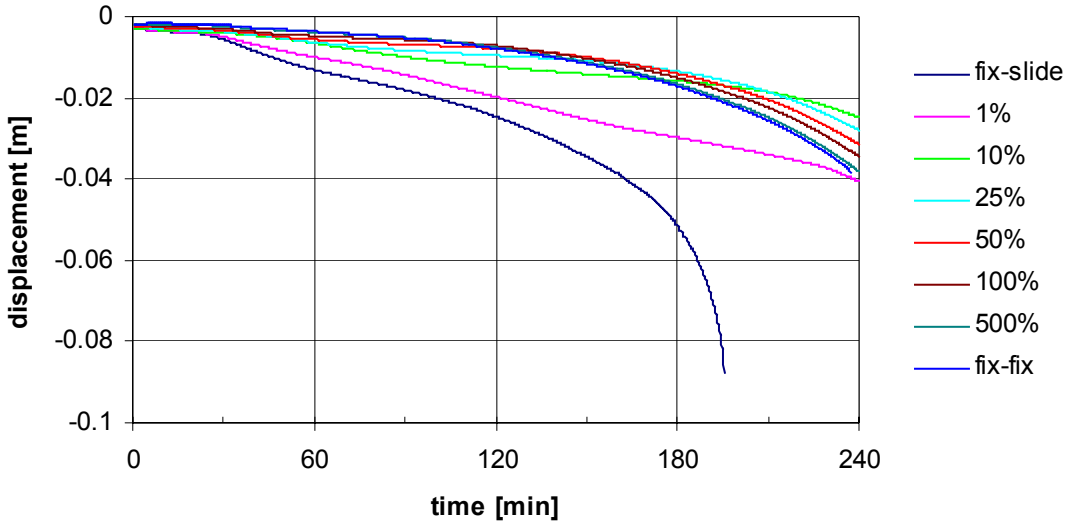

Figure 5.17: Vertical displacement at midspan versus time

The vertical displacement of the beams at midspan is shown in Figure 5.17. All beams showed a very small initial displacement which was smaller than for the pin-supported beams due to the rotational restraint at the ends of the beams. For the fix-slide beam and the beam with 1% horizontal restraint the displacement showed a steady increase at about 30 minutes. For the fix-slide beam this ended in a run-away failure whereas for the beam with 1% spring-stiffness the deflection increased gradually afterwards but did not lead to failure. At the initial stages of the fire, the lightly restrained beams (10% and 25% spring-stiffness) showed larger displacements than the highly restrained beams (100% to fix-fix); as the fire progressed this relationship reversed.

Figure 5.18 and Figure 5.19 show the variation of the bending moment versus time at the support and at midspan respectively.

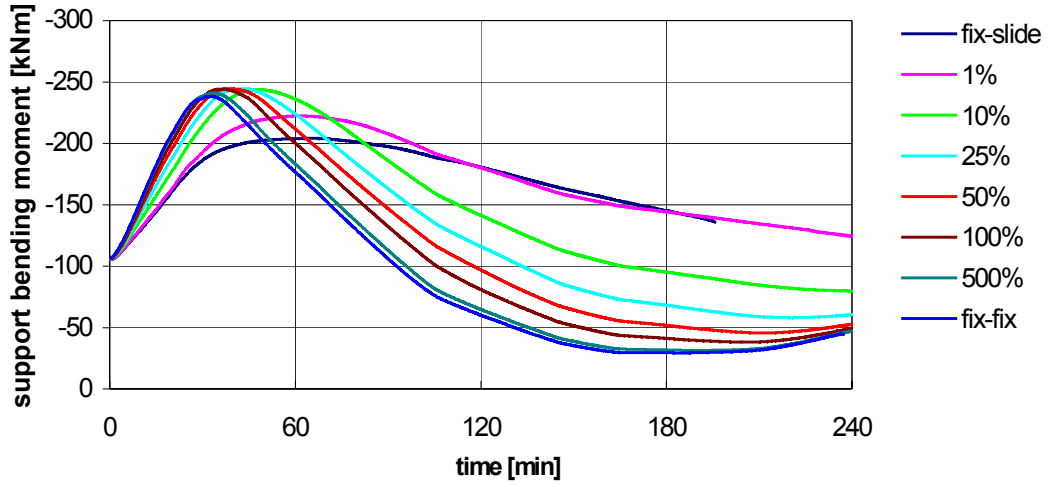

Figure 5.18: Support bending moment versus time

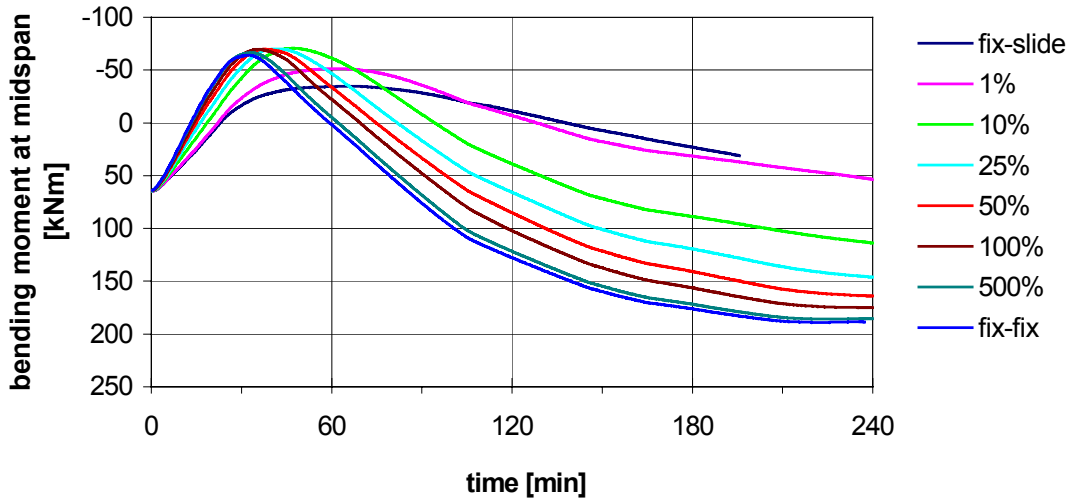

Figure 5.19: Midspan bending moment versus time

At the initial stages of the fire, the beams wanted to deflect downwards due to the thermal bowing effect caused by the expanding bottom parts of the beam. This caused the ends of the beam to tend to lift from their supports. As this movement was restrained, the bowing resulted in an increase of the support bending moments. Due to the unchanged imposed load, the midspan bending moment consequently decreased at the same rate.

For the fix-slide supported beam and the beam with 1% restraint, the bending moment at the supports showed a linear increase at the initial stage of the fire and reached a plateau at about 60 minutes. Afterwards, the moments slowly decreased. The increasing moment

led the top reinforcing bars to exceed their proportional limit and in the fix-slide case they yielded in tension, forming a plastic hinge. The support moments started to decrease as the strength-limit of the top reinforcing bars decreased due to the increasing temperatures.

For beams with restraint higher than 10%, the support bending moments initially increased rapidly until they reached a peak value and then dropped off. The peak values were reached when all the bottom reinforcement bars at the supports had reached their proportional compressive limit. From that point onwards, the support moment decreased as the negative moment capacity of the beam was diminished. Beams with lower axial restraint reached their peak bending moment at a later point of time.

In the decreasing branch, all the bending moments showed three turning points at about 110, 150 and 167 minutes. After these changes the decrease rate of the bending moment was diminished. These changes were caused by the bottom reinforcing bars at the supports. Above a temperature of 700°C, the rate of strength loss for steel lessens and therefore the rate of decrease in the moment capacity was reduced. For beams with restraint higher than 10%, the support bending moments dropped below their initial values. This was caused by the loss in stiffness of the concrete and the reinforcing bars.

The midspan bending moment increased slightly faster than the support moments decreased, this was due to the axial force acting at the supports imposing an additional positive bending moment.

For beams with stiffness of the spring higher than 25%, the support bending moment increased again at the later stages of the fire while the midspan bending moment reached a plateau. This increase in support bending moment was accompanied by the trend of the bottom reinforcing bars at midspan to go back into tension. As the capacity of these bars had already been severely depleted, a redistribution of the midspan bending moment to the supports is supposed.

Fix-slide:

The following figures show the stresses in the reinforcing bars for the fix-slide supported beam at midspan and at the supports respectively.

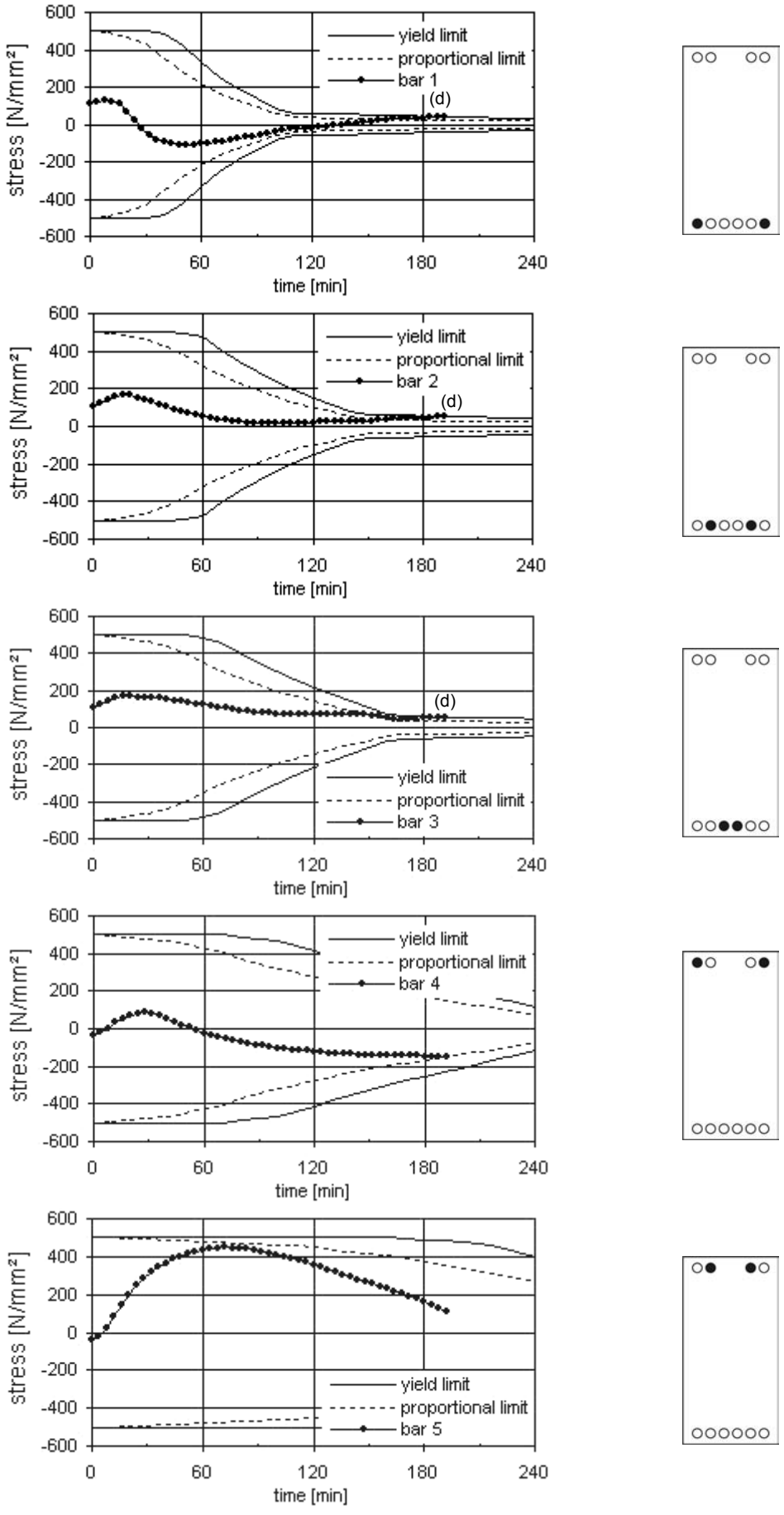

Figure 5.20: Stresses in reinforcing bars for the fix-slide supported beam, at midspan (tension positive)

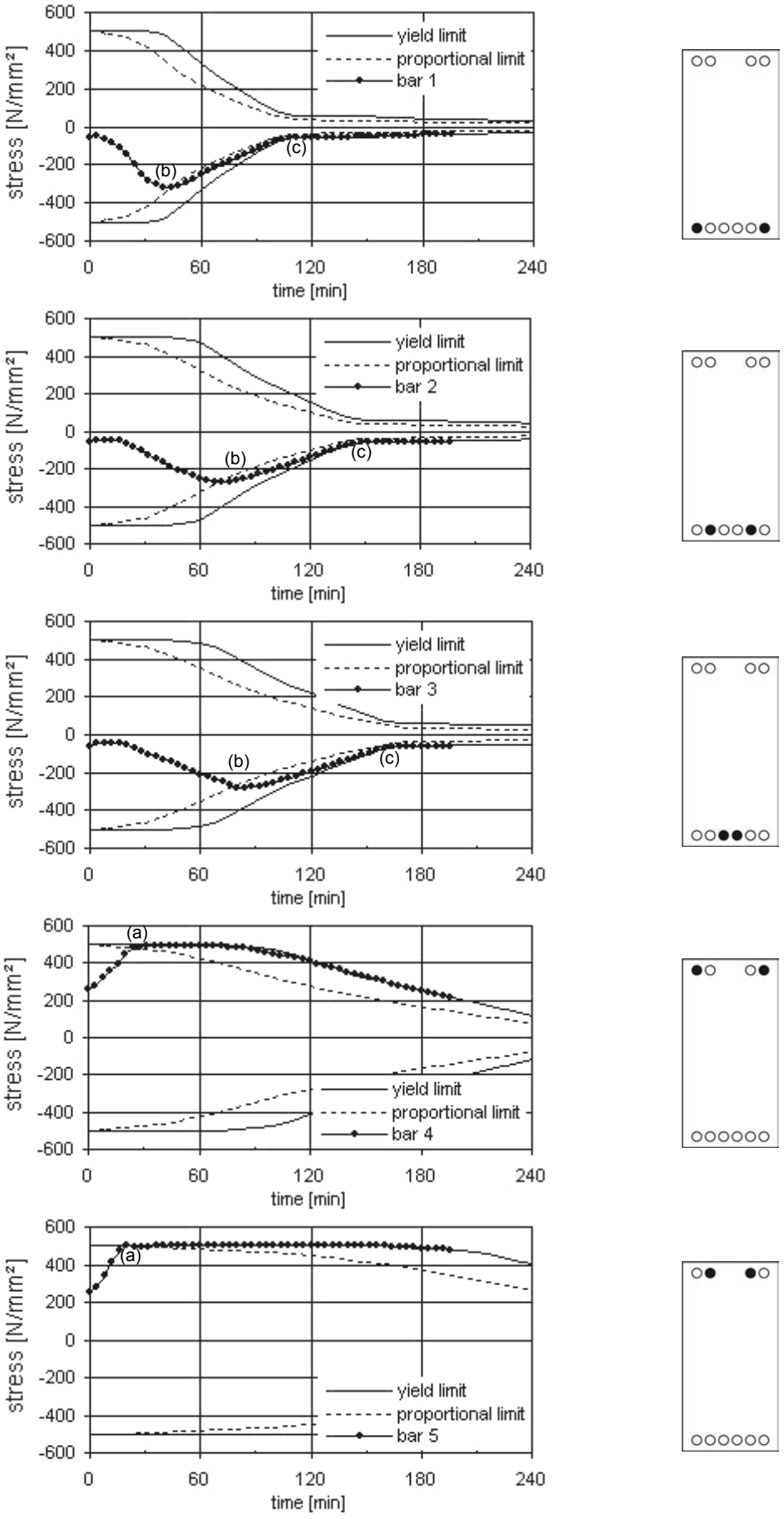

Figure 5.21: Stresses in reinforcing bars for the fix-slide supported beam, at the support (tension positive)

The tensile stresses in the top reinforcing bars at the supports increased linearly until they yielded in tension (points (a) in Figure 5.21). This led to the formation of a plastic hinge, which allowed the beam to rotate freely. This is indicated by the sudden increase in deflection at about 30 minutes (see Figure 5.17).

The bottom reinforcement bars at midspan were initially in tension. Their tensile stresses increased at the beginning of the fire although the bending moment decreased. This increase is again related to the thermal expansion of the outer layers which forced the inner parts of the cross-section into tension. The stresses in the bars started to decrease as the bending moment became negative, but only bar 1 went into compression.

The bottom bars at the supports showed a similar trend to the bars at midspan at the initial stage of the fire. The stresses then increased in compression until they reached their proportional compressive limits (points (b) in Figure 5.21) and dropped gradually afterwards until reaching the yield limits (points (c) in Figure 5.21). By the time these bars reached their compressive yield limit, the tensile stresses in the bottom bars at midspan showed a change of slope and increased afterwards until they yielded in tension (points (d) in Figure 5.20) which caused the beam to fail, as three plastic hinges had formed.

A general distribution of the stresses in the beam at midspan at failure time can be seen in Figure 5.22. All bottom bars were in tension due to the positive bending moment and the concrete above was cracked. The compression block at the top of the beam was limited to the outer layers due to the thermally induced stresses which caused the inner concrete fibres to crack and the inner reinforcing bars to go into tension.

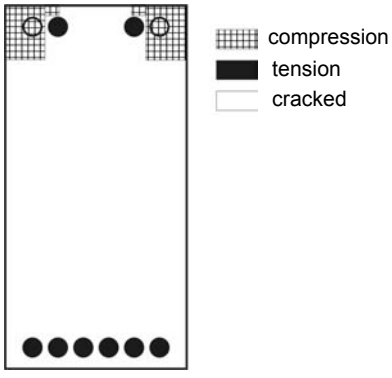

Figure 5.22: General stress distribution for the fix-slide beam at midspan at failure time

The stresses in the reinforcing bars of the beam with 1% spring stiffness showed similar behaviour, but the stresses did not reach the yield limit after exceeding the proportional limit and therefore failure did not occur.

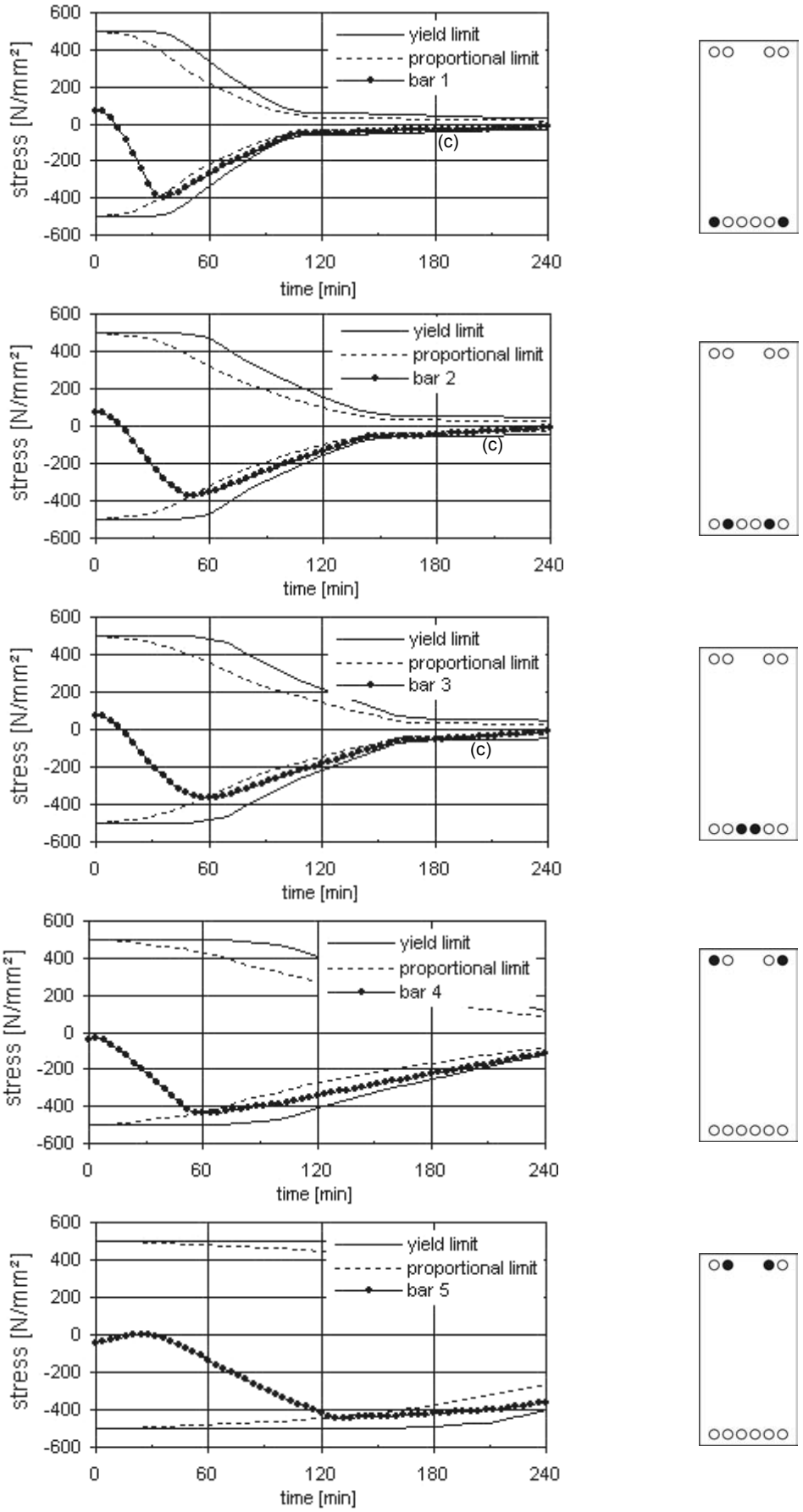

Figure 5.23: Stresses in the reinforcing bars for the fix-spring supported beam with 50% spring stiffness at midspan (tension positive)

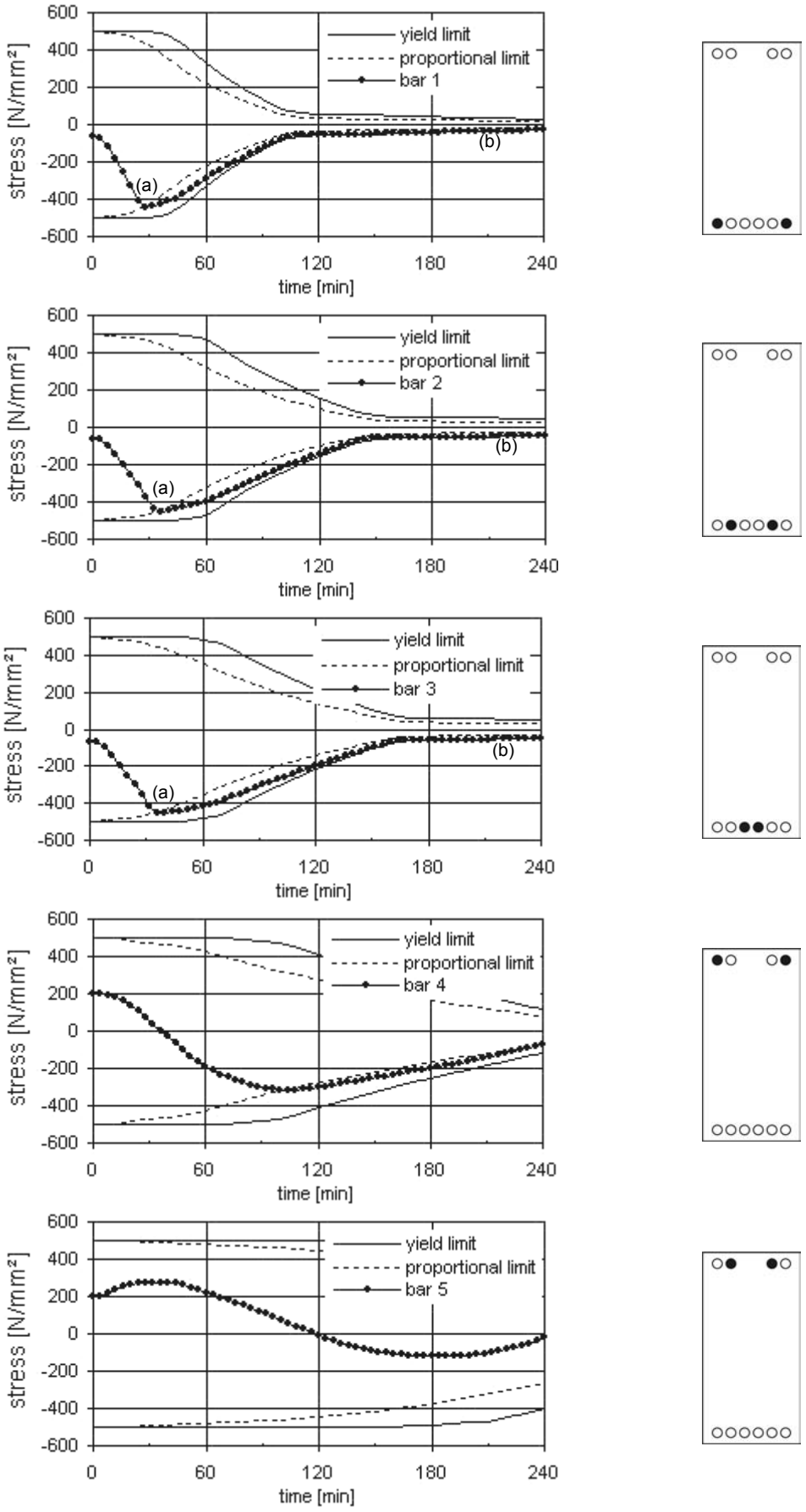

Figure 5.24: Stresses in the reinforcing bars for the fix-spring supported beam with 50% spring stiffness at the supports (tension positive)

Spring-stiffness > 10%

Figure 5.23 and Figure 5.24 show the stresses in the reinforcing bars for the beam with 50% spring-stiffness as example of the stress-development in the higher restrained beams, as all the beams showed similar trends.

The top reinforcing bars at the supports (bars 4 and 5 in Figure 5.24) initially showed tensile stresses, but in contrast to the fix-slide supported beam the steep increase in the negative bending moment did not lead to yielding of the bars. Governed by the developing axial compressive force, the stresses decreased and went into compression. Only bar 5 showed a slight increase in tension during the first 30 minutes which again can be related to thermal effects.

The bottom reinforcing bars at the supports (bars 1 to 3 in Figure 5.24) increased linearly in compression as the support bending moment increased. This increase reached its maximum as the bars reached the proportional compressive limit (points (a) in Figure 5.24). By the time all bars had reached their proportional limit, the maximum support bending moment was reached. This decreased as the strength of the bars decreased. At the final stages of the analysis the bars yielded in compression as the support bending moment increased again slightly (points (b) in Figure 5.24).

At midspan, the bottom reinforcement bars were initially in tension but showed the same trend as the bars at the supports as the axial force developed and went into compression. The compressive stresses reduced as the strength of the bars reduced. At the final stages of the analysis the bars showed the trend to turn back into tension (points (c) in Figure 5.23).

The top reinforcement at midspan showed the same trend as the bars at the supports but was in compression during the whole analysis.

It can be seen in the stress diagrams that the strength of the bottom reinforcing bars is severely reduced after a fire exposure of four hours, but this did not lead to failure of the beams.

Conclusions:

The analysis of the rotationally restrained beams with varying horizontal restraint showed that:

- Rotationally restrained beams have very good structural behaviour in fire. All beams exceeded their calculated fire resistance time of 120 minutes according to the tabulated data.
- The deflections during the fire exposure are very small and hardly exceeded 40 mm.
- The horizontal restraint was beneficial to the behaviour of the beams, as the horizontally restrained beams sustained the fire for the entire fire duration of four hours whereas the fix-slide beam failed after 197 minutes. The amount of horizontal restraint did not show a great influence on the behaviour of the different beams.
- Compared to the pin-supported beams, the developing axial force showed smaller values.

6 NUMERICAL ANALYSIS OF CONTINUOUS REINFORCED CONCRETE BEAMS SUBJECTED TO FIRE

6.1 Continuous two-bay beam

The following section discusses the analysis of a reinforced concrete beam which is continuous over one support (see Figure 6.1). Both ends of the beam are pin-supported and only one support is horizontally restrained, the other supports are free to move longitudinally. The scope of this analysis is to investigate the effect of continuity at the centre support and the influence of different lengths of reinforcing bars at the top of the beam. Both bays of the beam are subjected to the four-hour ISO-fire from the bottom and the sides.

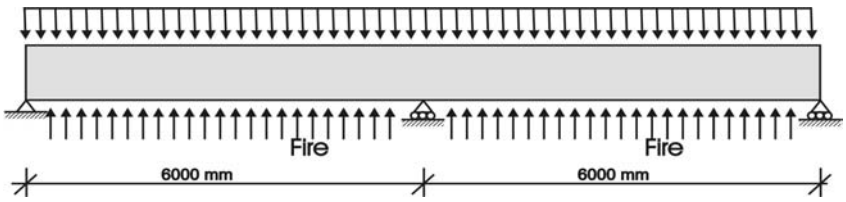

Figure 6.1: General view of the continuous two-bay beam

The analysis covers three differently reinforced beams. The geometry and the properties of the beams are the same as the ones stated in sections 5.1 and 5.3.1, only the reinforcement is adjusted to meet the requirements of a continuous beam and the length of the single beam elements is adjusted to the length of the reinforcing bars. Within this section only the structural analysis will be discussed, as the temperature profiles are similar to those in section 5.2.

BEAM 1

Beam 1 is designed according to the design rules of DIN 1045-1 (DIN-1045-1). The possibility of the occurrence of a fire has not been taken into account during the design process. The top reinforcement has been curtailed following the given design rules. The bottom reinforcement is continuous through the beam and has not been curtailed. The arrangement of the reinforcing bars is shown in Figure 6.2.

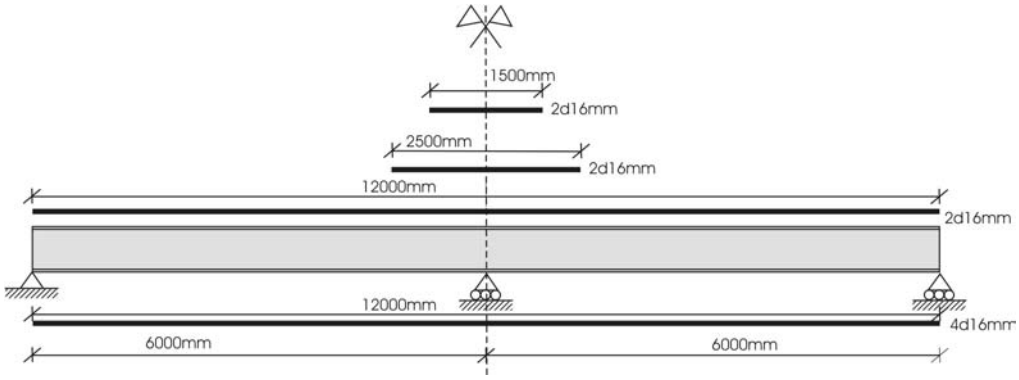

Figure 6.2: Arrangement of reinforcing bars for beam 1

BEAM 2

Beam 2 is also designed according to DIN 1045-1 but the top reinforcement bars at the centre support have been lengthened in order to fulfil the following design rule according to EC2 (EC2-02), where the area of the top reinforcement over each intermediate support should not be less than

$$A_{s,req}(x) = A_{s,req}(0) \cdot (1 - 2.5 \cdot x / l_{eff}) \tag{6.2}$$

where:

x is the distance from the section considered to the centre line of the support where $x \leq 0.3 \cdot l_{eff}$

$A_{s,req}(0)$ the area of the top reinforcement required at the support

$A_{s,req}(x)$ is the minimum area of top reinforcement required in the section considered but not less than $A_s(x)$ required without considering the rule

l_{eff} is the effective length of span.

Figure 6.3 shows the curtailment of the reinforcing bars for beam 2.

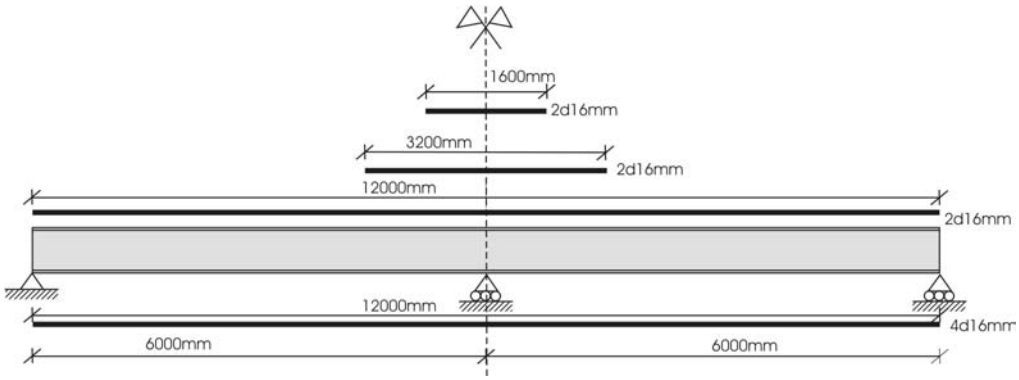

Figure 6.3: Arrangement of reinforcing bars for beam 2

BEAM 3

Beam 3 considers the design rules of „DIBt-Richtlinie zur Anwendung von DIN V ENV 1992-1-2 in Verbindung mit DIN 1045-1“ (DIBt-02). According to that regulation the top reinforcement bars at the supports have to fulfil the same regulations as beam 2 but must be elongated further for a length of $0.15 \cdot l_{eff}$ compared to the bars of beam 1. The resultant length of the reinforcing bars is shown in Figure 6.4.

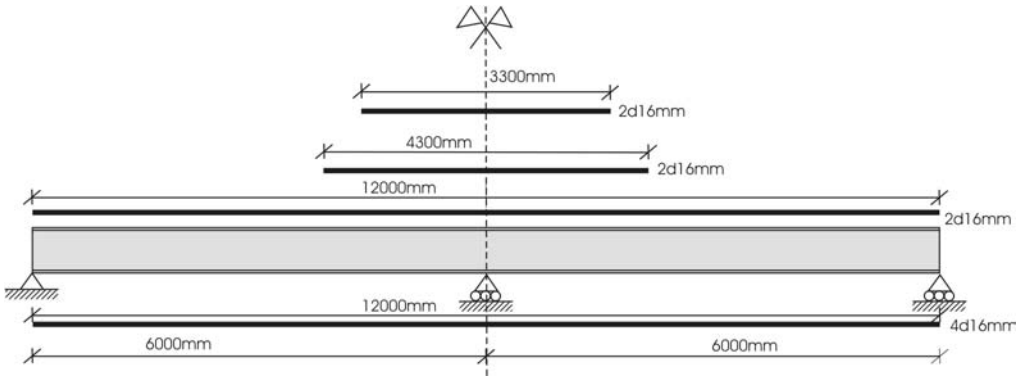

Figure 6.4: Arrangement of reinforcing bars for beam 3

In all design calculations the development length of the reinforcing bars needed for structural design has not been taken into account, as the SAFIR program is assuming that perfect bond exists between the steel and the concrete. Thus the modelling of the development length would imply additional flexural capacity (Lim-03).

Bending moments and deflections

Figure 6.5 shows the development of the bending moment at the inner support and at the location of the maximum positive bending moment in the span for the three different beams. The maximum vertical displacement of the span is shown in Figure 6.6.

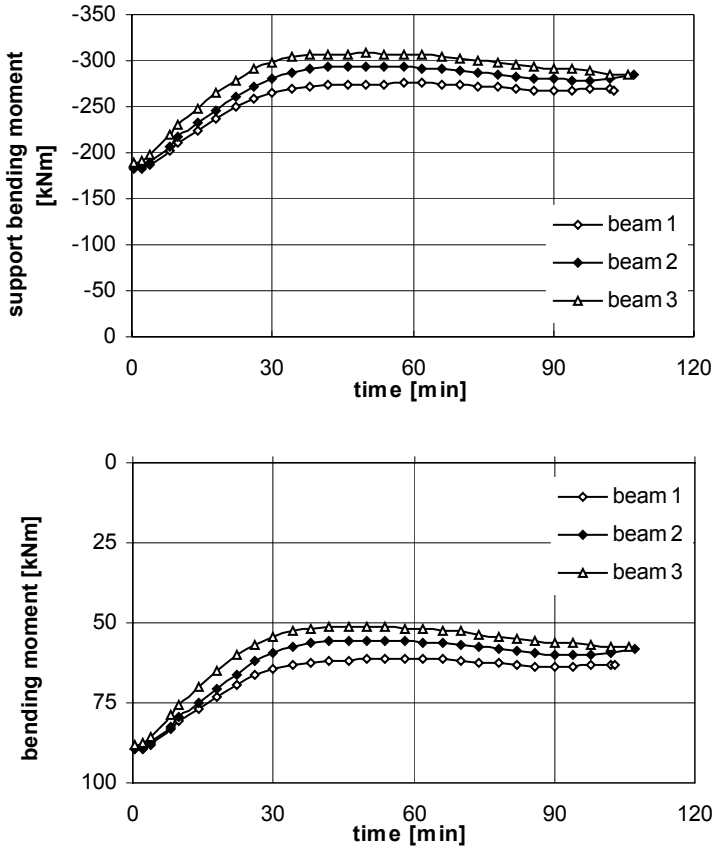

Figure 6.5: Development of the bending moment at the support and at the location of the maximum positive bending moment respectively

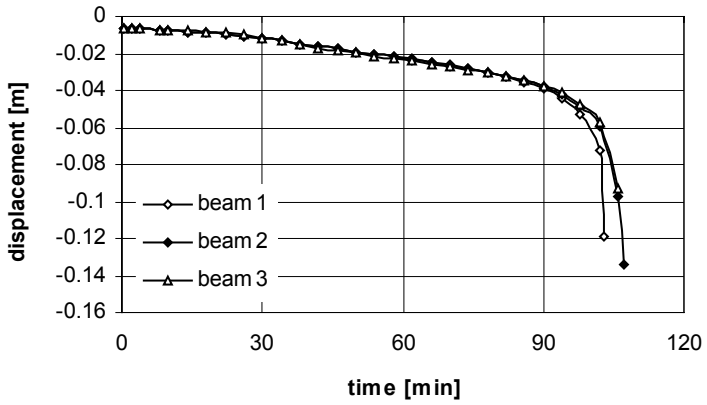

Figure 6.6: Vertical displacement of the span at the location of the maximum positive bending moment

Beam 1

The bending moment for beam 1 increased initially at the centre support and consequently decreased in the span. This increase was caused by the thermal bowing effect, as the beam wants to bow and thus lift from the end supports. Due to the continuity over the support this rotation was disabled and resulted in an increasing bending moment. The bending moment reached its maximum at about 46 minutes. At this time the top reinforcement bars at a distance of 1.25 m from the inner support (only two reinforcing bars were present at the top of the beam) started to yield in tension. After that time, the bending moment remained reasonably constant.

The deflection of beam 1 increased linearly until about 96 minutes, then a plastic hinge started to form in the midspan and the vertical deflection increased rapidly afterwards. Beam 1 failed after 103 minutes. This was when the bottom reinforcement at the location of the maximum positive bending moment yielded in tension and consequently formed a failure mechanism.

The deflected shape of the beam at failure is shown in Figure 6.7. It can be seen that the beam acted like a cantilever over the inner support, carrying the spans like pin supported beams, as the plastic hinges formed at the termination point of the top reinforcement (points (a) in Figure 6.7).

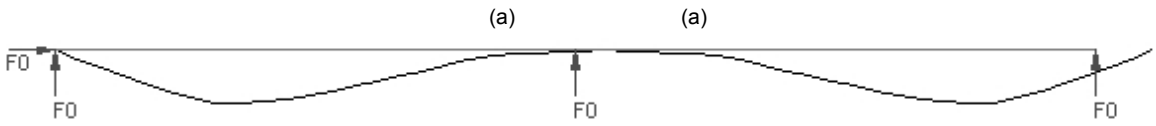

Figure 6.7: Deflected shape of beam 1 at failure

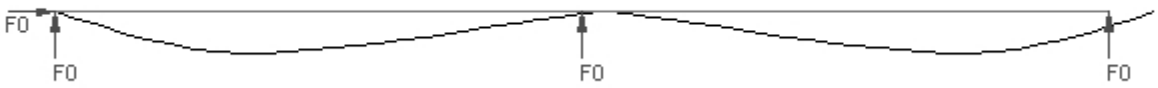

Figure 6.8: Deflected shape of beam 3 at failure

Beams 2 and 3

Beams 2 and 3 showed a slightly different behaviour during the fire exposure. The bending moments at the supports also increased at the initial stage of the fire due to the

thermal bowing, but higher values were reached at the inner support compared to beam 1. This increase is due to the elongation of the top reinforcing bars, which made the beams stiffer in bending at the supports and thus shortened the parts of the span which were free to bow.

This rise in the support bending moment led the top reinforcement at the support exceed its tensile proportional limit during the early stages of the fire and some bars started to yield in tension. Different to beam 1, the increase in bending moment did not led the reinforcing bars to yield at their termination points. The maximum bending moment for beam 2 was reached at about 53 minutes and for beam 3 at about 50 minutes. For beam 3 this was when all bars reached the tensile yield limit. After reaching the maximum, the bending moment kept reasonably constant until it decreased slightly after 70 minutes. For beam 2, the bending moment increased again at the final stages of the analysis which finally caused all top reinforcing bars at the support to yield in tension. This increase was caused by a redistribution of the bending moment, as a plastic hinge formed at the location of the maximum positive bending moment in the span. This redistribution was not possible for beam 3, as the flexural capacity at the support had already been reached before. The beams failed, when the bottom reinforcement in the span finally yielded in tension.

The deflected shape of beam 3 at failure time is shown in Figure 6.8. The plastic hinges are visible at the centre support and in both spans. The deflected shape for beam 2 is equivalent to that of beam 3.

Beam 2 failed after 107 minutes, whereas the analysis for beam 3 terminated after 106 minutes. This shows that the additional length of the top reinforcement at the centre support did not have a positive effect on the fire resistance of the analysed beam. The lengthening of the reinforcement led to an increased support bending moment, which led beam 3 to reach its flexural strength at a slightly earlier stage during the analysis.

Stresses in the reinforcing bars

As an example, the stresses in the reinforcing bars of beam 2 are shown in Figure 6.9 and Figure 6.10 at the inner support and at the location of the maximum positive bending moment in the span, respectively. The stresses for the other two beams showed similar behaviour.

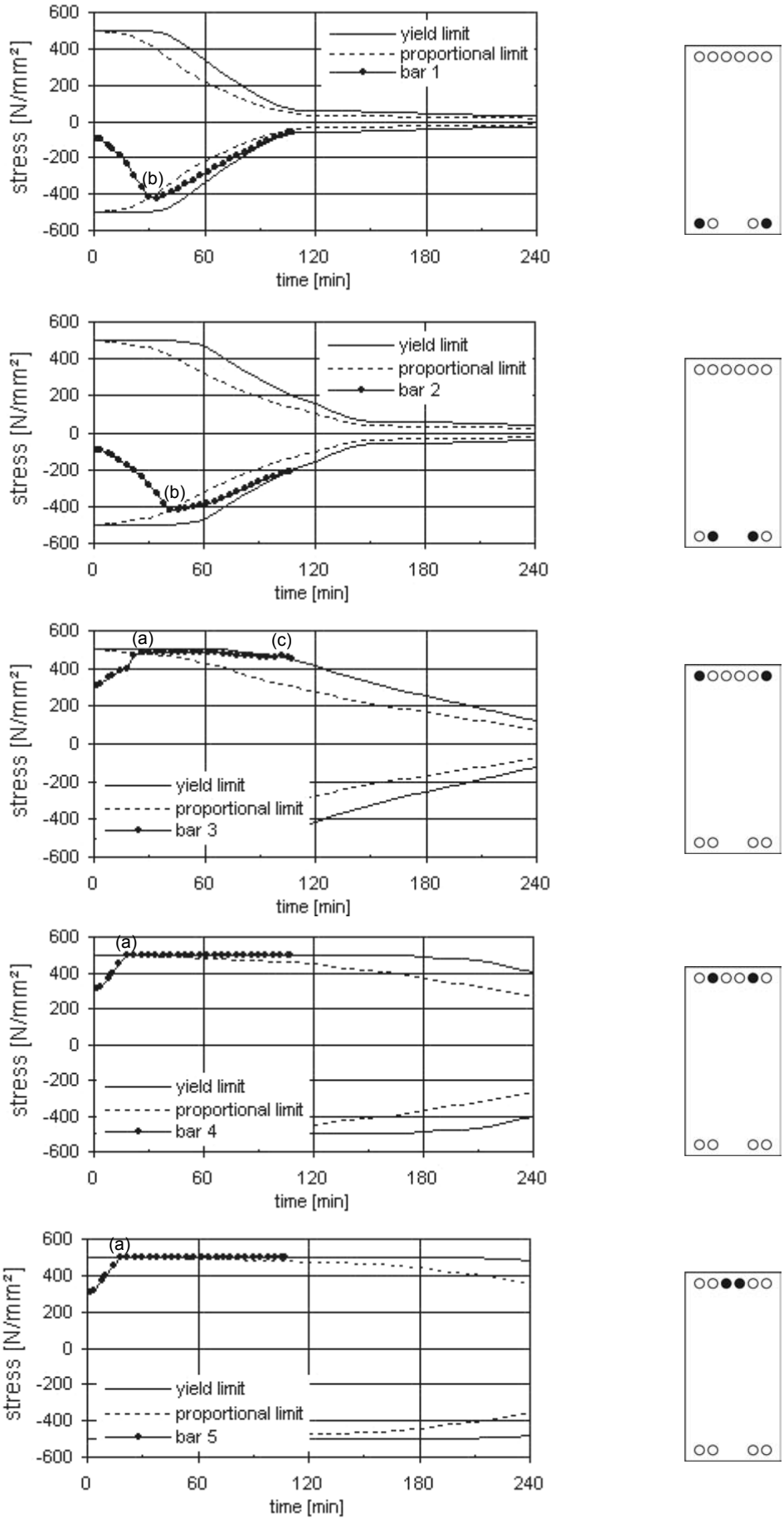

Figure 6.9: Stresses in the reinforcing bars at the centre support for beam 2 (tension positive)

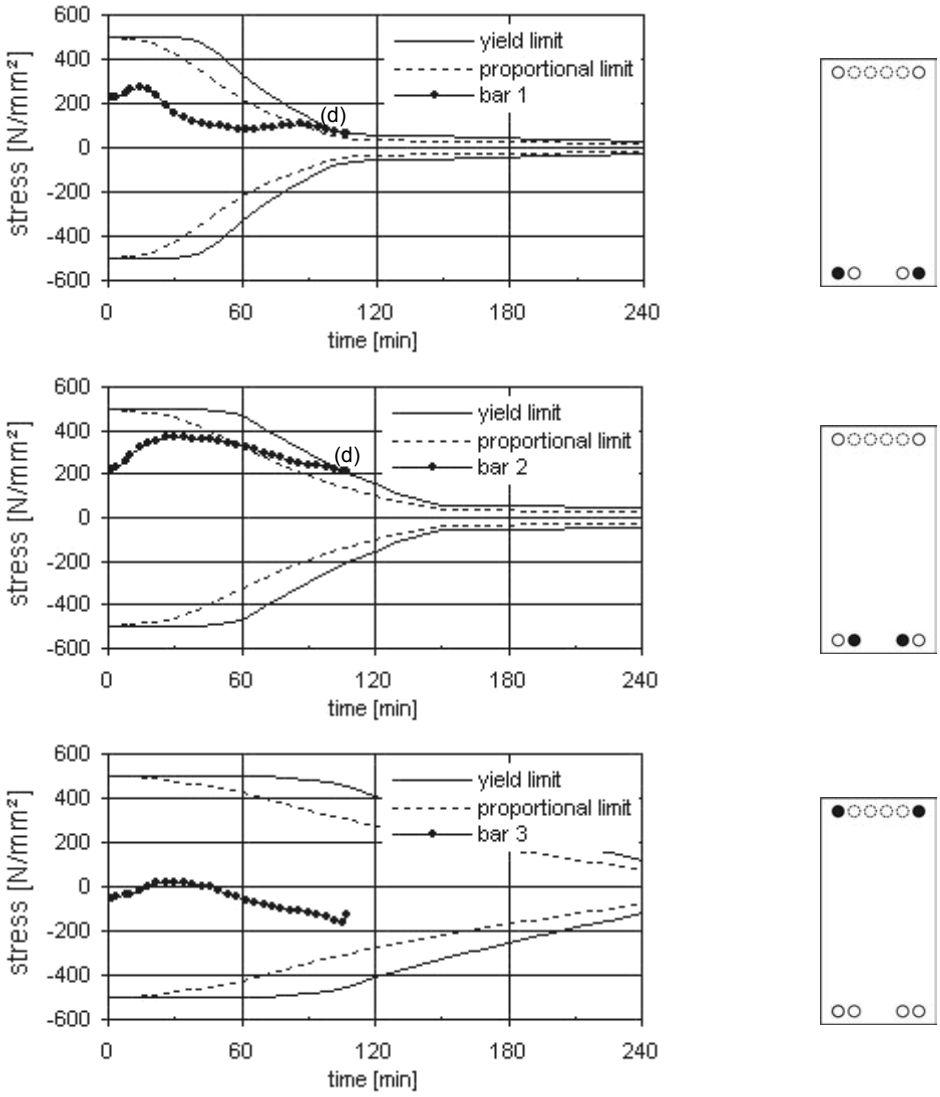

Figure 6.10: Stresses in the reinforcing bars at the location of the maximum positive bending moment for beam 2 (tension positive)

The top reinforcement bars at the centre support increased linearly in tension and reached their proportional limit after a short period of the fire exposure (at about 20 minutes) (points (a) in Figure 6.9) due to the increasing bending moment. Bars 4 and 5 started to yield in tension whereas the stresses in bar 3 stayed slightly below the yield limit.

The bottom bars at the support increased in compression until they exceeded the proportional compressive limit at 34 and 42 minutes respectively (points (b) in Figure 6.9), but this did not show any influence on the still increasing bending moment. The more rapid increase in compression of bar 1 is due to the thermally induced strains.

The bottom bars at the location of the maximum positive bending moment in the span initially showed tensile stresses which increased as the fire progressed, although the bending moment decreased. This increase was, as already stated in previous sections, due to the thermal expansion of the outer layers of the beam, which forced them into compression, as the inner, colder parts did not expand at the same rate. These compressive stresses had to be compensated by the steel bars. This initial increase can also be observed for the top bars in the span.

When a plastic hinge started to form in the span, the redistribution of the bending moment to the support led bar 4 finally reach its yield limit at the support (point (c) in Figure 6.9). Failure occurred when the bottom bars in the span yielded in tension (points (d) in Figure 6.10). At the final time step, even the top bars in the span showed a trend to go into tension. Along with the large increase in deflection at about 102 minutes as shown in Figure 6.6, these indicate that a plastic hinge was formed.

Tabulated data

According to the tabulated data of Eurocode (EC2-02) beam 2 and 3 have a fire resistance rating of 120 minutes. Following the rules of DIN 4102-4 (DIN-4102-4) beam 3 also has a fire resistance rating of 120 minutes. This rating could not be achieved by the analysis as the beams failed after 107 and 106 minutes respectively. However, a hand calculation according to the simplified calculation method stated in annex E of the Eurocode (EC2-02) using the temperature profiles given in annex A (EC2-02) could also not reach a fire resistance rating of 120 minutes. For a fire exposure of 90 minutes the stability criterion could be reached. It seems as if for this particular beam, which was designed at the limits of the values of the tabulated data, the different methods stated in the Eurocode show a slight inconsistency in the fire resistance ratings. The calculations following the simplified calculation method are shown in Appendix A.4.

Axial restraint

Due to the relatively poor behaviour of the continuous beams without horizontal restraint, two analyses were carried out with beam 2 restricting the horizontal movement with a spring restraint of 1% and 25%, respectively, to allow for a situation more representative of real structures.

The failure mode was not analysed in detail, but failure did occur after 209 minutes for the beam with 1% spring-stiffness and after 214 minutes for the beam with 25% spring-stiffness. Thus, the provision of some amount of horizontal restraint was very beneficial to the beam's behaviour, as it far exceeded the fire resistance rating of 120 minutes stated in the tabulated data.

Conclusions:

- Compared to a simply supported beam, a continuous beam showed better performance during the fire exposure.
- It is necessary to increase the length of the reinforcing bars at the supports in order to prevent yielding of the reinforcing bars at the termination point. The analysis showed that the length of the bars in beam 2 was sufficient to prevent failure occurring at the termination point.
- According to the results of the analysis, the difference in the fire resistance rating for beams which are designed without considering the additional length for the top reinforcing bars compared to those with lengthened bars can be neglected.
- The fire resistance rating of 120 minutes given in the tabulated data of DIN and Eurocode could not be reached during the analysis, but calculations according to the simplified method of Eurocode also predicted a fire resistance rating less than the tabulated data. According to the simplified method the beams can sustain the load for at least 90 minutes, this value was exceeded during the analysis with SAFIR.
- Axial restraint is very beneficial to the structure, therefore in a real structure, where some amount of restraint will always be available, the fire rating given in the tabulated data can be achieved.

6.2 Continuous three-bay beam

This section analyses the behaviour of a reinforced concrete beam which is continuous over two supports. The end supports are pin-connected and only one support is horizontally restrained. The single bays each span 6 metres. The cross-section and material properties are equivalent to those stated in section 5.1 and 5.3.1, only the number of reinforcing bars is adjusted to the structural behaviour of a three-bay beam and the length of the single beam elements is adjusted to the length of the reinforcing bars. All three bays are heated on three sides during the analysis. The layout of the beam is shown in Figure 6.11.

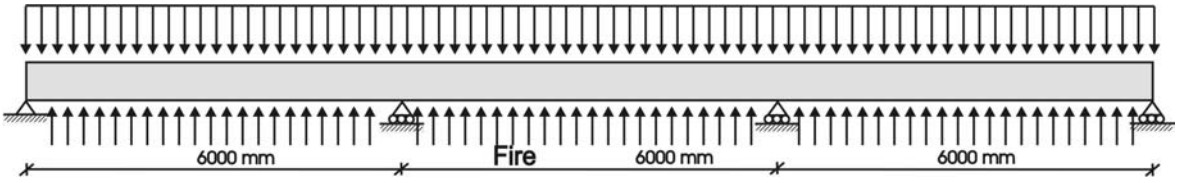

Figure 6.11: Layout of the three-bay beam

Three different beams are analysed:

BEAM 1

Beam 1 is designed according to the design rules of DIN 1045-1 (DIN-1045-1) without considering the case of a fire. Figure 6.12 shows the resultant reinforcement for beam 1. As the beam is reinforced symmetrically, only half of the beam is shown. Again, the development length has not been taken into account for any of the beams.

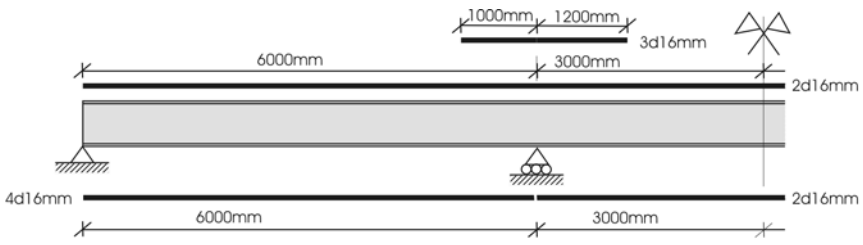

Figure 6.12: Arrangement of reinforcing bars of beam 1

BEAM 2

Beam 2 is also designed according to DIN 1045-1 (DIN-1045-1) but the design regulations following Eurocode 2 (EC2-02), as already stated in section 6.1, are taken into account. This results in an additional length of the bars for the edge bay of 45 cm and 25 cm for the inner bay compared to beam 1. Figure 6.13 shows the arrangement of the reinforcing bars for beam 2.

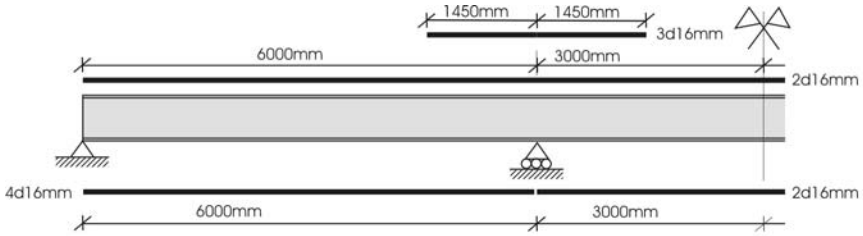

Figure 6.13: Arrangement of reinforcing bars of beam 2

BEAM 3

Beam 3 follows the regulations of „DIBt-Richtlinie zur Anwendung von DIN V ENV 1992 -1 -2 in Verbindung mit DIN 1045-1“ (DIBt-02). Consequently the reinforcing bars are further lengthened compared to beam 1 and beam 2. The resultant lengths of the bars are shown in Figure 6.14.

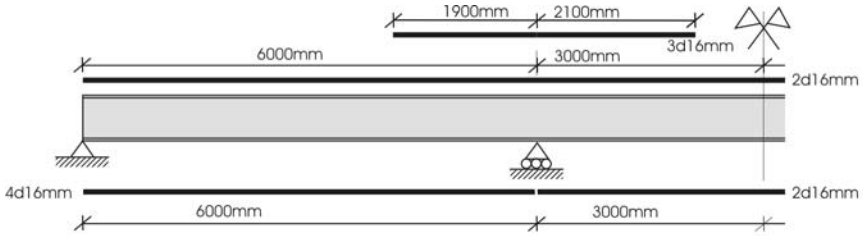

Figure 6.14: Arrangement of reinforcing bars of beam 3

Bending moments

Figure 6.15 to Figure 6.17 show the development of the bending moment for the three different beams at the inner supports, at the centre of the centre bay and at the location of the maximum positive bending moment at the outer bay respectively.

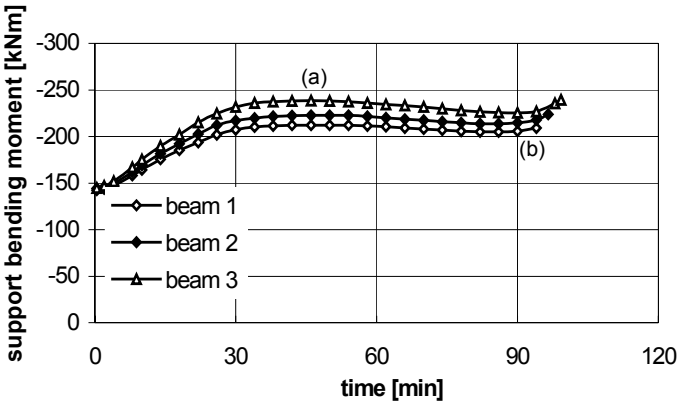

Figure 6.15: Bending moment at the inner support

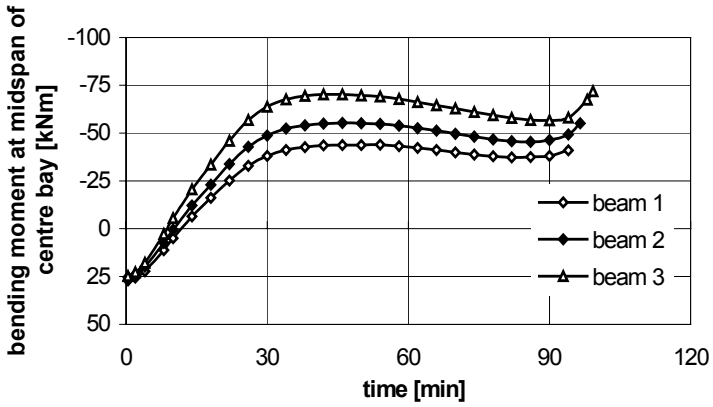

Figure 6.16: Bending moment at midspan of centre bay

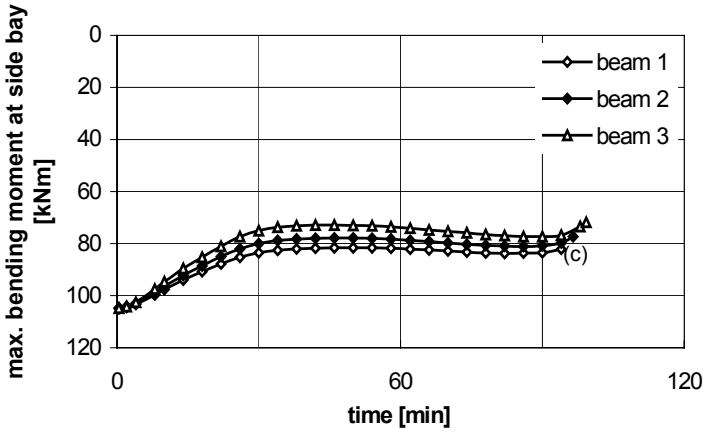

Figure 6.17: Maximum bending moment at the side bay

All beams showed an initial increase in the bending moment at the inner supports, due to the thermal bowing effect, followed by a slight decrease after about 50 minutes (point (a) in Figure 6.15). Towards the end of the analysis the support bending moments increased again (point (b) in Figure 6.15). It can be seen that the lengthening of the top reinforcement led to higher bending moments at the supports as has already has been observed for the two-bay beams. The bending moments of the spans showed equivalent trends due to the unchanged load. Figure 6.16 shows that for the inner span, the bending moments became negative as the fire progressed. For example, the shape of the bending moment at the final time of the calculation for beam 2 is plotted in Figure 6.18.

Figure 6.18: Shape of the bending moment of beam 2 at the end of the analysis

Displacements

The displacements at the outer bay and the centre of the inner bay are shown in Figure 6.19 and Figure 6.20 respectively. The different beams gradually deflected downwards linearly at the same rate at the outer bay. By the time failure occurred, the deflection rate had increased rapidly.

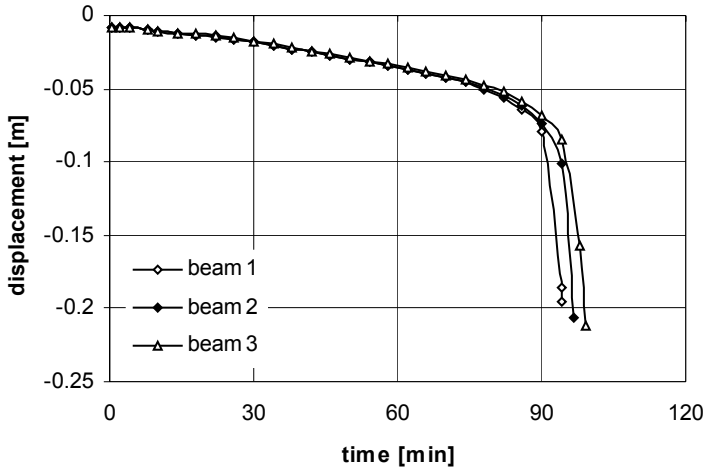

Figure 6.19: Displacement at outer bay

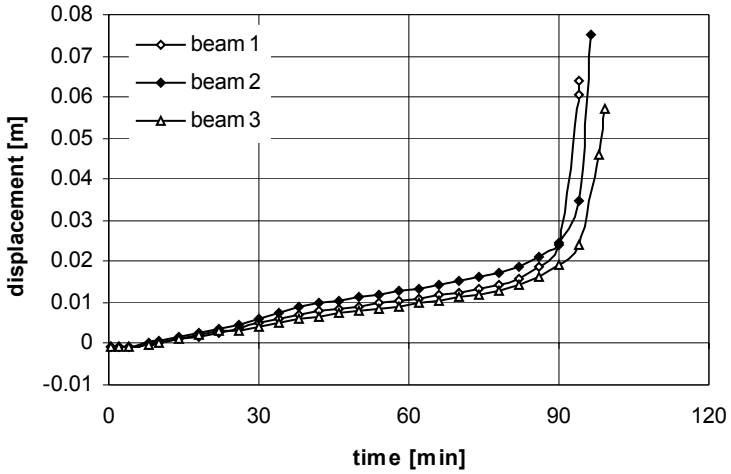

Figure 6.20: Displacement at inner bay

The centre bays of the beams showed an upward movement during the analysis, as the bending moment at the inner bay became negative. Beam 2 showed higher deflections compared to beam 1 due to the higher negative bending moment induced. However, beam 3 which was exposed to the largest negative bending moments did not show the largest deflections. This might be caused by the additional length of the top reinforcing bars which provided the beam with a higher stiffness in such a way that the increased bending moment did not result in the largest deflections.

Beams 1 and 2

Beams 1 and 2 showed similar behaviour during the fire exposure. For both beams the initial increase in the support bending moment led the top reinforcement at the support to get close to its tensile strength limit, but only one bar started to yield. At the location at the centre bay where the reinforcing bars were curtailed and only two bars were present at the top of the beam, the bars almost yielded in tension by the time the maximum bending moment was reached. As the bending moments dropped slightly, the stresses in the bars reduced as well.

At the final time steps, all bottom reinforcing bars at the location of the maximum positive bending moment in the outer span had exceeded the proportional tensile strength limit and started to yield in tension, forming a plastic hinge. This plastic hinge formation was followed by a redistribution of the bending moment to the inner supports. This

redistribution can be seen in the slight decrease in positive bending moment (point (c) in Figure 6.17) and the increase in the support bending moment (point (b) in Figure 6.15). The increase in the support bending moment also led to an increase of the negative bending moment for the centre span. This general increase in bending moment could be accommodated by the reinforcing bars at the support, which increased in tensile stress but did not all yield. In contrast, the flexural strength was reached in the centre bay at the location where the reinforcing bars were curtailed. Thus, the top reinforcement yielded in tension forming a plastic hinge and consequently a mechanism in the beam. By the time, the plastic hinges formed, the displacements in the spans increased rapidly. Failure occurred for beam 1 after 94 minutes and beam 2 sustained the applied loads for 96 minutes. The deflected shape of beam 2 at failure time is shown in Figure 6.21. The plastic hinges (ph) are indicated.

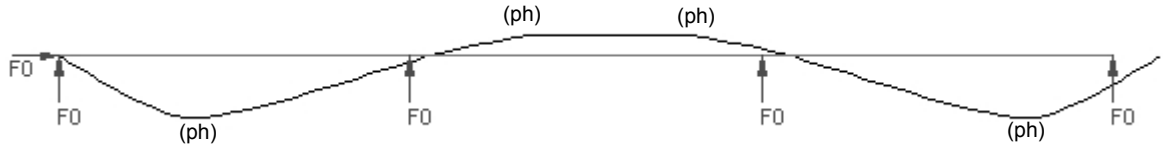

Figure 6.21: Deflected shape of beam 2 at the final time step

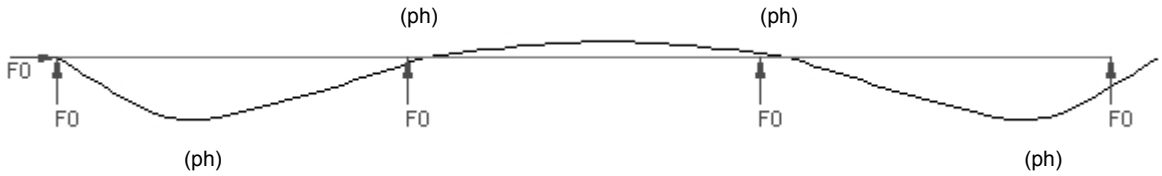

Figure 6.22: Deflected shape of beam 3 at the final time step

Beam 3

The longer top reinforcement of beam 3 compared to beams 1 and 2 resulted in a slightly different behaviour of the beam during the fire exposure. The longer reinforcement led to higher support bending moments induced by the thermal bowing effect. These higher moments caused the top reinforcement bars at the inner supports to get close to their yield limit, but they did not yield in tension initially. When the bottom reinforcement in the

outer span started to yield in tension and a plastic hinge formed, the bending moment was redistributed to the supports. For beam 3 the reinforcing bars at the inner span were long enough to prevent failure at the location where the bars were terminated as the bending moment increased, thus the increase in bending moment led the top reinforcement at the inner supports to yield in tension. Figure 6.22 shows the deflected shape of beam 3 at the final time step with the locations of the plastic hinges. The beam sustained the fire exposure for 99 minutes and thus showed the best behaviour of the three analysed beams.

Tabulated data

Beam 2 and beam 3 have a fire resistance rating of 120 minutes according to the tabulated data of Eurocode (EC2-02). This rating could not be achieved during the calculation process as the beams failed after 96 minutes and 99 minutes respectively. But again, the hand calculation according to the simplified calculation method stated in the Eurocode (EC2-02) only reached the stability criterion for 90 minutes, which was exceeded during the analysis.

Axial restraint

Due to the poor behaviour of the beams, two further analyses have been carried out with beam 3 allowing for horizontal restraint at the end support. Springs with 1% and 25% spring-stiffness were used to determine the fire resistance rating of the beams in a situation which is more likely to occur in real structures.

The horizontal restraint showed beneficial influence on the behaviour of the beams. The failure mode was not analysed in detail, but the beam with 1% spring-stiffness survived the fire exposure for 141 minutes and for the beam with 25% horizontal restraint the analysis continued for more than 175 minutes. Thus, the provision of some amount of restraint led the beam exceed the fire resistance rating of 120 minutes stated in the tabulated data.

Conclusions:

- The elongation of the top reinforcement bars at the support showed a slight positive effect on the fire endurance of the three-bay beams as the beam with the longer reinforcement sustained the fire for longer time periods. The length of the reinforcing bars of beam 3 was needed to prevent yielding at the termination point of the reinforcement, but the lengthening of the bars did not greatly improve the fire resistance rating, as all beams failed within a time range of 5 minutes.
- Compared to the two-bay beams analysed in section 6.1, the three-bay beams failed earlier while exposed to the ISO-fire.
- Compared to the simply supported beam, the continuity over the supports did not result in a great improvement of the fire resistance rating, as the simply supported beam failed after 87 minutes, while the three-bay beams failed after 94, 96 and 99 minutes.
- The provision of some amount of restraint led to a great increase in the fire resistance rating, exceeding the rating of 120 minutes stated in the tabulated data, which could not be reached for the unrestrained beams.

7 NUMERICAL ANALYSIS OF REINFORCED CONCRETE BEAMS SUBJECTED TO ISO-FIRE WITH A DECAY PHASE

The ISO fire used in the previous analyses is increasing in temperature during the whole fire exposure. As it is not very likely for a real fire to last for four hours with constant increase in temperature, this section deals with ISO-fires growing for 30, 60, and 90 minutes followed by a decay phase. The beams analysed include the one-bay, two-bay and three-bay beam, all with pinned supports but without horizontal restraint. The beams chosen are those which sustained the 4-hour ISO-fire for the longest time period.

The decay phase is modelled according to the specifications of the Eurocode for the decay phase of parametric fires. The decay rate is equal to 625°C per hour for fires with a burning period less than half an hour and decreases to 250°C per hour for fires which increase for more than 2 hours. The decay rate is shown in Figure 7.1 and the resulting fire temperatures are shown in Figure 7.2.

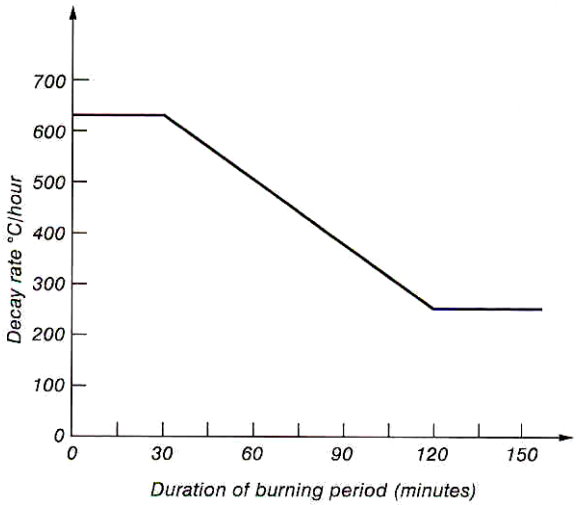

Figure 7.1: Rate of temperature decay in Eurocode parametric fires (Buc-01)

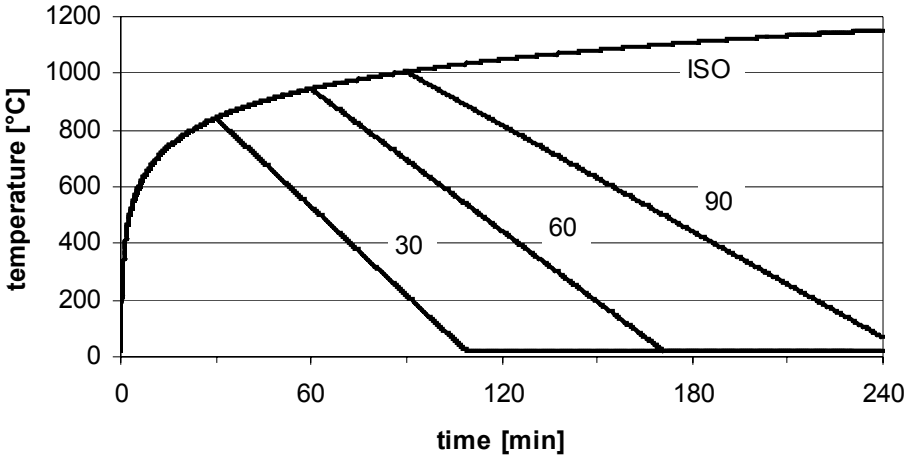

Figure 7.2: Fire temperatures during ISO-fires with decay phase

7.1 Thermal analysis

This section shows the temperature development in the reinforcing bars for the two-bay beam for the three different fires. The temperatures for the steel bars in the one-bay and three-bay beams are similar.

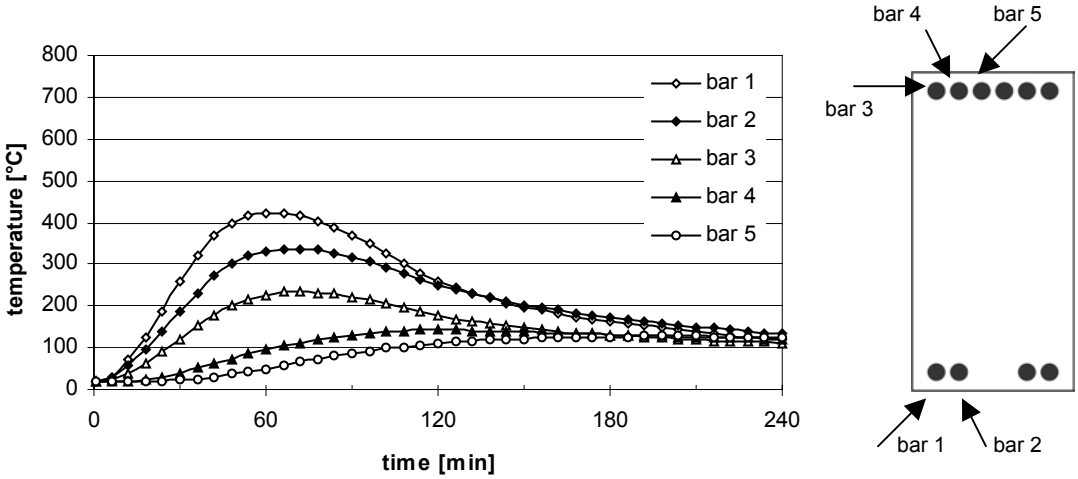

Figure 7.3: Temperatures in the reinforcing bars for 30 min ISO fire with decay phase

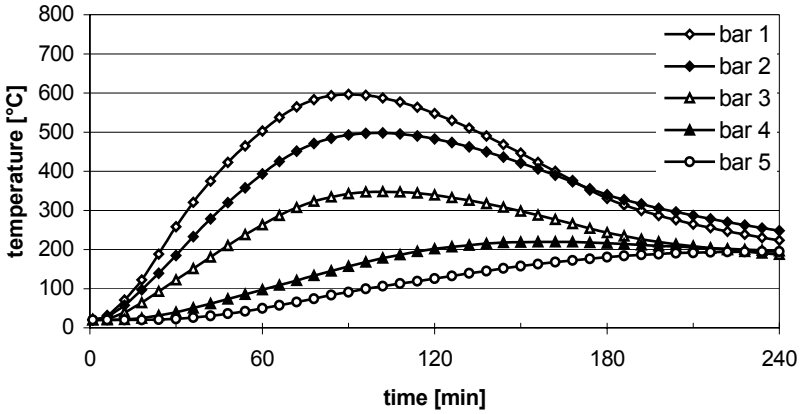

Figure 7.4: Temperatures in the reinforcing bars for 60 min ISO fire with decay phase

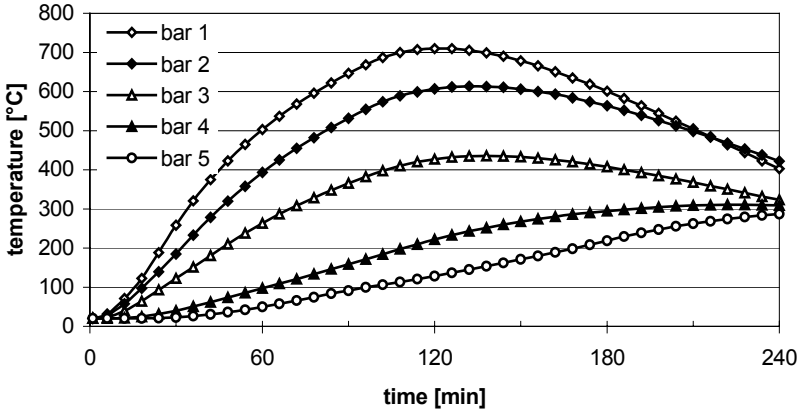

Figure 7.5: Temperatures in the reinforcing bars for 90 min ISO fire with decay phase

It can be seen in all three cases, that the temperatures in the steel bars still continued to increase after the fire temperature has begun to decrease. This is due to the concrete which still conducts heat from the outer layers to the cooler inner parts as long as the outer layers are hotter.

The bottom bars (bar 1 and 2) and the outer top bar (bar 3) showed a general decrease in temperature about 30 minutes after the fires went out. The temperatures in the inner top bars increased during the whole calculation period, as the heat flow was still directed inwards due to the quite cold centre of the cross section. This increase in temperature slowed down for the 30 and 60 minute fires in the final minutes. At the end of the analysis for the 30 minutes fire, the temperatures in all the steel bars reached almost the same value.

7.2 Structural analysis

7.2.1 One-bay beam

The statically determinate single bay beam, spanning 6 metres, subjected to the different fires showed a good behaviour during the analysis for the 30 and 60 minute fire as failure did not occur during the calculation time of 4 hours. Under the ISO fire the beam failed after 87 minutes, thus the investigation of a 90 minutes decay fire would not give any different results.

Figure 7.6 shows the deflection at the centre of the beam for the different fire exposures. For comparison, the deflection for the 4-hour ISO-fire is plotted as well.

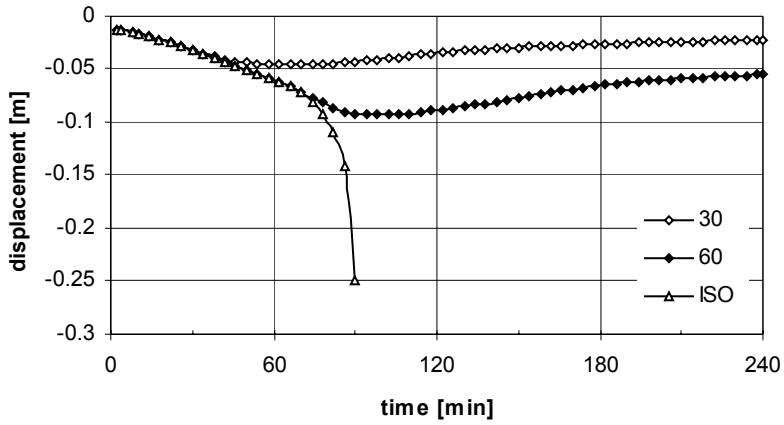

Figure 7.6: Deflection at the centre of the one-bay beam for the different fires with decay phase.

The beams deflected downwards as the temperatures increased. By the time the fire temperatures began to decrease, the deflection rate slowed down as the temperatures in the steel bars still increased and thus their strength still dropped, but at a slower rate compared to the 4-hour ISO-fire. The maximum deflection was reached when the maximum temperatures in the bottom bars were reached as well. This was at about 60 minutes for the 30 minute fire and at about 80 minutes for the 60 minute fire. Afterwards, the deflections decreased gradually as the steel regained its strength, the temperatures across the section got more uniform and the steel and concrete started to contract.

Stresses in reinforcing bars

Figure 7.7 shows the stresses in the reinforcing bars for the beam which was subjected to the 60 minute fire.

The initial increase in the tensile stresses of the bottom bars is, as stated already in section 5.3.2, due to the expanding outer concrete layers. These went into compression as their elongation was restrained by the cooler inner concrete fibres, which consequently had to go into tension. As the concrete fibres cannot take any tensile stress, this tension had to be carried by the reinforcing bars. The tensile stress in the outer bottom bar (bar 1) decreased after about 18 minutes (point (a) in Figure 7.7). This drop in tensile stress might be caused by the increasing temperature of the bar which reduces the difference in expansion between the surrounding concrete and the bar and thus leads to a decrease in the induced tensile stress, as well as the higher reduction in strength and modulus of elasticity due to the higher temperatures compared to the inner bars. This decrease had to be accommodated by the other reinforcing bars which carried on increasing stress until they reached their proportional limits (point (b) in Figure 7.7). This limit was reached first for bar 3 as this one was the coldest and thus the stiffest one, attracting most of the stress. As the strength and the modulus of elasticity of the inner bars dropped due to the rising temperatures, the outer bar had to increase in tension in order to enable the beam to sustain the imposed load.

All bottom bars nearly reached the yield limit by the time the steel bars showed the maximum temperature (point (c) in Figure 7.7), but failure did not occur. As all bars reached values between the proportional limit and the yield limit, they all experienced plastic deformations, which resulted in some permanent deflections, as can be seen in Figure 7.6. By the time the temperatures decreased, the tensile stresses for the inner bars (bar 2 and 3 in Figure 7.7) dropped, but the corner bar (bar 1) was forced into high tensile stresses almost reaching the yield limit (point (d) in Figure 7.7). This behaviour can basically be explained by the plastic strains the steel bars exhibited during the fire. Figure 7.8 shows that the thermal expansion of the outer bar was higher than for the inner bars due to the higher temperatures. Thus, the plastic strains developed in the bars to obtain equal total strains were larger in the inner than in the outer bars, if the contribution of the elastic strain is assumed to be equal in both bars. When the temperatures decreased, the thermal strains were reduced and the difference in total strain mainly resulting from the plastic strains had to be accommodated.

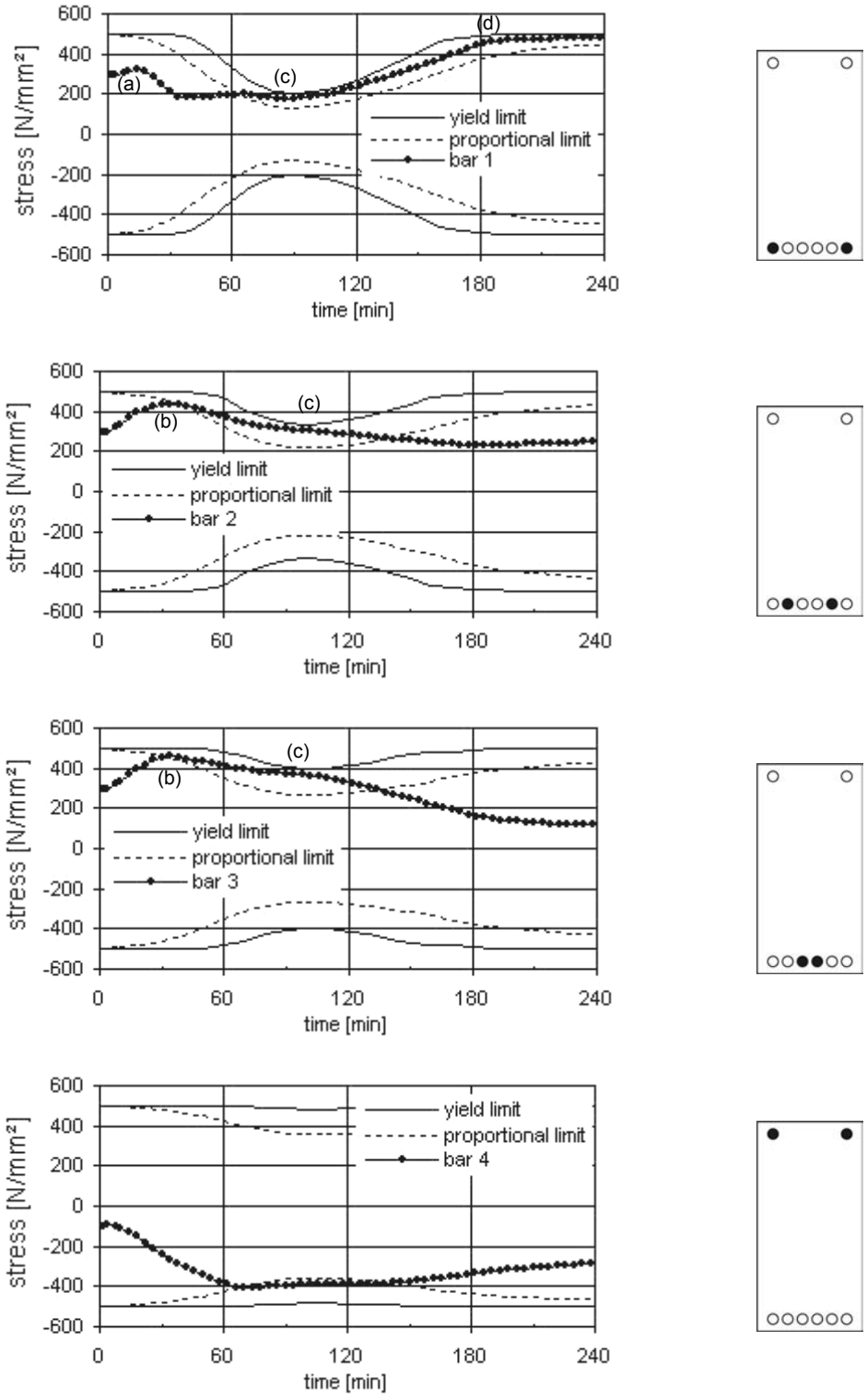

Figure 7.7: Stresses in the reinforcing bars for the beam with 60 minutes fire with decay phase (tension positive)

This was only possible with a lengthening and thus an increase in tensile stress of the outer bars and a shortening and thus compressive stresses for the inner bars. Additionally the complex processes in steel and concrete occurring at elevated temperatures, influencing the materials mechanical and thermal properties will effect this behaviour as well.

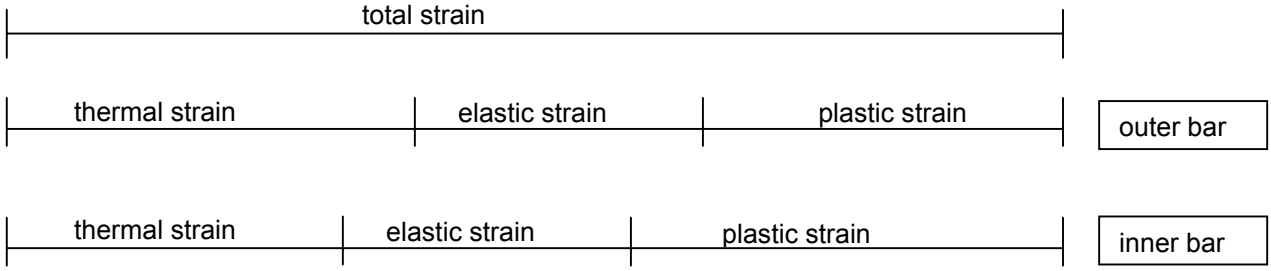

Figure 7.8: Indicative strains in the reinforcing bars at a given time during the analysis

7.2.2 Two-bay beam

The beam analysed within this section is the same as beam 2 of section 6. The beam was exposed to fires with a decay phase for 30, 60 and 90 minutes. For the purpose of comparison, the data for the 4-hour ISO-fire is also plotted in the following figures. The two-bay beam could sustain the fire for 30 and 60 minutes, but the beam subjected to the 90 minute fire failed during the analysis.

Bending moments

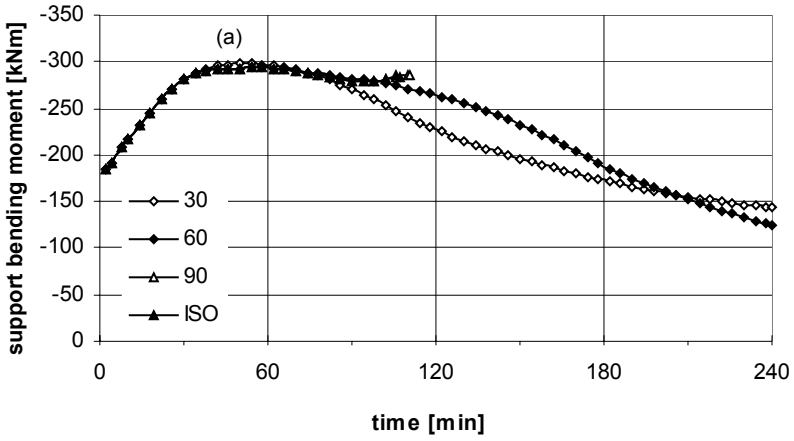

Figure 7.9: Bending moment at the support for different fires with decay phase

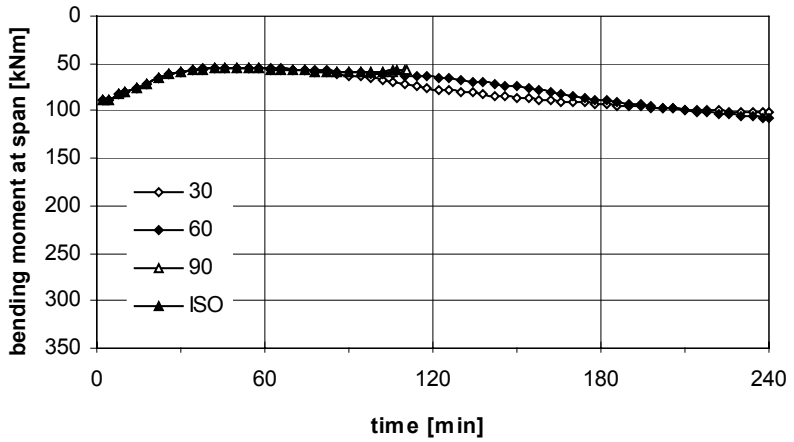

Figure 7.10: Maximum bending moment at the span for different fires with decay phase

Figure 7.9 and Figure 7.10 show the development of the bending moment at the inner support and at the span for the different fires with a decay phase. The bending moments at the inner support shown in Figure 7.11 are derived from the analyses without imposing a mechanical load on the beam and show the effect of thermal loading only.

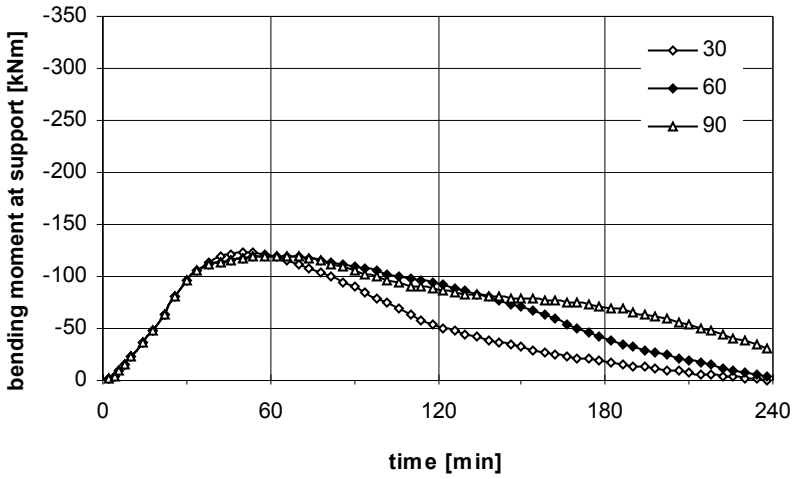

Figure 7.11: Bending moment at the support for different fires with decay phase without mechanical loads

The bending moments at the inner support increased initially due to the thermal bowing effect. The beam subjected to the 30 minute fire showed the highest bending moment, which was reached at about 50 minutes (point (a) in Figure 7.9). This increase is consistent with the bending moment only induced by thermal loading, which also reached its peak after 50 minutes for the 30 minute fire. The beams with 60 and 90 minute fires reached their peak bending moment at about 60 minutes. As the decay phase had not started for both of the beams, the values reached were equal. In contrast to the beam exposed to the 30 minute fire, the bending moment for the other two beams did not show an increase after the fire went out, but decreased after reaching the peak value. The beam subjected to the 90 minute fire followed the bending moment curve derived from the exposure to the 4-hour ISO fire and showed an increased support bending moment at the final time steps, as moment redistribution from the span occurred. This beam failed after 110 minutes, which means that the beam could sustain the imposed load 3 minutes longer than for the 4-hour ISO-fire. This is due to the slightly lower temperatures in the outer steel bars during the final time steps, which enabled the beam to sustain the load for some more minutes, but could not prevent failure.

The support bending moments for the beams with 30 and 60 minute fire exposure

decreased with a similar slope as the moments induced by thermal loading only (see Figure 7.9 and Figure 7.11). The thermally induced bending moments returned to zero at the end of the analysis, but the bending moments shown in Figure 7.9 dropped below their initial values. This drop might be due to plastic deformations that caused a permanent deflection on the beam that reduced its moment capacity.

Displacements

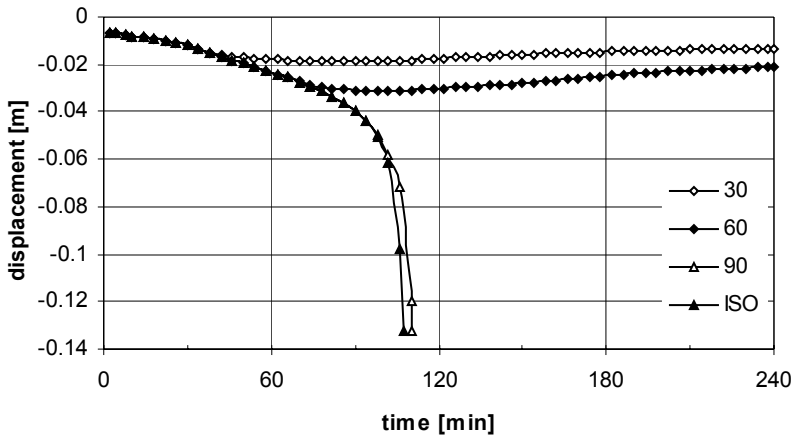

Figure 7.12: Displacements at the span for different fires with decay phase.

Figure 7.12 shows the displacements at the span for the two-bay beam subjected to different fires with decay phase. The deflections for the beams subjected to the fire for 30 and 60 minutes reached their maximum values at about 85 minutes and 100 minutes respectively. Afterwards, the deflection decreased gradually. The beam subjected to the 90 minute fire followed the deflection of the ISO-fire curve initially and showed run-away failure at the end of the analysis, which was slightly delayed, compared to the beam subjected to the ISO-fire due to the slightly lower temperatures in the reinforcing bars.

Stresses in reinforcing bars

The stresses in the reinforcing bars for the beam exposed to the 60 minute fire with decay phase are shown in Figure 7.14 and Figure 7.13 at the span and at the support respectively.

The stresses are equal to the ones shown in Figure 6.9 and Figure 6.10 and described in section 6.1 for the initial 60 minutes. It can be seen in Figure 7.13 that although the temperatures in the bottom reinforcing bars increased after the fire went out, the strength reduction in the bottom bars did not result in yielding of the reinforcement in the span. After the maximum steel temperatures were reached, the stresses in the outer bars increased in tension and the stresses in the inner bars decreased.

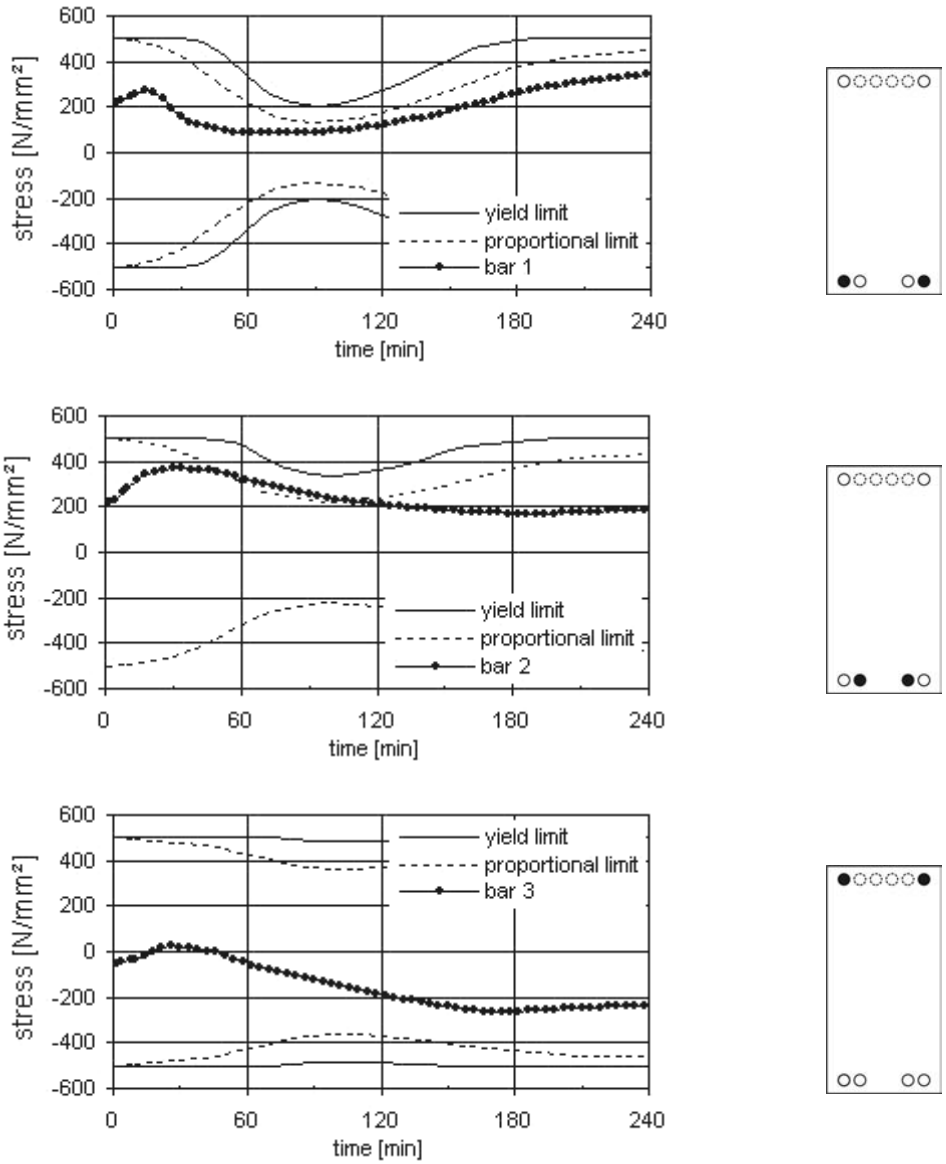

Figure 7.13: Stresses in the reinforcing bars at the span for the beam with 60 minute fire (tension positive)

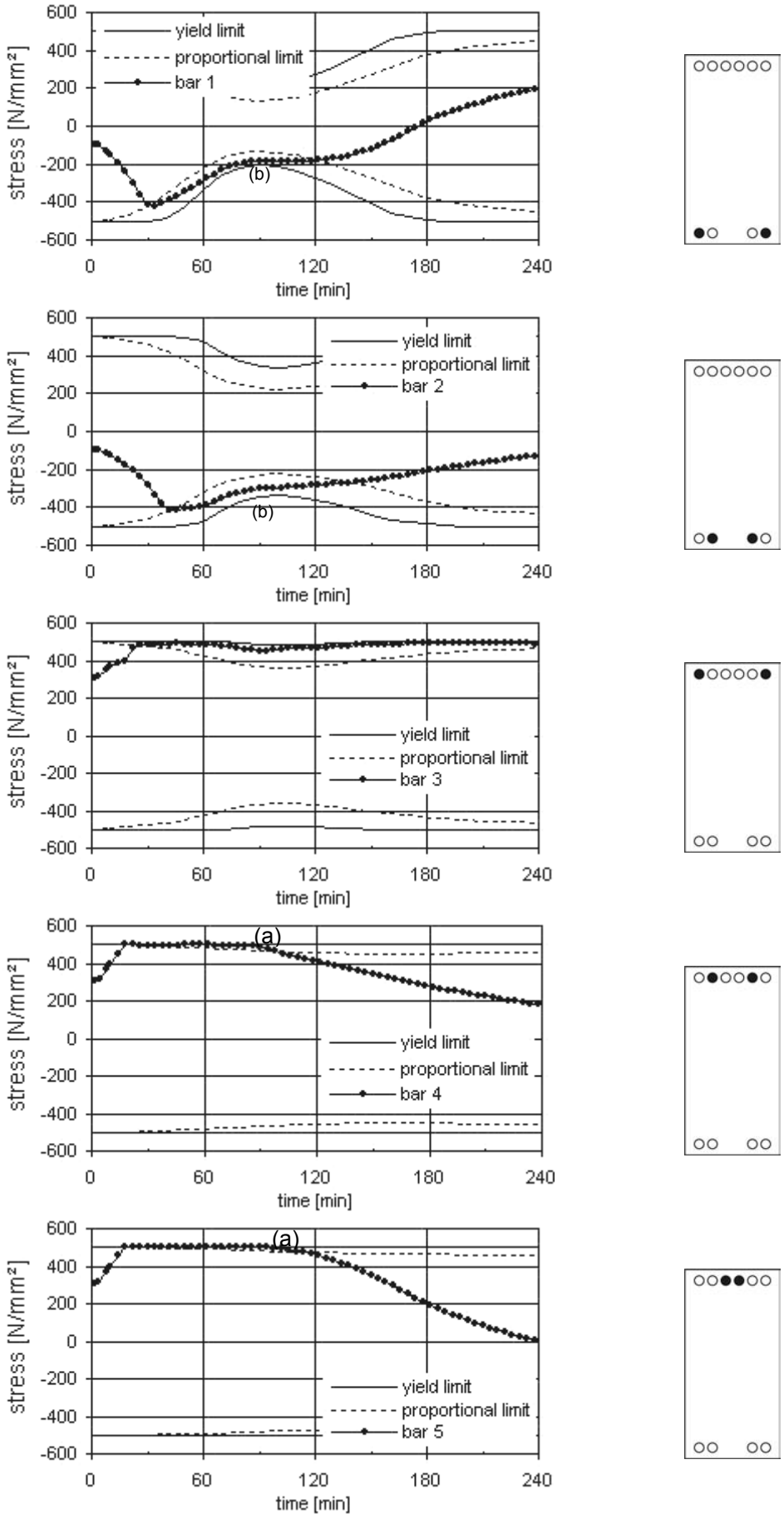

Figure 7.14: Stresses in the reinforcing bars at the inner support for the beam with 60 minutes fire (tension positive)

At the central support bars 4 and 5 yielded in tension and bar 3 showed values slightly below the yield limit during the early stages of the fire exposure. The stresses did not decrease until about 90 minutes after the start of the fire. Afterwards, the stresses in the inner bars decreased in a linear trend (points (a) in Figure 7.14), as the temperatures and thus the bending moment decreased as well. The stresses reached were below the bars initial values. In contrast, the stresses in the corner bars kept values close to the tensile yield limit.

The behaviour for the tensile reinforcement is equivalent to the one observed for the tensile reinforcement of the one-bay beam analysed in section 7.2.1 and is basically due to the difference in plastic strain exhibited during the fire exposure.

For the bottom bars at the support, the stresses nearly reached the compressive yield limit at the time when the highest temperatures in the bars occurred (points (b) in Figure 7.14). As the bending moment at the support dropped, the compressive stresses were reduced and eventually went into tension for the outer bar (bar 1), although this bar was surrounded by a complete compression block (see Figure 7.15).

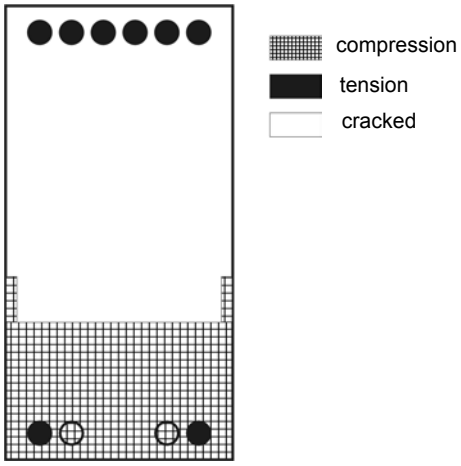

Figure 7.15: General stress distribution on the cross-section at the support at the end of the analysis for the 60 minute fire.

It is assumed that this behaviour of the compression reinforcement is also related to the plastic strains exhibited during the fire exposure but shows a slightly different behaviour due to the load imposed compressive stresses.

7.2.3 Three-bay beam

This section covers the analysis of a three-bay beam subjected to the ISO-fire for 30, 60 and 90 minutes with a following decay-phase, as described in section 7.1. The beam analysed is equal to the three-bay beam with the longest top reinforcing bars analysed in section 6.2 (beam 3). During the analysis all three bays were heated from the bottom and the sides.

The beams subjected to the 30 and 60 minute fire sustained the imposed load during the analysis period of four hours without collapse, while the beam subjected to the 90 minute fire failed after 99 minutes, as it did during the ISO-fire.

Displacements

The displacements of the beam at the outer span and at midspan for the different fire exposures are shown in Figure 7.16 and Figure 7.17 respectively.

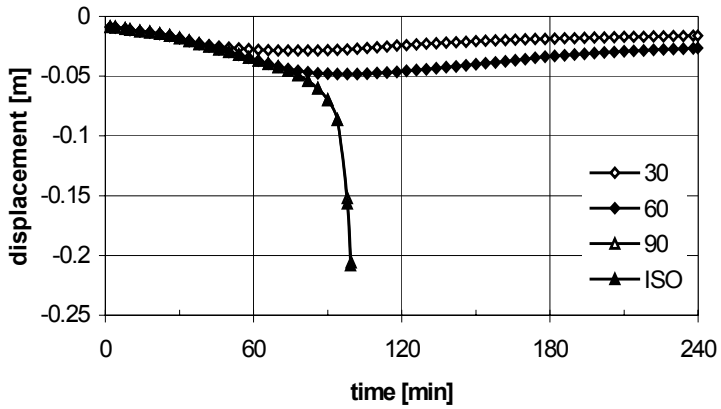

Figure 7.16: Displacements at the outer span for different fires with decay phase

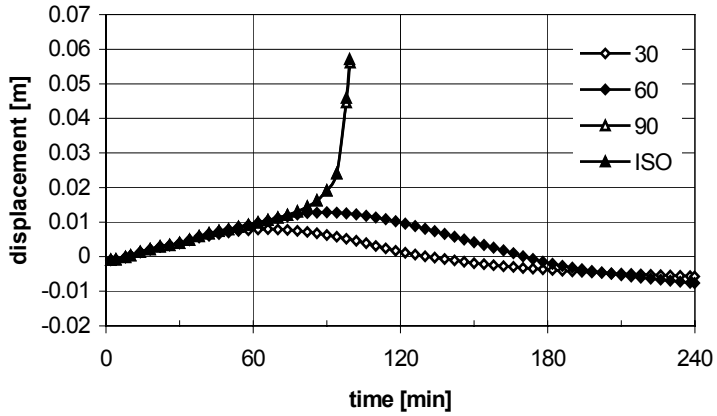

Figure 7.17: Displacements at the inner span for different fires with decay phase

It can be seen in Figure 7.16 that the beams deflected downwards in the outer span at the initial stages of the analysis. As the temperatures in the steel bars reduced and the concrete cooled down as well, the deflections for the beams with 30 and 60 minute fire exposure reduced gradually, but did not recover completely due to plastic deformations. The beam with 90 minute fire exposure followed the curve derived with the ISO-fire and showed run-away failure after 99 minutes.

The initial upwards movement of the inner bay (see Figure 7.17) reversed as the temperatures dropped. The beams then deflected downwards gradually and exceeded the initial downwards displacement. This was due to plastic deformations occurring at the supports which were higher for the beam with 60 minute fire exposure and thus led to higher resultant deflections in that beam.

Bending moments

The development of the bending moments at the inner supports, the centre of the inner span and the outer span are shown in Figure 7.18 to Figure 7.20. The bending moment at the support increased initially. At about 40 minutes the beams reached their maximum bending moment, which was the highest for the beam with 30 minutes fire exposure, although the fire for that beam had already gone out. The bending moment dropped gradually afterwards for the beams with 30 and 60 minute fire exposure, whereas the beam with 90 minutes fire exposure followed the curve derived with the ISO-fire. This beam failed as the moment was redistributed from the outer span to the support. The bending moment at the support for the beams with 30 and 60 minute fire exposure dropped below their initial values at the end of the analysis due to plastic deformations at the supports, as has already been observed for the two-bay beams. The bending moments at the centre and the outer bay followed the behaviour of the bending moment at the support due to the unchanged load.

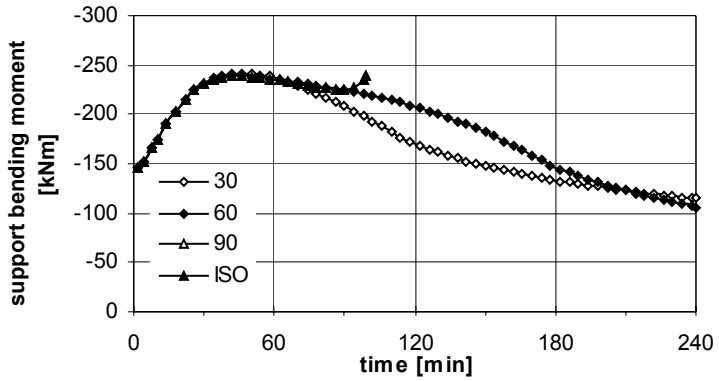

Figure 7.18: Bending moment for the three-bay beam at the support for different fires with decay phase

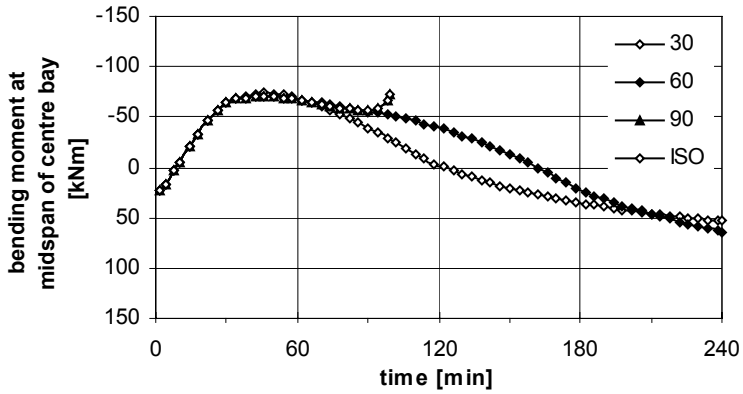

Figure 7.19: Bending moment for the three-bay beam at the inner span for different fires with decay phase

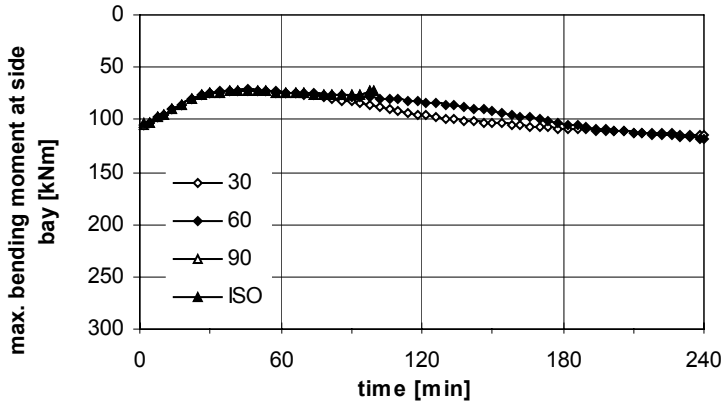

Figure 7.20: Bending moment for the three-bay beam at the outer bay for different fires with decay phase

Stresses in reinforcing bars

The stresses in the reinforcing bars showed similar behaviour to the stresses shown for the one-bay and two-bay beams in sections 7.2.1 and 7.2.2 and therefore are not shown explicitly.

Conclusions:

The analyses of the one to three-bay beams subjected to ISO-fires for 30, 60 and 90 minutes with a decay phase have shown:

- The temperatures in the steel bars still increase at a reasonable rate after the fire goes out.
- The concrete beams showed a good structural behaviour during the more realistic fire conditions. Failure only occurred when the start of the decay-phase of the fire was close to the failure time reached during the ISO-fire.
- The different number of spans did not appear to have great influence on the beams behaviour.
- The deflections occurring during the fire exposure were mainly recovered at the end of the analysis. Only small permanent deflections could be observed.
- The stresses in the reinforcing bars did not return to their initial stress level. High residual tensile stresses can be induced into the bars during the decay phase of the fire.

8 CONCLUSIONS AND RECOMMENDATIONS

8.1 Conclusions

This research project was conducted to study the effect of various support conditions on the fire behaviour of a reinforced concrete beam with a rectangular cross-section. Analyses were carried out on the behaviour of single span beams with pinned and rotationally restrained supports, allowing for varying levels of horizontal restraint in both cases. The effect of continuity was studied with beams spanning over two and three bays. Within this analysis, the influence of different length of top reinforcement at the supports was investigated. These beams were subjected to the ISO-fire for a duration of four hours. Implementing the full process of a fire development, the behaviour of one, two and three-bay beams during the exposure to a growing ISO-fire with a decay phase has also been analysed. The study was performed with 2D finite element analyses using SAFIR.

8.2 ISO-fire

8.2.1 Pin-supported single span beams

The analyses for the pin-supported beams have shown that horizontal restraint is usually beneficial to the beam's structural behaviour compared to an unrestrained beam. The axial force that developed due to thermal elongation acted like prestressing on the beam and improved its moment capacity. Best performance was obtained for beams with levels of horizontal restraint that were intermediate between zero and full restraint. Within real buildings almost all beams will have some intermediate level of axial restraint.

For high levels of restraint, the axial forces that developed during the fire exposure were very large and would have to be implemented into the design process of the surrounding structure in order to enable the beneficial behaviour to be achieved.

The SAFIR program was not able to predict the final failure time of the restrained beams, because of convergence problems near the time of failure. However, the highly restrained beams appeared to fail in compression while less highly restrained beams appeared to fail in tension.

The fire resistance rating obtained in the analysis for the unrestrained beam exceeded the value stated in Eurocode (EC2-02) and DIN (DIN-4102-4).

8.2.2 Rotationally restrained single span beam

The provision of full rotational restraint at the supports resulted in a large increase in the fire resistance rating compared to the pin-supported beams, as the redundant structure allowed for the redistribution of the bending moments. Horizontal restraint improved the beam's structural behaviour but the amount of restraint did not appear to have a great influence, as all beams with some amount of restraint sustained the fire for the four-hour fire exposure. The deflections occurring during the fire exposure were very small for the rotationally restrained beams.
The fire resistance rating stated in the tabulated data could be exceeded during the analysis.

8.2.3 Continuous beams

The analyses of continuous beams, spanning over two and three bays without horizontal restraint, showed that for the two-bay beam the fire resistance compared to a simply supported beam was noticeably improved, but for the three-bay beam the continuity over the supports did not greatly enhance the fire resistance compared to a simply supported beam.

Three different lengths of the reinforcement bars at the top of the beams at the inner supports were analysed. The length of the bars was determined following the design rules of DIN 1045-1 (DIN-1045-1) for the cold design, the design rules of EC 2 (EC2-02) for fire conditions and the regulations of „DIBt-Richtlinie zur Anwendung von DIN V ENV 1992-1-2 in Verbindung mit DIN 1045-1“ (DIBt-02) respectively, which resulted in a continuously increasing length of the bars. The analysis showed that the lengthening of the reinforcing bars was necessary to prevent the beam from forming a plastic hinge at the points were the bars were terminated when the support bending moments increased due to the effects of thermal bowing and moment redistribution. For the two-bay beam the length according to EC 2 was sufficient whereas for the three-bay beam the bars had to be lengthened according to the DIBt-regulation. However, the lengthening of the bars did not result in a great increase in the fire resistance rating.

When running SAFIR, the beams failed at a time less than the value in the tabulated data of EC 2 (EC2-02) and DIN-4102-4 (DIN-4102-4). But the simplified method of EC 2 (EC2-02) also predicts fire-resistance ratings less than the values in the tabulated data. The time to failure obtained in SAFIR was closer to the simplified method than to the tabulated data. However, this is not a serious problem in real buildings because the provision of some amount of restraint enabled the beams to sustain the imposed load for the stated duration. Even 1% restraint, based on the stiffness of one bay of the beams, was sufficient.

8.3 ISO-fire with decay phase

Beams spanning one, two and three bays without horizontal restraint were subjected to a growing ISO-fire for 30, 60 and 90 minutes followed by a decay phase. The beams analysed were those which sustained the full ISO-fire for the longest time period.

The beams exposed to the full process of fire development showed good behaviour during the analysis. Collapse of the beams only occurred when the start of the decay phase was close to the failure time reached during the analysis with the full ISO-fire. The deflections which developed during the fire exposure mostly recovered and only small permanent deflections could be observed. During the decay phase of the fire, some of the reinforcing bars developed large residual tensile stresses.

8.4 Recommendations for further research

It is recommended that further research should include:

- The effects of varying the vertical position of the supports of the reinforced concrete beams.
- The modelling of more realistic support conditions allowing for some amount of rotational and horizontal movement.
- The behaviour of differently shaped beams (changed dimensions, T-beams).
- A more detailed analysis of the behaviour of continuous beams with varying horizontal restraint.
- The analysis of reinforced concrete beams built into a frame structure.
- The analysis of beams with horizontal restraint subjected to fires with a decay-phase.
- A comparative analysis using the new SAFIR program which could allow the determination of the final failure mode of the pin-supported beams.
- A more detailed analysis of the observed stress development within the cross-section. This needs a more user-friendly output of the fibre stresses to allow the analysis of the stress development with time.
- An experimental verification of the analytical results.

A APPENDIX

A.1 Effect of varying the nodeline

In the SAFIR program, one of the items that needs to be specified is the “nodeline”. This is the line where the elements are connected to each other and the supports, and also the reference line for determining the displacements and bending moments. In many cases, this nodeline would be taken as being at the mid-depth of the section and in the case of homogenous, symmetric cross-sections this would also be the neutral axis. In the case of a concrete beam, the neutral axis is not at the mid-depth, but would be for an uncracked section with symmetric reinforcing.

When a pin-supported beam is loaded, it’s ends rotate due to the curvature imposed on the beam. The neutral axis of the beam will not change in length. Thus, the rotation results in an inwards movement of the endpoint of the neutral axis, which is situated close to the top of the cross-section for pin-supported concrete beams (see Figure A 1). The centroidal axis of the beam moves outwards.

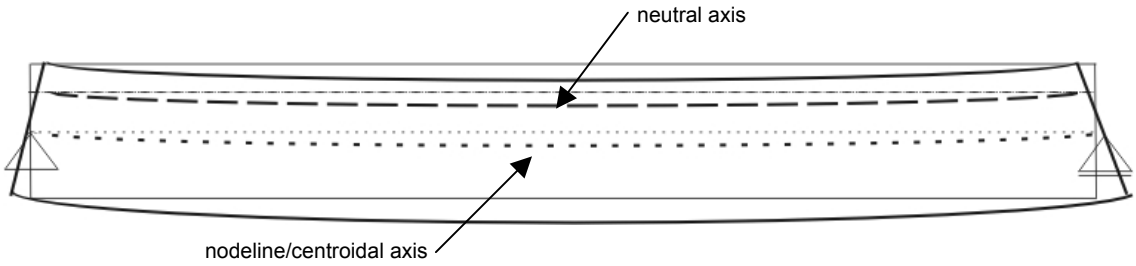

Figure A 1: Pin-supported beam

When the nodeline and thus the supports of a pin-pin beam are set at the height of the centroidal axis, the outward movement is restrained and results in a compressive force induced on the cross-section.

When the nodeline and the supports are set at the height of the neutral axis, the inward movement of the neutral axis is restrained, which causes a tensile force in the beam. The change of height of the supports results in a different structural behaviour of the beam under fire exposure, as the axial force is induced closer to the top of the beam.

When the nodeline is defined at the height of the neutral axis, but the supports are positioned at the centre of the cross-section, using vertical rigid elements as links in between (see Figure A 2), the beam acts like a beam supported and linked together at the centre of the cross-section. The stresses, the axial force and the deflections are the same,

but the obtained bending moment is related to the shifted nodeline and thus shows a distinct difference.

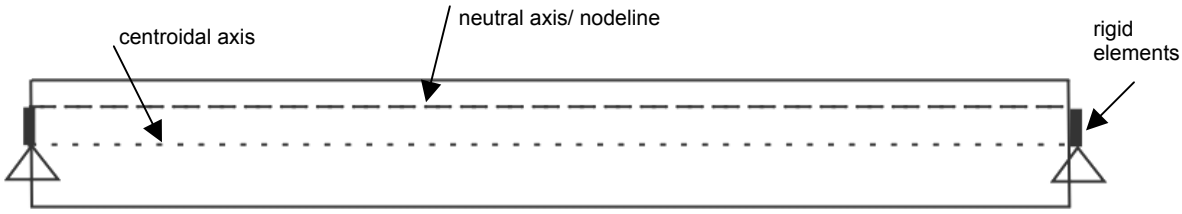

Figure A 2: Pin-supported beam with rigid elements

The bending moments, axial forces and vertical displacements at midspan for a pin-pin supported beam subjected to the ISO fire for the three different models mentioned above are shown in Figure A 3 to Figure A 4.

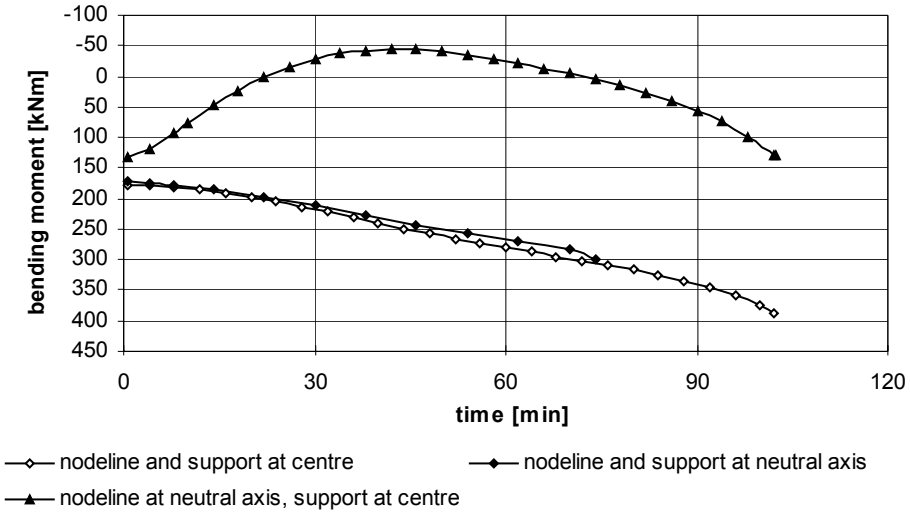

Figure A 3: Bending moment at midspan for varying support conditions

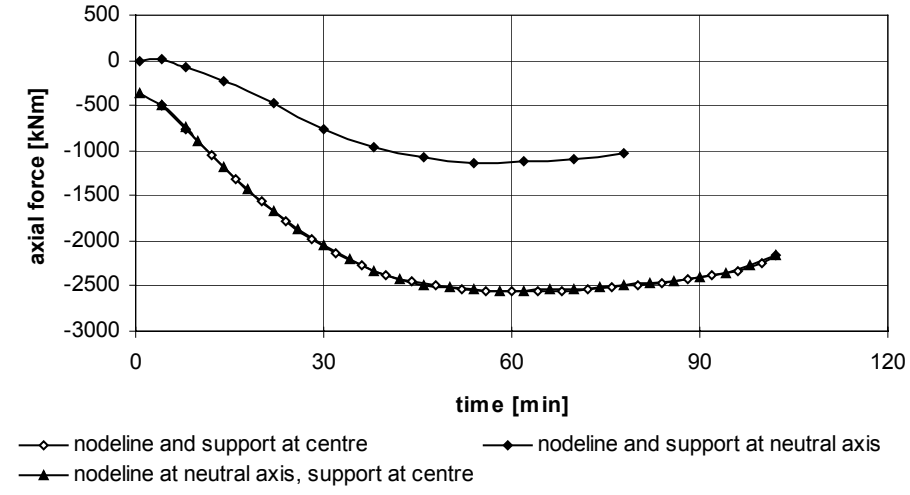

Figure A 4: Axial force for varying support conditions

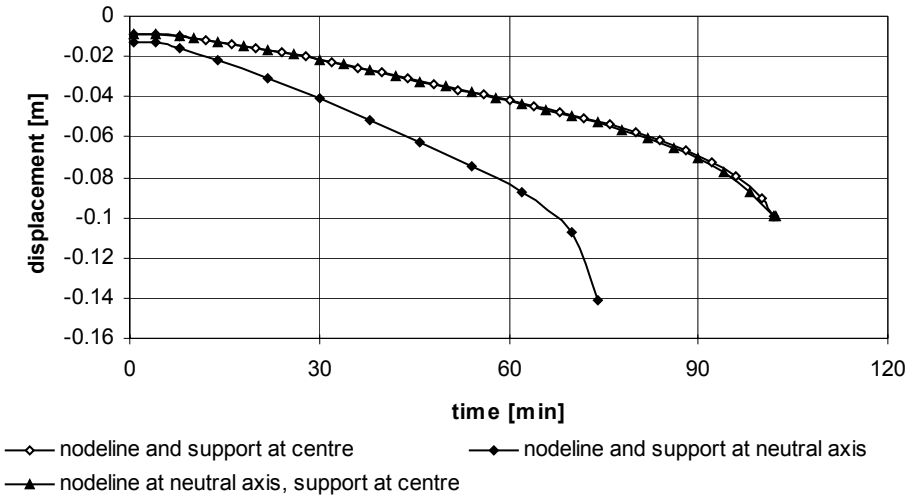

Figure A 5: Displacement at midspan for varying support conditions

For continuous beams the height of the neutral axis changes with the position along the beam, thus it is not possible to define the nodeline co-incident with the neutral axis. In order to get comparable results within this report, the nodeline and the supports have been positioned at the centre of the cross-section in all cases.

A.2 Stress-strain relationship of concrete according to EC2

a) Version 2002

Concrete temp. θ	Siliceous aggregates			Calcareous aggregates		
	$f_{c,\theta} / f_{ck}$	$\varepsilon_{c1,\theta}$	$\varepsilon_{cu,\theta}$	$f_{c,\theta} / f_{ck}$	$\varepsilon_{c1,\theta}$	$\varepsilon_{cu,\theta}$
[°C]	[-]	[-]	[-]	[-]	[-]	[-]
1	2	3	4	5	6	7
20	1,00	0,0025	0,0200	1,00	0,0025	0,0200
100	1,00	0,0040	0,0225	1,00	0,0040	0,0225
200	0,95	0,0055	0,0250	0,97	0,0055	0,0250
300	0,85	0,0070	0,0275	0,91	0,0070	0,0275
400	0,75	0,0100	0,0300	0,85	0,0100	0,0300
500	0,60	0,0150	0,0325	0,74	0,0150	0,0325
600	0,45	0,0250	0,0350	0,60	0,0250	0,0350
700	0,30	0,0250	0,0375	0,43	0,0250	0,0375
800	0,15	0,0250	0,0400	0,27	0,0250	0,0400
900	0,08	0,0250	0,0425	0,15	0,0250	0,0425
1000	0,04	0,0250	0,0450	0,06	0,0250	0,0450
1100	0,01	0,0250	0,0475	0,02	0,0250	0,0475
1200	0,00	-	-	0,00	-	-

Table A 1: Stress-strain relationship of concrete according to EC 2 (EC2-02)

b) Version 1995

Concrete Temperature (°C)	$f_c(\Theta)/f_c(20°C)$		$\epsilon_{c1}(\Theta)$ x 10^{-3}
	siliceous	calcareous	
20	1,00	1,00	2,5
100	0,95	0,97	3,5
200	0,90	0,94	4,5
300	0,85	0,91	6,0
400	0,75	0,85	7,5
500	0,60	0,74	9,5
600	0,45	0,60	12,5
700	0,30	0,43	14,0
800	0,15	0,27	14,5
900	0,08	0,15	15,0
1000	0,04	0,06	15,0
1100	0,01	0,02	15,0
1200	0,00	0,00	-

Table A 2: Stress-strain relationship according to EC2 (1995) (EC2-95)

A.3 Mathematical model of stress-strain relationship of steel

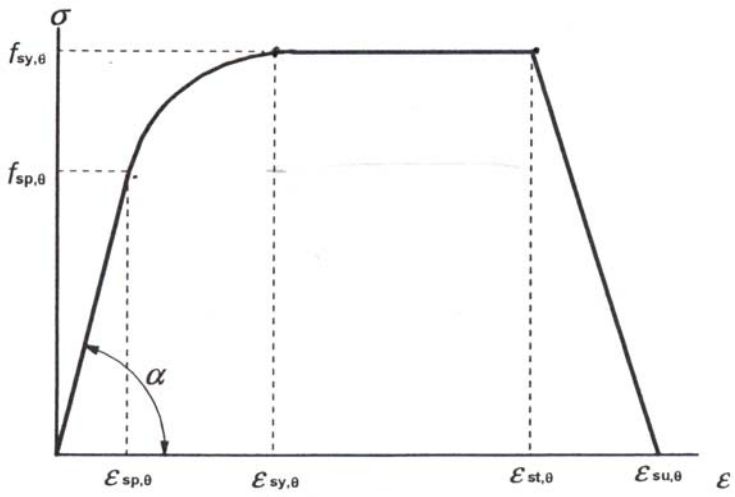

Range	Stress $\sigma(\theta)$	Tangent modulus
$\varepsilon_{sp,\theta}$	$\varepsilon E_{s,\theta}$	$E_{s,\theta}$
$\varepsilon_{sp,\theta} \le \varepsilon \le \varepsilon_{sy,\theta}$	$f_{sp,\theta} - c + (b/a)[a^2 - (\varepsilon_{sy,\theta} - \varepsilon)^2]^{0,5}$	$\frac{b(\varepsilon_{sy,\theta} - \varepsilon)}{a\left[a^2 - \left(\varepsilon - \varepsilon_{sy,\theta}\right)^2\right]^{0,5}}$
$\varepsilon_{sy,\beta} \le \varepsilon \le \varepsilon_{st,\theta}$	$f_{sy,\theta}$	0
$\varepsilon_{st,\beta} \le \varepsilon \le \varepsilon_{su,\theta}$	$f_{sy,\theta}[1-(\varepsilon - \varepsilon_{st,\theta})/(\varepsilon_{su,\theta} - \varepsilon_{st,\theta})]$	-
$\varepsilon = \varepsilon_{su,\theta}$	0,00	-
Parameter *)	$\varepsilon_{sp,\theta} = f_{sp,\theta} / E_{s,\theta}$ $\varepsilon_{sy,\theta} = 0,02$ $\varepsilon_{st,\theta} = 0,15$ $\varepsilon_{su,\theta} = 0,20$ Class A reinforcement: $\varepsilon_{st,\theta} = 0,05$ $\varepsilon_{su,\theta} = 0,10$	
Functions	$a^2 = (\varepsilon_{sy,\theta} - \varepsilon_{sp,\theta})(\varepsilon_{sy,\theta} - \varepsilon_{sp,\theta} + c/E_{s,\theta})$ $b^2 = c\,(\varepsilon_{sy,\theta} - \varepsilon_{sp,\theta})\,E_{s,\theta} + c^2$ $c = \frac{(f_{sy,\theta} - f_{sp,\theta})^2}{(\varepsilon_{sy,\theta} - \varepsilon_{sp,\theta})E_{s,\theta} - 2(f_{sy,\theta} - f_{sp,\theta})}$	

Figure A 6: Mathematical model of the stress-strain relationship of steel according to EC2 (EC2-02)

A.4 Calculations according to the simplified calculation method

Stated below are the calculations following the simplified calculation method given in annex E of the Eurocode (EC2-02) using the temperature profiles given in annex A of the Eurocode (EC2-02) for the two-bay beam analysed in section 6.1.

The table below states the temperatures in the reinforcing bars at **120** min according to Figure A.8 (EC2-02) and the strength reduction factors for the steel bars $k_s(\theta_{cr})$ according to Figure 5.1 (EC2-02) :

number of bars	**temperature in °C**	**$k_s(\theta_{cr})$**
top		
2	420	0.82
4	<200°C	1.00
bottom		
2	740	0.092
2	620	0.31

Table A 3: Temperatures and strength reduction factors for steel bars at 120 min

Data needed out of the cold design:

$M_{ed,\ support}$= 267.3 kNm

$A_{s,\ req,\ support}$= 11.97 cm²

$M_{ed,\ span}$= 162.0 kNm

$A_{s,req,span}$= 6.99 cm²

d= 56.5 cm

$w_{ed,\ fi}$= 38.5 kN/m

The support bending moment at the support after 120 min according to equation E.4 (EC2-02) can be calculated as:

$M_{Rd,fi}$ = $(\gamma_s/\gamma_{s,fi})M_{ed}(A_{s,prov}/A_{s,req})(d-a)/d$

=$(1.15/1.0) \cdot 267.3 \cdot (0.82+1+1) \cdot 2 \cdot \pi \cdot 1.6^2/(4 \cdot 11.97) \cdot (565-55)/565$

=<u>262.9 kNm</u>

The resulting bending moment at the span thus can be calculated to:

$M_{max,span}$= <u>66.7 kNm</u>

The moment resistance at span according to equation (E.3) (EC2-02) is:

$M_{Rd,fi}$ = $(\gamma_s/\gamma_{s,fi})\ k_s(\theta_{cr})\ M_{ed}(A_{s,prov}/A_{s,req})$

= $(1.15/1.0)\ 162 \cdot (0.092+0.31) \cdot 2 \cdot \pi \cdot 1.6^2/(4 \cdot 6.99)$

= <u>43.1 kNm < 66.7 kNm</u> = $M_{max,span}$

→ the fire resistance in not provided for 120 minutes

The table below states the temperatures in the reinforcing bars at **90** min according to Figure A.8 (EC2-02) and the strength reduction factors for the steel bars $k_s(\theta_{cr})$ according to Figure 5.1 (EC2-02):

number of bars	**temperature in °C**	**$k_s(\theta_{cr})$**
top		
2	380	0.92
4	<200	1.00
bottom		
2	650	0.24
2	550	0.49

Table A 4: Temperatures and strength reduction factors for steel bars at 90 min

The support bending moment at the support after 90min according to equation E.4 (EC2-02) can be calculated as:

$M_{Rd,fi} = (\gamma_s/\gamma_{s,fi})M_{ed}(A_{s,prov}/A_{s,req})(d-a)/d$

$=(1.15/1.0)\cdot 267.3\cdot (0.92+1+1)\cdot 2\cdot\pi\cdot 1.6^2/(4\cdot 11.97)\cdot (565-40)/565$

$=\underline{280.2\ kNm}$

The resulting bending moment at the span thus can be calculated to:

$M_{max,span}= \underline{68.8\ kNm}$

The moment resistance at span according to equation (E.3) (EC2-02) is:

$M_{Rd,fi} = (\gamma_s/\gamma_{s,fi})\ k_s(\theta_{cr})\ M_{ed}(A_{s,prov}/A_{s,req})$

$= (1.15/1.0)\ 162\cdot (0.24+0.49)\cdot 2\cdot \pi\cdot 1.6^2/(4\cdot 6.99)$

$= \underline{78.2\ kNm > 68.8kNm} = M_{max,span}$

→ fire resistance in provided for 90 minutes

A.5 SAFIR input files

Typical input file for thermal analysis

```
concrete beam 300X600mm
6d16 @ bottom, 4d16 @ top

    NPTTOT       782
      NODE 1541
      NDIM    2
 NDIMMATER    1
   NDDLMAX    1
      FROM    1   TO 1541 STEP    1 NDDL    1
  END_NDDL
  TEMPERAT
      TETA       0.9
  TINITIAL      20.0
  MAKE.TEM
 LARGEUR11     40000
 LARGEUR12         2
   NORENUM
beam1.tem
      NMAT    2
  ELEMENTS
     SOLID 1452
        NG    2
     NVOID    0
  END_ELEM
     NODES
      NODE    1     -0.30    -0.150
     GNODE    3     -0.30    -0.140    1
     GNODE   23     -0.30     0.000    1
    REPEAT   23     0.007     0.000   10
    REPEAT   23     0.010     0.000   46
    REPEAT   23     0.007     0.000   10
  NODELINE            0.0       0.0
     YC_ZC            0.0       0.0
 FIXATIONS
   END_FIX
NODOFSOLID
      ELEM    1    1    2   25   24    1    0
     GELEM   22   22   23   46   45    1    0    1
    REPEAT   22   23    3
      ELEM   89   93   94  117  116    1    0
     GELEM   94   98   99  122  121    1    0    1
      ELEM   95   99  100  123  122    2    0
      ELEM   96  100  101  124  123    2    0
      ELEM   97  101  102  125  124    1    0
     GELEM  100  104  105  128  127    1    0    1
      ELEM  101  105  106  129  128    2    0
      ELEM  102  106  107  130  129    2    0
    REPEAT    6    6    1
      ELEM  109  113  114  137  136    1    0
      ELEM  110  114  115  138  137    1    0
    REPEAT   22   23    1
```

```
      ELEM  133  139  140  163  162    1    0
     GELEM  154  158  159  181  180    1    0    1
    REPEAT   22   23   53
      ELEM 1321 1381 1382 1405 1404    1    0
     GELEM 1326 1386 1387 1410 1409    1    0    1
      ELEM 1327 1387 1388 1411 1410    2    0
      ELEM 1328 1388 1389 1412 1411    2    0
    REPEAT    6    6    1
      ELEM 1335 1395 1396 1419 1418    1    0
     GELEM 1342 1402 1403 1426 1425    1    0    1
    REPEAT   22   23    1
      ELEM 1365 1427 1428 1451 1450    1    0
     GELEM 1386 1448 1449 1472 1473    1    0    1
    REPEAT   22   23    3
  FRONTIER
         F    1      FISO        NO        NO        NO
        GF   22      FISO        NO        NO        NO    1
         F    1        NO        NO        NO      FISO
        GF 1431        NO        NO        NO      FISO   22
 END_FRONT
  SYMMETRY
     YSYM
    ENDSYM
 PRECISION     1.E-3
 MATERIALS
SILCONCEC2
92 25 9 0.5
  STEELEC2
25 9 0.5
      TIME
                10.      600.
                20.    14400.
  END_TIME
IMPRESSION
 TIMEPRINT       60.
```

Typical input file for structural analysis

```
pin-supported beam with 50% spring-stiffness

    NPTTOT    120000
     NNODE    50
      NDIM    2
 NDIMMATER    1
   NDDLMAX    3
      FROM    1   TO   49 STEP    2 NDDL    3
      FROM    2   TO   48 STEP    2 NDDL    1
      FROM   50   TO   50 STEP    1 NDDL    3
  END_NDDL
    STATIC
     NLOAD    1
   OBLIQUE    0
  COMEBACK     0.002
 ARCLENGTH     0.005
 LARGEUR11       550
 LARGEUR12        50
   NORENUM
      NMAT    3
  ELEMENTS
      BEAM   24    1
        NG    3
    NFIBER 1452
     TRUSS    1    1
  END_ELEM
     NODES
      NODE    1   0.00000   0.00000   0.00000
     GNODE   49   6.00000   0.00000   0.00000
      NODE   50   7.00000   0.00000   0.00000
 FIXATIONS
     BLOCK    1             F0        F0        NO
     BLOCK   49             NO        F0        NO
     BLOCK   50             F0        F0        F0
   END_FIX
 NODOFBEAM
beam1.tem
 TRANSLATE    1    1
 TRANSLATE    2    2
 END_TRANS
      ELEM    1    1    2    3    1
     GELEM   24   47   48   49    1    2
NODOFTRUSS
myfire.fct          0.18         0    3
      ELEM    1   49   50    1
 PRECISION     1.e-6
     LOADS
  FUNCTION     FLOAD
 DISTRBEAM         1        0.   -38500.
GDISTRBEAM        24        0.   -38500.    1
  END_LOAD
 MATERIALS
SILCONCEC2
        .2    30.E+6    0.0E+6                              1
  STEELEC2
   210.E+9        .3   500.E+6
```

```
 ELASTIC
    1.5E+9        .3
      TIME
                   8.      600.
                  16.    14400.
   ENDTIME
LARGEDISPL
     EPSTH
IMPRESSION
 TIMEPRINT        1.
PRINTREACT
   PRINTMN
PRNSIGMABM   13    1
```

A.6 List of tables

A.7 List of figures

A.8 References

(ACI-81) Report No. ACI 216R-81:
Guide for Determining the Fire Endurance of Concrete Elements,
American Concrete Institute, 1981

(And-76) Anderberg,Y.; Thelandersson,S.:
Stress and deformation characteristics of concrete at high temperatures,
Lund Institute of Technology, Lund, Sweden, 1976

(And-82) Anderberg,Y.; Forsén, N.E.:
Fire Resistance of Concrete Structures;
Lund Institute of Technology, Lund, Sweden, 1982

(Bai-02) Bailey,C.:
Holistic behaviour of concrete buildings in fire;
in Proceedings of the Institution of Civil Engineers, Structures &
Buildings 152, Issue 3, pp.199-212, 2002

(Bai-99) Bailey,C.G; Lennon.T.; Moore,D.B.:
The behaviour of full-scale steel-framed buildings subjected to
compartment fires;
in The Structural Engineer, Vol.77; No.8;pp.15-21, 1999

(Baz-96) Bažant,Z.P.; Kaplan,M.F.:
Concrete at High Temperatures: Material Properties and Mathematical
Models,
Longman Group Ltd., Essex, England, 1996

(Bob-75) Bobrowski,J.:
Fire resistance of concrete structures;
Report of Joint Committee of the Institution of Structural Engineers and
the Concrete Society; The Institution of Structural Engineers, London,
1975

(Bra-03) Bratina,S.; Planinc,I.; Saje,M.; Turk,G.:
Non-linear fire-resistance analysis of reinforced concrete beams,
in Structural Engineering and Mechanics, Vol.16, No.6, pp.695-712,
2003

(Buc-01) Buchanan,A.H.:
Structural Design for Fire Safety,
John Wiley & Sons, West Sussex, 2001

(Cai-03) Cai,J.; Burgess,I.; Plank,R.:
A generalised steel/reinforced concrete beam-column element model for
fire conditions,
in Engineering Structures, Elsevier, Vol.25,pp.817-833, 2003

(Car-62) Carlson,C.C.:
Fire Resistance of Prestressed Concrete Beams Study A - Influence of thickness of concrete covering over prestressing steel strand;
Research Development Laboratories of the Portland Cement Association, Research Department, Bulletin 147, 1962

(Car-65) Carlson,C.C.; Selvaggio,S.L.;Gustaferro,A.H.:
A Review of Studies of the Effect of Restraint on the Fire Resistance of Prestressed Concrete, Portland Cement Association Research and Development Laboratories, Bulletin 206, Skokie, Illinois, 1965

(Cha-03) Chana,P.; Price,B.:
The Cardington Fire Test;
in Concrete, The Concrete Society, Berkshire, UK, Vol.37,No.1;
pp.28-33, 2003

(Cru-66) Cruz,C.R.:
Elastic properties of concrete at high temperatures,
in Journal of the Portland Cement Association Research and Development Laboratory (PCA Bulletin 191), January, 1966

(Des-98) Desai,S.B.:
Design of reinforced concrete beams under fire exposure conditions;
in Magazine of Concrete Research, Thomas Telford Services Ltd,
Vol.50, No.1, pp.75-83, 1998

(DIBt-02) Deutsches Institut für Bautechnik:
DIBt-Richtlinie zur Anwendung von DIN V ENV 1992-1-2 in Verbindung mit DIN 1045-1,
DIBt-Mitteilungen, 2/2002

(DIN-1045-1) Eibl,J.:
Ergänzungsband zum Betonkalender 2002, Ernst & Sohn, Berlin, 2002

(DIN-4102-22) DIN 4102-22 Entwurf (November 2003);
Brandverhalten von Baustoffen und Bauteilen:
Teil 22: Anwendungsnorm zu DIN 4102-4; Deutsches Institut für Normung e.V., Beuth Verlag, Berlin,2003

(DIN-4102-4) DIN 4102-4 (März 1994);
Brandverhalten von Baustoffen und Bauteilen: Zusammenstellung und Anwendung klassifizierter Baustoffe, Bauteile und Sonderbauteile;
Deutsches Institut für Normung e.V., Beuth Verlag, Berlin, 1994

(EC1-03) DIN EN 1991-1-2: Eurocode 1: Einwirkungen auf Tragwerke Teil 1-2:
Allgemeine Einwirkungen Brandeinwirkungen auf Tragwerke
Deutsche Fassung EN 1991-1-2:2002;
Deutsches Institut für Normung e.V., Beuth Verlag, Berlin, 2003

(EC2-02) Eurocode 2: Design of concrete structures. prEN 1992-1-2 part 1.2:
General rules – Structural fire design,
European Committee for Standardization, Brussels, 2002

(EC2-95) Eurocode 2: Design of concrete structures. ENV 1992-1-2 part 1.2: General rules – Structural fire design, European Committee for Standardization, Brussels, 1995

(EC3-02) Eurocode 3: Design of steel structures. draft prEN 1993-1-2 part 1.2: General rules – Structural fire design, European Committee for Standardization, Brussels, 2002

(Ehm-65) Ehm,H.; von Postel,R.: Versuche an Stahlbetonkonstruktionen mit Durchlaufwirkung unter Feuerangriff, in Fire resistance of prestressed concrete, proceedings of a symposium held at Braunschweig Germany by the Federation Internationale de la Precontrainte, pp.24-31, 1965

(Elg-01) Elghazouli,A.Y.; Izzuddin,B.A.: Analytical assessment of the structural performance of composite floors subjected to compartment fires; in Fire Safety Journal, Elsevier, Vol.36, pp.769-793, 2001

(Ell-80) Ellingwood,B.; Shaver,J.R.: Effects of Fire on Reinforced Concrete Members, in Journal of the Structural Division, Proceedings of the American Society of Civil Engineers, Vol.106, No.St.11, pp.2151-2166, 1980

(Ell-91) Ellingwood,B.; Lin,T.D.: Flexure and Shear Behaviour of Concrete Beams during Fires, in Journal of Structural Engineering, American Society of Civil Engineers, New York, Vol.117, No.2, pp.440-458 1991

(FIP-78) FIP Commission on fire resistance of prestressed concrete structures, chairman: K.Kordina: FIP/CEB Report on methods of assessment of the fire resistance of concrete structural members, Fédération Internationale de la Précontrainte by the Cement and Concrete Association, Wexham Springs, 1978

(Fra-00) Franssen,J.M.; Kodur,V.K.R.; Mason,J.: USER'S MANUAL FOR SAFIR2001, A Computer Program for Analysis of Structures submitted to the Fire, University of Liège,2000

(Fra-02) Franssen,J.M.;Kodur,V.K.R.;Mason,J.: USER'S MANUAL FOR SAFIR 2001 free, A Computer Program for Analysis of Structures submitted to the Fire, University of Liège, 2002

(Fra-04) Franssen, J.M.; Gens,F.: Dynamic Analysis used to cope with partial and temporary failures; in Proceedings of the Third International Workshop Structures in Fire, Ottawa, pp.297-310, 2004

(Fra-04) Franssen,J.-M.:
Numerical determination of 3D temperature fields in steel joints;
in Fire and Materials, Vo.28, No 2-4, pp.63-82, 2004

(Fra-97) Franssen,J.M.; Bruls,A.:
Design and Tests of Prestressed Concrete Beams;
in Proceedings of the Fifth International Symposium of Fire Safety Science, Melbourne, Australia, Ed. Hasemi.Y.; International Association for Fire Safety Science, pp.1081-1092, 1997

(Gil-00) Gillie,M.:
The Behaviour of Steel-Framed Composite Structures in Fire Conditions;
University of Edinburgh, 2000,
source: http://www.civ.ed.ac.uk/research/fire/project/thesis/MGillie.pdf

(Gil-04) Gillie,M.; Usmani,A.; Rotter,M.:
Bending and membrane action in concrete slabs;
in Fire and Materials, Vol.28, p.139-157, 2004

(Gus-71) Gustaferro,A.H.; Abrams,M.S.; Salse,E.A.B.:
Fire Resistance of Prestressed Concrete Beams Study C: Structural Behaviour During Fire Test;
Research and Development Bulletin, Portland Cement Association, 1971

(Gus-86) Gustaferro, A.H.:
Design Implementations – Concrete Structures;
in Design of Structure against Fire, ed. Anchor,R.D., Elsevier, Essex, pp.189-211; 1986

(Gut-80) CRSI Concrete Reinforcing Steel Insitute; Chairman: Gustafson,J.A.;
Reinforced Concrete Fire Resistance,
Concrete Reinforcing Steel Institute, Chicago, 1980

(Har-93) Harmathy,T.Z.:
Fire Safety Design of Concrete;
Longman Scientific & Technical, Essex, England, 1993

(Her-03) Hertz, K.D.:
Limits of spalling of fire-exposed concrete,
in Fire Safety Journal,Vol. 38, Elsevier, pp.103-116, 2003

(Hua-00) Huang,Z.; Burgess,I.W.; Plank,R.J.:
Non-linear modelling of three full-scale structural fire test;
Proceedings of the first international workshop – Structures in Fire,2nd edition; Copenhagen; Denmark; Editor: J.-M. Franssen, pp.53-70, 2000

(Hua-01) Huang,Z.; Burgess,I.W.; Plank,R.J.:
Non-linear structural modelling of a fire test subjected to high restraint;
in Fire Safety Journal, Elsevier, Vo.36, No.8, pp.795-814, 2001

(Iss-70) Issen,L.A.; Gustaferro,A.H.; Carlson,C.C.:
Fire Tests of Concrete Members: An Improved Method for Estimating Thermal Restraint Forces; American Society for Testing and Materials, Philadelphia, USA, 1970

(Kho-85) Khoury,G.A.; Grainger,B.N.; Sullivan,P.J.E.:
Strain of concrete during first heating to 600°C under load,
in Magazine of Concrete Research, Cement and Concrete Association, Wexham Springs, Slough, Vol.37, No.133, pp.195-215, 1985

(Kho-85b) Khoury,G.A.; Grainger,B.N.; Sullivan,P.J.E.:
Transient thermal strain of concrete: literature review, conditions within specimen and behaviour of individual constituents,
in Magazine of Concrete Research, Cement and Concrete Association, Wexham Springs, Slough, Vol.37, No.132, pp.131-144, 1985

(Kir-88) Kirby,B.R.; Preston,R.R.:
High Temperature Properties of Hot-rolled, Structural Steels for Use in Fire Engineering Design Studies,
in Fire Safety Journal, Elsevier, Vo.13, No.1, pp.27-37, 1988

(Kor-65) Kordina,K.:
Der Einfluß von Abplatzungen, Schutzschichten und des Spannsystems auf die Feuerwiderstandsdauer,
in Fire resistance of prestressed concrete, proceedings of a symposium held at Braunschweig Germany by the Federation Internationale de la Precontrainte, pp.51-56, 1965

(Lam-01) Lamont,S.:
The Behaviour of Multi-storey Composite Steel Framed Structures in Response to Compartment Fires;
University of Edinburgh, 2001,
source: http://members.fortunecity.com/911/fire/Slamont.htm

(Lim-03) Lim,L.:
Membrane Action in Fire Exposed Concrete Floor Systems, research Report No. 03/2, University of Canterbury, Christchurch, New Zealand, 2003

(Lim-04) Lim,L; Buchanan,A.H.; Moss,P.J.:
Restraint of re-exposed concrete floor systems;
in Fire and Materials, Vol. 28, Issue 2-4, p.95-125, 2004

(Lim-04b) Lim,L.; Buchanan,A.; Moss,P.; Franssen,J.-M.:
Numerical modelling of two-way reinforced concrete slabs in fire;
in Engineering Structures, Elsevier, Vol.26, pp.1081-1091, 2004

(Lin-81) Lin,T.D.; Gustaferro, A.H.; Abrams,M.S.:
Fire Endurance of Continuous Reinforced Concrete Beams;
Research and Development Bulletin RD072.01B,
Portland Cement Association, Illinois, USA, 1981

(Lin-88) Lin,T.D.; Ellingwood,B.; Piet,O.:
Flexural and Shear Behaviour of Reinforced Concrete Beams During Fire Test
Research and Development Bulletin RD091T,
Portland Cement Association, Illinois, USA, 1988

(Mal-69) Malhotra,H.L.:
Fire resistance of structural concrete beams ;
Fire Research Note No.741, Fire Research Station, Borehamwood, UK, 1969

(Mal-82) Malholtra,H.L.:
Design of fire-resisting structures,
Surrey University Press, London, 1982

(Mal-84) Malhotra,H.L.:
Spalling of concrete in fires,
Construction Industry Research and Information Association, Technical Note 118, London, 1984

(Mos-04) Moss,P.J.; Clifton,G.C.:
Modelling of the Cardington LBTF steel frame building fire tests;
in Fire and Materials, Vol.28, No 2-4; pp.177-198, 2004

(NZS-95) Standards New Zealand:
NZS 3101: Part 1: 1995, Concrete Structures Standard: Part 1- The Design of Concrete Structures,
Standard Council, Wellington, 1995

(PCI-77) Gustaferro,A.H.; Martin, L.D.:
PCI Design for fire resistance of precast prestressed concrete;
Prestressed Concrete Institute, USA, 1977

(Pur-86) Purkiss,J.A.:
High Temperature Effects,
in Design of Structure against Fire, ed. Anchor,R.D., Elsevier, Essex, 1986

(San-00) Sanad,A.M.; Rotter,J.M.; Usmani,A.S.; O'Conner, M.A.:
Composite beams in large buildings under fire-numerical modelling and structural behaviour;
in Fire Safety Journal, Elsevier, Vo. 35, No.3, pp.165-188, 2000

(Schn-82) Schneider,U.:
Verhalten von Beton bei hohen Temperaturen,
DAfStb Heft 337,Ernst & Sohn, Berlin, 1982

(Schn-88) Schneider,U.:
Concrete at High Temperatures – A General Review,
in Fire Safety Journal, Elsevier, Vo.13, No.1, pp.55-68,1988

(Sel-63) Selvaggio,S.L.; Calson,C.C.:
Effect of restraint on fire resistance of prestressed concrete;
Portland Cement Association, Illinois, USA, 1963

(Sel-64) Selvaggion,S.L.; Carlson,C.C.:
Fire Resistance of Prestressed Concrete Beams Study B. Influence of Aggregate and Load Intensity;
Research and Development Laboratories of the Portland Cement Association, Research Department, Bulletin 171, 1964

(Sul-94) Sulivan,P.J.E.; Terro,M.J.; Morris,W.A.:
Critical Review of fire-dedicted thermal and structural computer programs;
in Journal of Applied Fire Science, Baywood Publishing Company, New York, Vol.3(2), p.113-135,1994

(Ter-98) Terro,M.J.:
Numerical Modelling of the Behaviour of Concrete Structures in Fire;
in ACI Structural Journal, American Concrete Institute, Michigan,
Vol. 95, No.2, p.183-193, 1998

(Wad-91) Wade,C.:
Method for Fire Engineering Design of Structural Concrete Beams and Floor Systems,
BRANZ (Building Research Association of New Zealand),
Technical Recommendation No:8,1991

(Zha-03) Zha,X.X.:
Three-dimensional non-linear analysis of reinforced concrete members in fire;
in Building and Environment, Elsevier, Vol.38, pp.297-307, 2003